Cloning and characterization of voltage-gated sodium and calcium channel homologs from the single-cell choanoflagellate, *Salpingoeca rosetta*

by

Amrit Mehta

A thesis
presented to the University of Waterloo
in fulfillment of the
thesis requirement for the degree of
Master of Science
in
Biology

Waterloo, Ontario, Canada, 2016

Author's Declaration

I hereby declare that I am the sole author of this thesis. This is a true copy of the thesis, including any required final revisions, as accepted by my examiners.

I understand that my thesis may be made electronically available to the public.

Abstract

We have isolated a complement of gene homologs from the simplest extant eukaryotic species to possess voltage-gated sodium (Na^+) and calcium (Ca^{2+}) channels, *Salpingoeca rosetta*. The isolated channels share the same 4 Domain, 6 Transmembrane helices (4x6TM) architecture characteristic of voltage-gated ion channels and do not exhibit any alternative splicing. Transfection and expression of both channels in Human Embryonic Kidney-293T (HEK-293T) cells generate voltage-dependent ionic currents. SroNa$_v$2 codes for an 1831 amino-acid transmembrane protein of four repeat domains with a selectivity filter ring, DEEA, resembling Ca^{2+}-selective sodium channel genes found exclusively in non-vertebrate animals. The structurally similar to Na$_v$1, SroNa$_v$2 shows non-selective ion permeability and allows the passage of both divalent and monovalent ions. The SroNa$_v$2 selectivity filter mutant, DEKA, produced to mimic neuronal vertebrate Na$_v$1 channels, produces a highly selective channel that exclusively passes monovalent ions. SroCa$_v$1 codes for a 1664 amino-acid transmembrane protein, requires co-expression of a native β auxiliary subunit, and is highly selective and does not allow the passage of sodium. SroCa$_v$1 lacks obvious calcium-dependent inactivation and does not exhibit the same long-lasting currents characteristic of L-type channels with Ba^{2+} as a charge carrier. We envisage that these homologs of voltage-gated Ca^{2+} and Na^+ channels found in single cell choanoflagellate *Salpingoeca rosetta* may generate Ca^{2+}-dependent action potentials that signal between cells of choanoflagellate colonies, regulate intra-cellular events, or control movement of it's single flagellum or cilia.

Acknowledgements

I would like to first and foremost say thank you to Dr. David Spafford. You took a chance on me when no one else would. You spent countless hours designing PCR primers, analyzing sequences and collected electrophysiology data, creating figures and graphs, and developing strategies for making this project a success. Your enthusiasm for the research, knowledge, guidance, and patience are what have brought this project to where it is today. You pushed me when I needed it most, and provided support when it was necessary. I am thankful for your contribution in making me who I am today.

To my committee members, Dr. Warren Gallin, Dr. Moira Glerum, and Dr. Joe Quadrilatero, as well as Dr. Cheryl Duxbury. Thank you for taking time out of your busy schedules to read my proposal and my thesis. Thank you for asking the difficult questions, providing guidance and support as a student and a person. I would especially like to thank Wendy Guan, Robert Stephens and Julia Fux for taking me under their wings as a volunteer and teaching me what I needed to know to become successful in science.

To my lab mates Jenn Czekus and Cynthia Quan. You guys taught me things that science could not and kept me sane when the science had other ideas. Thank you to Priya Jani, Cynthia Quan, Khevna Patel, Devon Travo, Ronak Saluja, Kathleen Zhang, Sumit Nakra, Sunny Nakra, and all of OSS.

And finally my family, my mother and father. Your love, guidance and patience in me as I pursue bigger and bigger ventures have been my strengths as I progress. I hope to always make you proud. To my brother, Arun, the ever-lasting competition between us has manifested in other areas of my life and keeps pushing me to be the best in everything I do.

Dedication

I dedicate this thesis to my mother, Neena. We may argue at times but the love and support you've shown me is unparalleled. I can only hope to repay a fraction of what you've given me.

Table of Contents

List of Figures

List of Tables

Chapter 1

Introduction

1.1 The origin of animals in the Opisthokonts

The appearance of a nervous system was a major event at the roots of evolution of multicellular organisms from single cell ancestors. For nervous systems to evolve, it required specific ion channels, especially the voltage-gated sodium- and calcium-selective channels, to generate the electrical activity for neural communication and neurotransmission at nerve synapses. In this thesis, I will describe our discovery of homologs of voltage-gated sodium- and calcium-selective channels in the simplest extant organisms to have them, the single cell choanoflagellates. Before proceeding with an introduction to ion channels in simple organisms, I will first explain why it is important for us to study single cell eukaryotes as a model organism to gain insights into animal and nervous system evolution.

Understanding the roots of human and animal evolution remains a topic of great debate and source of curiosity for scientists and researchers. Categorizing and defining the biological world rose independently in both the Eastern (Chinese) and Western (Greek, Roman) worlds thousands of years ago by the efforts of early scientists such as Aristotle, Theophrastus, and Brunfels. Modern efforts in research have been put into uncovering the roots of our last common ancestors on both fundamental organismal and molecular levels (Fairclough et al., 2013; King, 2004; Lang, et al., 2002; Nichols et al., 2012; Richter & King, 2013; Ruiz-Trillo et al., 2007; Shalchian-tabrizi et al., 2008; Tarvin et al., 2016; Watanabe et al., 2009). Inconsistencies and gaps in fossil records lead to reconstructing the identity of the last common Metazoan ancestors by observing differences and similarities to extant species (Borowiec et al., 2015; Burger et al., 2003; Fairclough et al., 2013; Love et al., 2009; Nosenko et al., 2013; Parfrey et al., 2011; Philippe et al., 2005; Richter & King, 2013; Ruiz-Trillo et al., 2007). The current widely accepted hypothesis suggests that *Homo sapiens*, animals and many other eukaryotes, reside within a single super-group known as the Opisthokonta (Richter & King, 2013; Ruiz-Trillo et al., 2008; Torruella et al., 2012). The Opisthokonta clade is divided into two sub-groups, the ‘holozoa’ and ‘holomycota’, the former of which encompass not only all animals but also includes choanoflagellates, filasterea, ichthyosporea (Fig. 1.1) (Paps et al., 2015; Richter & King, 2013).

The ability to discern, analyze and evaluate the relationships of the clade's members cannot be done without understanding the fundamentals that make them members of the Opisthokonta. Identifying the similarities and differences between members can help to establish relationships in hopes to allow for a better understanding and possible predictions of basic homologous biological processes that may be integral or in some ways beneficial to life.

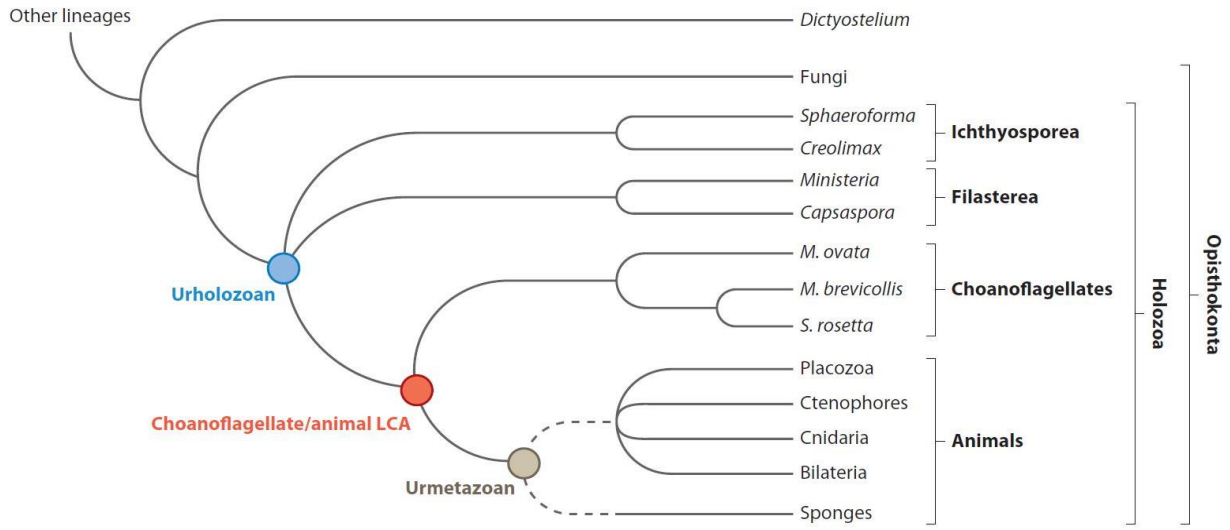

Figure 1.1 Phylogenetic representation of Opisthokonta

Nodes represent a proposed single relative for branching outgroups. Choanoflagellates are proposed at the most closely related sister group to animals. Dotted lines indicate uncertainty in relationships of early branching animals. (Adopted from Richter and King, 2013)

1.2 The timeline for the evolution of the eukaryotes

The methods currently employed to study basal organisms make use of small subunit ribosomal RNA (rRNA) and mitochondrial DNA, body patterning genes, body plan and tissue specific genes, various enzyme encoding genes and other bio-markers (Hedges et al., 2004; Osigus et al., 2013; Pakendorf & Stoneking, 2005; Paps et al., 2015; Sogin, 1991; Torruella et al., 2012). Current fossil records place eukaryotic origins approximately 600 million years, while biochemically and molecular-derived estimates place the emergence and diversification of the earliest eukaryotes at nearly 1900 million years ago (Mya) (Hedges et al., 2004; Richter & King, 2013; Wegener et al., 2011).

Fungi present the first divide in the Opisthokonta and create the dichotomy of holomycota (fungi) and holozoa. Within the holozoa the ichthyosporea and filasterea (Choanozoa) appear to represent the first divergent sub-lineages, while choanoflagellates diverged next and are more closely related to metazoans (Paps et al., 2015; Torruella et al., 2012). Holomycota divergence estimates place them at just over 1,500 Mya, while ichthyosporea, filasterea and choanoflagellates diverged at later time estimates of ~1,200 Mya (Bullerwell et al., 2003; Carr et al., 2008; Parfrey et al., 2011; Richter & King, 2013; Wakefield et al., 2010). The remaining sub-group contains more than 1.3 million 'higher' members known as the Metazoa or Animalia (which include lophotrochozoa and deuterostomia), and identifiable non-bilaterian members including placozoa, cnidarian, ctenophora and porifera (sponge) (Moran et al., 2015; Nosenko et al., 2013).

Ichthyosporea, filasterea and choanoflagellates are often grouped together because they are often used as model organisms for studying the origins of eukaryotic multicellularity (Ruiz-Trillo et al., 2007). Several research initiatives have screened and analyzed cellular characteristics and molecular markers of these species and have consistently implied their relationships as the closest relatives to the Metazoa, or modern day animals (Carr et al., 2008; Hedges et al., 2004; Nosenko et al., 2013; Richter & King, 2013; Shalchian-tabrizi et al., 2008). All currently acknowledged members of these groups appear to at least divide through binary fission but also posses the genes for sexual reproduction within their genomes (Suga, 2015). Choanoflagellates have recently been experimentally shown to undergo sexual reproduction marking the earliest signs of gender-mediated procreation (Levin & King, 2013). Several representative strains within each species appear to share biological characteristics including the ability to aggregate into a multicellular form, a flagellum (likely for movement) and a sponge-like cellular morphology that is characteristics of choanocytes (Carr et al., 2008; Glockling et al., 2013; King, 2004; Paps et al., 2015; Suga, 2015). The presence of choanocyte-related aspects provides the first evidence for a close relationship to Porifera (sponge) – a non-bilaterian member of Metazoa. Demospongiae fossils analyzed based on hydrocarbon sterane biomarker content date the earliest porifera species at ~751 Mya, a time frame several million years prior to early Metazoa fossils (Love et al., 2009). Porifera is an enigmatic group of extant organisms. Sponge genomes possess genes associated with a central nervous system (CNS) and neurons yet they lack a central nervous system and many critical CNS developmental genes (Moroz, 2015;

Watanabe et al., 2009). The close relationship between choanoflagellates and metazoans has been well-supported implying that the eukaryotic last common ancestor was likely similar to a choanoflagellate (Hedges et al., 2004; Paps et al., 2015; Richter & King, 2013; Torruella et al., 2012).

1.3 *Salpingoeca rosetta* as a representative of the closest single-cell ancestor to the Metazoans

The current accepted hypothesis places the first definitive Metazoan animals appearing at a time over six hundred million years ago (Richter & King, 2013), a proposed time when unique microbial eukaryotes (protists), mainly single-celled organisms, first began to undergo a "diversification explosion" that would eventually lead to the organisms that currently exist today (Fairclough et al., 2013; Jekely, 2013; Richter & King, 2013; Ruiz-Trillo et al., 2007; Wegener et al., 2011). One specific candidate has come to light with strong evidence as being closely related to the last common ancestor of animals, the choanoflagellate *Salpingoeca rosetta* (referred to as *Salpingoeca* henceforth in this work). Choanoflagellates are considered by many as being a sister evolutionary lineage to the Metazoa, and their divergence from that lineage may mark a pivotal transitioning point of multicellularity (King, 2004; Richter & King, 2013; Ruiz-Trillo et al., 2007). First characterized as part of the *Proterospongia* family due to its high degree of structural similarity to sponge choanocytes (porifera), *Salpingoeca* is actually an extant choanoflagellate with fossil records dating back to more than 1,200 million years ago (Carr et al., 2008; Richter & King, 2013; Wegener et al., 2011). Genome evaluation with *Salpingoeca* has revealed a surprising number of gene homologs present in higher species within the animal clade that were previously thought to be exclusive to more complex, multicellular species.

1.4 Cellular differentiation, life cycles, and sexual reproduction of *Salpingoeca rosetta*

A unique characteristic of *Salpingoeca* is its ability to undergo several life stages including three solitary stages; fast or slow swimming, and a single cell-attached/anchored stage (thecate), and two multicellular colonial stages; rosette colonies where cell connections are robust and resistant to mechanical stressors, and chain colonies with weaker intercellular

connections (Dayel et al., 2011; Levin, 2014) (Fig.1.2). A possible origin of multicellular colonies of single cell organisms is illustrated in the observation that colonies form by cell division and incomplete cytokinesis, and not aggregation. (Fairclough et al., 2010). Incomplete cytokinesis may have been a possible way that tissues evolved from a single cell. The membranes of adjoining cells in *Salpingoeca* colonies are continuous with each other as a result of the incomplete cytokinesis, and electron- dense plates bridging the cells prevent mixing of cellular contents between adjacent cells (Dayel et al., 2011). *Salpingoeca rosetta* can colonize into a rosette pattern, but this life stage transition requires a commensal bacteria that normally resides with *Salpingoeca*, such as Bacteroides, *Algoriphagus machipongonensis* (Dayel et al., 2011). *A machinpongonensis* produces a C-type lectin-like protein that triggers the formation of *Salpingoeca* rosette colonies. Treatment with antibiotics that eliminate the commensal bacteria prevent rosette formation. The gene responsible for rosette multicellularity has been identified in a mutant strain of *Salpingoeca rosetta* insensitive to the extracellular C-type lectin-like protein, dubbed "Rosetteless" (Levin et al., 2014). The relationship that *Salpingoeca* shares with *A. machipongonensis* presents one of the earliest branching commensal relationships currently described for an extant eukaryote. Such research in animal-bacteria relationships are of a growing interest, especially as it relates to the human gut microbiome (Ley et al., 2008).

Salpingoeca rosetta differentiate into at least five distinct cell types, including three solitary cell types (slow swimmers, fast swimmers, and thecate cells) and two colonial forms (rosettes and chains). *Salpingoeca* cells are also observed to transition from haploid to diploid cell states via fusion of male and female gametes in response to an unenriched growth environment (Levin & King, 2013).

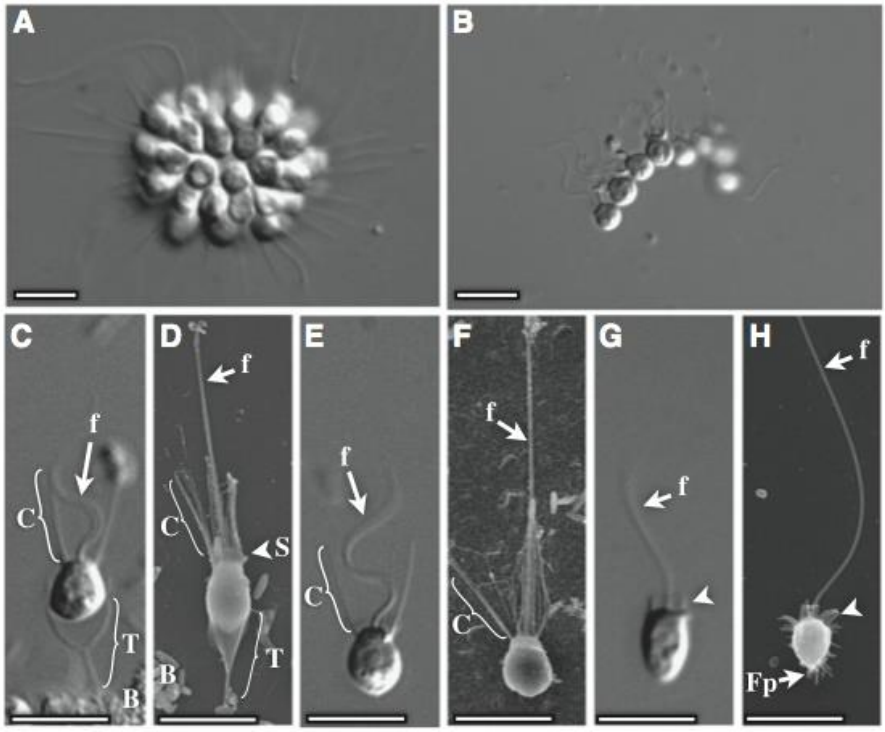

Figure 1.2 Life stages of *Salpingoeca rosetta*

(A) *Salpingoeca rosetta* in rosette colony. (B) *S. rosetta* in chain colony (C-D) Cells in surface-attached thecate stage. (E-F Slow swimmers. Morphology more closely resembles thecate stage (G-H) Fast swimmers, prominent flagellum. Unlabelled arrow indicates short ciliary collar. C: cilia collar, T: thecate stem, S: skirt, f: flagellum, Fp: filipodia. (Adopted from Dayel et al., 2011)

1.5 Prey capture and phagocytosis

Salpingoeca exhibits a commensal relationship in its native environment with many strains of bacteria, including the Bacteriodes, *Algoriphagus machipongonensis* and closely related strains. The bacteria are prey and a source of sphingolipids capable of inducing rosette formation in the basal eukaryote (Alegado et al., 2012, 2013). Prey capture has been observed in the thecate where the out-facing flagellum beats in a sinusoidal pattern likely as a method to draw bacteria towards the cell where they are then 'caught' in the microvilli collar. Prey capture occurs in the rosette colony life stage as well. Rosette colonies lack a prominent collar skirt but create a phagocytic cup that is capable of engulfing large bacterial prey and in some observed cases, large yeast cells such as *Saccharomyces cerevisiae* (Dayel & King, 2014). Ingestion of

bacterium is restricted to within 700nm of the apical pole where large groupings of food vacuoles exist.

1.6 Phylogenetic and molecular patterns

Phylogenetic studies using small subunit and large subunit ribosomal DNA (Carr et al., 2008), mitochondrial DNA (Lang et al., 2002; Ruiz-Trillo et al., 2008), and fragmented whole genome DNA (Fairclough et al., 2013) consistently place the choanoflagellates as a closest single cell pre-metazoan group to the human lineage.

The *Salpingoeca* genome is approximately 55Mb (mega-bases) and is comprised of greater than 9,400 ortholog gene clusters. Work by Fairclough and colleagues (2013) compared these ortholog clusters to Metazoa, fungi, and the sister choanoflagellate *Monosiga brevicolis* to theorize that *Salpingoeca* most closely represents the gene content of an animal precursor. *Salpingoeca* expresses genes previously thought to be specific to higher organisms within the Metazoan clade. Genes involved in cell adhesion, including δ-catenin and a form of classic cadherin are integral to multicellularity and are identified in *Salpingoeca* (Dayel & King, 2014). Tyrosine kinases (TK) and associated receptors, and voltage-gated ion channels, including calcium (Ca_v) and sodium (Na_v) channels (Fairclough et al., 2013; Fairclough, 2011; Moran et al., 2015; Moran & Zakon, 2014; Nichols et al., 2012). Salpingoeca has a voltage-gated sodium channel (Na_v2), a high voltage-activated calcium channel Ca_v1, and a low voltage-activated Ca_v3 calcium channel. These channels are involved in neuronal signalling, pain sense, pace-making, muscle contraction, and neurotransmitter release among other functions in higher animals, many of which are functions that are not present in single-celled eukaryotes. Studies of these sodium and calcium channels in *Salpingoeca rosetta* will provide insights into the roles that these ion channels played before the advent of multicellularity. These channels are of the most distant and basally positioned calcium and sodium channel homologs, which provides opportunities to evaluate the different structure and functional features related to key ion channel functions such as their calcium and sodium selectivity, their voltage and drug sensitivity, and kinetics.

1.7 Structure of voltage-gated ion channels

The ion channel superfamily members are divided based on their respective permeant ions; calcium (Ca^{2+}), sodium (Na^{+}), potassium (K^{+}), and/or chloride (Cl^{-}) ions and are denoted "I_v", where *'I'* represents primary conducted ion and 'v' - voltage. The first experimental evidence for the structure of a member of the superfamily of ion channels was achieved by Doyle and colleagues (Doyle et al., 1998) who resolved the crystal structure of the inward rectifying potassium channel (K^{+}) from the Actinobacterium *Streptomyces lividans* to a resolution of 3.2 angstroms (Å). Since then other research teams have been able to further isolate the crystal structure of a member of the *Shaker* family K^{+} channel (Long et al., 2005) and of a bacterial voltage-gated sodium channel from *Arcobacter butzleri* to a resolution of 2.7Å (Payandeh et al., 2012). All resolved ion channel structures serve as a template in the predictions on the structures and mechanisms of other ion channels.

Ca_v, Na_v, and K_v channel types possess a homologous core protein structure and have the ability to interact with auxiliary subunits that can affect functional channel expression patterns and kinetic/gating properties (Canti et al., 2003; Doyle et al., 1998; Fang & Colecraft, 2011; Lory et al., 1992; Moran & Zakon, 2014; Murakami et al., 2002; Simms & Zamponi, 2014; Spafford et al., 2004; Wiser et al., 1996). The ability to differentiate and allow or block certain ions is attributed to the channels' selectivity filters and extracellular turret domains linked to the conduction pore (Catterall, 2012; Favre et al., 1996; Hille, 1975; Krauss et al., 2011; Senatore et al., 2014; Senatore et al., 2014; Stephens et al., 2015; Yamagishi et al., 1997). The pore-forming α-subunit of Ca_v and Na_v channels consists of 24 transmembrane helices, a four homologous domain protein comprised of six transmembrane helices (S1-S6) per domain (4x6TM) that are connected via inter-domain linkers that protrude into the cell, along with the N- and C-termini (Fig. 1.3). The α subunit is the primary conducting component of the ion channel protein and in some cases is capable of full functional expression without any associated auxiliary subunit. The four domain architecture is proposed to have risen from two rounds of duplication of a 1x6TM channel, and resulted in domain-pairing pattern where Domains I-III and Domains II-IV are more similar than the others (Stephens et al., 2015). Each homologous domain is divided into two distinct functional components, a voltage sensor domain (S1-S4) and a pore domain (S5-S6). The pore domain contains a short re-entrant loop, the pore-loop or P-loop, between S5 and S6

segments that is responsible for forming the extracellular component of the pore, while S5 and S6 form the narrow intracellular-facing portion (Catterall et al., 2007; Senatore et al., 2014; Senatore et al., 2014).

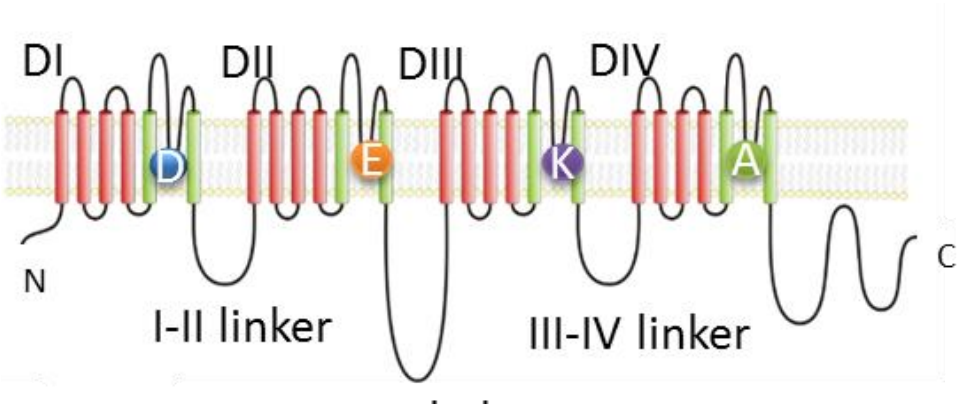

Figure 1.3 Expanded transmembrane view of 4x6TM voltage-activated ion channels

Eukaryotic voltage-activated calcium and sodium channels formed by a single peptide divided into 4 Domains (DI-DIV) of 6 transmembrane helices. Red indicates voltage-sensor helices; green indicates pore helices. Indicated residues represent location of selectivity filter residues in calcium and sodium channels (Na_v1 family filter depicted)

The ability to, and the physiological mechanics for conducting ions through the channel have been theorized by Eisenman (Eisenman, 1962; Krauss et al., 2011). Eisenman proposes that monovalent alkali ions act as charged spheres that must coordinate between attraction and entry into a channel's binding site, or remaining part of a hydration shell (Eisenman, 1962; Krauss et al., 2011). These two states are constantly in competition as a single ion must shed parts of its hydration shell in order to fit into the binding site of its channel. This is one way that channels are able to differentiate between extracellular ions; the correct ion will have the greatest affinity for the channel's binding site due to adequate reduction of hydration state and resultant size. Eisenman defined the binding site of ions as either 'high field strength' or 'low field strength' which correspond to a small or a large ion sphere, respectively. The purpose of the proposed model was based on the theory first proposed by Hille who theorized that ions face barriers to diffusion and must coordinate in a manner that maximally reduces such barriers in order to pass through the hydrophobic membranes of cells at rates nearing free diffusion (Hille, 1975).

Before ions are able to enter the high or low field strength site they must first overcome the barrier of the outer selectivity filter and an extracellular turret (Stephens et al., 2015). The turret of an ion channel is likened to an extracellular dome that contributes to passing or blocking of specific ions. Both the selectivity filter and turret are retained within the P-loops of each domain of the ion channel. The N-terminal end of each P-loop, closest to S5, first extends up over the protein and forms a cap-like structure (P-loop turrets are joined in a pairwise manner with the opposing domain; DI-DIII, DII-DIV). The pore loop then descends to the pore helix which ascends to forming the narrowest extracellular facing constriction point where key selectivity residues reside (Stephens et al., 2015). The narrowest amino acid contributing to the selectivity filter are 4 key amino acid residue side chains, one from each domain P-loop, that function cooperatively to highly regulate the ion selectivity of the channel. Calcium channels selectivity filter are an EEEE/EDEE configuration and sodium channel selectivity filters are DEKA, DKEA, and DEEA (Bendahhou et al., 1999; Boda et al., 2015; Borowiec et al., 2015; Sands et al., 2005; Stephens et al., 2015). Both the extracellular turret and selectivity filters are variable and highly influence ionic selectivity both independently and cooperatively (Senatore et al., 2014; Senatore et al., 2014; Stephens et al., 2015).

1.8 Function and biophysical properties

Voltage-gated channels conduct ions, possess regulatory gates, and are modified by post-translational modification such as phosphorylation or regulated by auxiliary subunits or other proteins (Catterall et al., 2007). Voltage sensor domains (S1-S4) are positioned laterally and outward from the central pore and are responsible for detecting changes in membrane voltage. The S4 segment of the voltage sensor is composed of a repeating motif of a positively charged amino acid residue in every third position of the channel pore gates (Catterall et al., 2007). Recordings of gating currents and the modeling of crystalized ion channels in different conformations has provided a hypothesis that the S4 segment, upon membrane depolarization, moves outward (towards the extracellular region) in a helical or corkscrew motion (Bezanilla, 2000; Payandeh et al., 2012). Gating charges denoted ‘R2’ and ‘R3’ interact with extracellular negatively charged clusters while an ‘R4’ charge interacts with an intracellular negatively charged cluster in a manner that stabilizes the voltage sensor domain during the conformation

change that occurs with the movement of the S4 segment during depolarization. Segments S1, S2 and S3 provide a set of counter-charges that interact with S4 charges as the S4 helix corkscrews up and down the membrane (Payandeh et al., 2012).

Ion channel gating is assessed by looking at kinetic properties such as activation, deactivation and inactivation. Activation and deactivation in sodium and calcium channels refer to the opening and closing of these channels in response to membrane depolarization and repolarization, respectively (Canti et al., 2003; Catterall, 2012; Gerster et al., 1999; Senatore et al. 2012; Simms & Zamponi, 2014). Inactivation however refers to refractory state that the sodium or calcium channel enters following a prolonged channel opening during accumulative membrane depolarization. In this state the sodium or calcium channel is no longer able to respond to any depolarizing stimulus regardless of its amplitude, and its recovery from inactivation is facilitated by hyperpolarization. Normally inactivation is a process that accumulates during rapid trains of action potential spikes, which in whole cell patch clamp recording, is evaluated by the rate of change (tau of inactivation) of the decaying current during prolonged voltage steps clamped to depolarizing potentials. Deactivation is measured in whole cell patch clamp as the rate of channel closure (tau activation), upon removal of a rapid depolarizing step that opens channels. The activation is measured in whole cell patch clamp as the time to peak current, or the slope of the current increase to peak current over time upon depolarizing voltage step. Recovery from inactivation is measured as the percent fractional recovery of maximal peak current size after time intervals have passed after a protocol that depolarizes ion channels to maximal (100%) inactivation.

1.9 Voltage-gated sodium channels

Two classes of voltage-gated cation channels include the sodium-selective (Na_v) channels and the calcium-selective (Ca_v) channels. Voltage-gated sodium channels have been found to predate the divergence of animals, choanoflagellates and fungi by their presence in apusozoans (Cai, 2012, Liebenskind, 2011). The apusozoans are a group of small heterotrophic flagellates that are proposed as a sister group to the Opisthokont superfamily in several molecular phylogenies (Cavalier-Smith and Chao, 1995, Paps et al., 2013). *Thecamonas trahens* (a representative organism of the apusozoans) possesses a four-domain homolog of sodium

channels, TtrNa$_v$2, an Na$_v$2 family sodium channel that is also found in choanoflagellates and most non-vertebrate animals, but missing in fungi, a sister group to the animals (Cai, 2012). A key determinant for ion selectivity is the single residue in the selectivity filter contributed by each of the four domains located as the most constricted point of the aqueous pore. *T. trahens* selectivity filter key amino acids are DEES, and similar to *Salpingoeca rosetta* (DEEA), where DEEA is the configuration of almost all Na$_v$2 channels (Cai, 2012). While Nav2 channels possess DEEA selectivity filters typically, all Nav1 channels have a lysine residue in either the second position (DKEA, cnidarians) or the third position (DEKA- all non-cnidarian Nav1 channels in metazoans). Na$_v$2 channels are related to Nav1 channels with an overall homology including their genomic structure with twenty intron splice sites conserved in all Na$_v$2 and Na$_v$1 channels. DEEA Na$_v$2 channels likely predate Na$_v$1 channels, since Na$_v$2 channels are present in single cell choanoflagellates, while DEKA/DKEA Na$_v$1 channels are only present in more advanced, multicellular organisms with nervous systems (eg. cnidarians and other metazoans).

The choanoflagellate *Salpingoeca rosetta* possess the most primitive Na$_v$2 sodium channel with a DEEA selectivity filter. This homolog represents the most basal DEEA sodium channel to arise following the animal-fungal split, and may be the progenitor for the evolution of other Na$_v$2 and Na$_v$1 sodium channel genes within the Metazoa.

Voltage-gated sodium and calcium channels are postulated to have evolved as a result of gene duplications of a one domain channel such as a potassium K^+ channel. Sodium channels are responsible for the rapid rising phase of nerve, muscle and endocrine cell action potentials (Catterall et al., 2007; Hille, 2001; Hodgekin & Huxley, 1952; Lipkind & Fozzard, 2008) and calcium channels play a role in excitability and activation of calcium dependent intracellular processes. Sodium channels are divided into two distinct groups, Na$_v$1 channels, containing 10 genes in humans (Na$_v$1.1 – Na$_v$1.9 and NaX), and Na$_v$2 channels, with only one gene in most invertebrates to more rarely, as many as four members (Na$_v$2.1 – Na$_v$2.4) in Anthozoa (e.g. sea anemone) cnidarians. In many cases the core α_1 subunits of the sodium channel are sufficient for functional expression but still possess the propensity to be modulated by auxiliary subunits (i.e. β subunits). The two sub-families are distinguished from another in several ways, including expression patterns, selectivity filters, ion conductance and drug-binding properties (Boda et al., 2015; Catterall, 2012; Gur Barzilai et al., 2012; Watanabe et al., 2002). Expression patterns of

the vertebrate α_1 subunits are tissue specific where $Na_v1.1$-$Na_v1.3$ and $Na_v1.6$ are the primary channels of the central nervous system, and $Na_v1.7$-$Na_v1.9$ are found in the peripheral nervous system. $Na_v1.4$ is abundant in skeletal muscle, and $Na_v1.5$ is located in the heart (Catterall, 2012). The appearance of a highly sodium selective channel is hypothesized as the trigger for the evolution of nervous systems. The first class of organisms identified to possess a nervous system are in the cnidarians, an example of which is jellyfish containing a centralized ring of interconnected neurons with sensory and motor neurons (Anderson & Spencer, 1989; Mackie, 2004; Spafford et al., 1996; Spencer, 1979; Spencer, 1995; Watanbe at al., 2009). Na_v2 sodium channels differ functionally from Na_v1 channels in lacking rapid N-type channel inactivation kinetics of Na_v1 channels, primarily influenced by a putative 'hinged-lid' formed by the intracellular III-IV linker connecting Domains III and IV. They also lack a lysine in the selectivity filter that engenders sodium-selectivity in Na_v1 channels, expressed Na_v2 channels to date are non-selective allowing Ca^{2+}, Ba^{2+}, $Na^{+,}$ K^+ to pass through the pore(Dong et al., 2015; Gur Barzilai et al., 2012b; Zhang et al. 2011). Functionally expressed Na_v2 channels have significantly slower kinetics of channel inactivation than classical Na_v1 channels that generate nerve action potentials, suggesting that a lack of a "hinged lid" responsible for rapid inactivation may be lacking in Na_v2 channels.

1.10 Selectivity filter

Based on crystal structure architecture analysis, the selectivity filter creates the tightest bottleneck of the channel pore of approximately 3.1 x 5.1Å, which leads into a highly electronegative conduction pathway that allows the movement of partially hydrated Na^+ ions (Hille, 1975; Krauss et al., 2011; Payandeh et al., 2011). A major difference between Na_v1 and Na_v2 channels lies within their selectivity filters, which then lead to dramatically different ion permeation kinetics. Na_v1 channels are only found expressed in vertebrates, and possess the selectivity filter of DEKA or DKEA which makes the members of this group highly selective for sodium ions; whereas Na_v2 channels have only been identified in invertebrates and possess selectivity filters of DEEA or DEES, and thus far been shown to be non-selective (Gur Barzilai et al., 2012a; Moran et al., 2015; Stephens et al., 2015). The difference between the selectivity filters lies in the presence (or absence) of a lysine residue in either second or third position of the

filter, where substitution of the positively charged lysine residue results in dramatic alterations in channel properties including sodium ion permeability (Favre et al., 1996; Kim et al., 1993; Lipkind & Fozzard, 2008; Yamagishi et al., 1997). Mutations of the lysine residue in the rat muscle $Na_v1.4$ sodium channel results in a shift of the current-voltage (IV) relationship of channel opening and peak current to a more depolarized/positive direction, and changes in ion permeability ratios for K^+/Na^+ and Ca^{2+}/Na^{2+} to favor passage of ions other than sodium ions as the dominant charge carrier. Mimicking the calcium channel selectivity filter (DEKA → EEEE) results in a calcium permeant channel (Heinemann, 1992). Furthermore, substitution of the basic charged lysine (DIII) with an equal basic charge arginine (R) does not maintain sodium selectivity over calcium ions and allows potassium to permeate (Favre et al., 1996; Heinemann et al., 1992). It may relate to a stabilizing effect of the charged lysine (DIII) and a carboxyl group from the adjacent glutamate (DII) residue to the selectivity filter glutamate residue with the hydrated sodium ion in the pore to create an energetically favourable binding site (Lipkind & Fozzard, 2008).

1.11 Rapid deactivation and inactivation

A definitive characteristic of sodium channels is their rapid opening and closing, in that once sodium channels open upon membrane depolarization, channel conductance is quickly minimized (<4 ms) by a [1] rapid N-type inactivation and [2] slower C-type inactivation (Kass, 2004; Vandenberg & Bezanilla, 1991). Activation, deactivation and inactivation are voltage-dependent gating mechanisms. Activation is the state of channel opening and deactivation is a state of channel closing. Inactivation is the state where a channel becomes refractory to re-open (Catterall, 2012).

The opening and closing is evident in single channel recordings, where channels flicker between different opening and closed states. The opening (activation) and closing (deactivation) states are related to occlusion or extension in diameter of the pore, while a slow pore collapse is considered to be associated with a slow C-type inactivation. A fast N-type inactivation of sodium channels is regulated outside the pore domain, by a 'capping off' of the internal portion of the conduction pathway by the intracellular linker connecting domains III and IV; the rapid inactivation mechanism has been likened to a "hinged-lid" (Catterall, 2012; West et al., 1992).

Once occluded the channel is refractory (inactivated) for a period of time. A three amino acid cluster (IFM: Ile-1488, Phe-1489, Met-1490) in the III-IV linker (West et al., 1992) interact with docking site residues located on linkers between S4-S5 of domains III and IV (Ala-1329[III], Asp-1662[IV]) (Goldin, 2003; West et al., 1992) of the rat $Na_v1.2$ channel. Injection of a protease in the cytoplasm (Armstrong et al., 1973) or mutating residues of the IFM motif results in abolishment of inactivation during depolarization (West et al., 1992) and altering the residues of S4-S5 linkers serving in the reception of the putative "hinged lid" leads to a slower channel inactivation (Smith et al., 1997). Nervous systems encode information in the rate of generation of action potentials. So the appearance of elements on Na_v1 sodium channels that allowed for fast action potential spikes was a key requirement for evolution of nervous systems (Vandenberg & Bezanilla, 1991).

1.12 Unconventional "sodium" channel, Na_v2

Many invertebrate species possess a single Na_v1 channel homolog, that is representative of the ten Na_v1 channels isolated in mammals including humans. Besides an Na_v1 channel, many invertebrates possessed a different sodium channel gene not present in vertebrates dubbed Na_v2. The first Na_v2 channel was isolated from American cockroach, *Blattella germanica* and functionally expressed by Ke Dong in *Xenopus* oocytes. *Blattella* Sodium Channel 1 (or BSC1) bore a likeness to close homolog DSC1 which was functionally characterized from the fruit fly, *Drosophila melanogaster*. Outside of insects, four different Na_v2 channel homologs dubbed $Na_v2.1$ to $Na_v2.4$, were cloned and characterized from sea anemone *Nematostella vectensis*. The sea anemone Na_v2 channels, as well as the insect ones characterized are permeable to both calcium ions and monovalent sodium and potassium ions, and possess the DEEA selectivity filter (Gur Barzilai et al., 2012; Zhou et al., 2004). Substitution of entire p-loop regions, the short 2-helix segment that connects transmembrane helices S5 and S6 and harbours selectivity filter residues, from another *N. vectensis* channel $NvNa_v2.5$ with the selectivity filter DKEA results in greater monovalent ion selectivity than substitution of selectivity filter residues alone (Gur Barzilai et al., 2012a). In contrast to the rapid nature of Na_v1 kinetics, the insect and sea anemone Na_v2 channels activate and inactivate at much slower rates requiring up to 40ms to reach peak conductance and remain open for a significantly longer period (>500 ms) (Dong et

al., 2015; Gur Barzilai et al., 2012; Song et al., 2004; Zhou et al., 2004). Furthermore, these channels possess a "MFL" motif in their III-IV linker place of the "IFM" motif (mammalian), and appear to be resistant to tetrodotoxin (TTX), a potent sodium channel blocker routinely used as a marker for sodium channels (Song et al., 2004; Zhang et al., 2011).

Thus far DSC1 mutants in *Drosophila* fruit flies reveal that Na_v2 channels are involved in odorant sensing (Kulkarni et al., 2002) and involved in the neural circuits of the 'giant fibre system' that mediates the fight-or-flight response in *Drosophila* (Zhang et al., 2013). The Na_v2 channel genes of sea anemone *Nematostella* have been shown to be spatiotemporally expressed during development. The form and function of Na_v2 channels is not well understood, outside what little we can infer from a few studies in insects by the Dong group (Dong et al., 2015; Zhang et al., 2013, 2011; Zhou et al., 2004) and a study in sea anemone by Moran group (Gur Barzilai et al., 2012b). In this thesis, we describe the characterization of an Na_v2 channel with a DEEA selectivity filter, from the simplest organism known to have an Na_v2 channel, the $SroNa_v2$ channel from the single cell choanoflagellate, *Salpingoeca rosetta*.

1.13 Voltage-gated calcium channels

Voltage-gated calcium channels are a different group of related cation channels and play central roles in neurotransmitter transmission, muscular contraction and pain sensation (Simms & Zamponi, 2014; Yu et al., 2005; Cox & Dunlap, 1992; Huang et al. 2010; Murakami et al., 2002; Weissgerber et al., 2006).). Voltage-gated calcium channels are segregated into two categories: High Voltage-Activated (HVA) and Low Voltage-Activated channels are activated by depolarisations to high voltages or lower voltages closer to resting membrane potentials, respectively (Bean, 1985) (Simms & Zamponi, 2014). HVA channels are comprised of 7 members in vertebrates, $Ca_v1.1$-$Ca_v1.4$ (exclusively L-type) and $Ca_v2.1$-$Ca_v2.3$(N-, P/Q-, R-type), while LVA channels are a 3-member family in vertebrates: $Ca_v3.1$-$Ca_v3.3$ (T-type). Alongside differing voltage-sensitivities and kinetic properties between calcium channels types, they are distinguished by blockade using different classes of drugs, peptides and natural toxins. L-type channels are susceptible to modulation by a class of drugs known as dihydropyridines (Catterall, 2011; Hofmann et al., 2014; Senatore et al., 2011). Ca_v2 group channels ($Ca_v2.1$ – $Ca_v2.3$), while all HVA channels can be disrupted by gabapentin which targets their auxiliary

alpha2 delta subunits (Cox & Dunlap, 1992; Hendrich et al., 2008; Marais et al., 2001). LVA (T-type) channels are highly sensitive to the piperidine-derived molecule TTA-P2 with near complete block of mammalian Ca_v3 channel currents in the low micromolar range (Dreyfus et al., 2010).

Besides a sensitive block to dihydropyridines, L-type or Ca_v1 calcium channels have several distinct characteristics including long lasting currents when barium ion is substituted as the charge carrier for calcium ion. Both Ca_v1 and Ca_v2 channels require the co-expression of auxiliary subunit proteins, in 1:1 stoichiometric ratios, to not only promote membrane expression but also to regulate kinetic properties (Buraei & Yang, 2010; Dzhura & Neely, 2003; Fang & Colecraft, 2011; Gerster et al., 1999; Hendrich et al., 2008; Lory et al., 1992; Opatowsky et al., 2004; Van Petegem et al., 2004). The kinetic properties of calcium channels are also highly influenced by highly conserved, calcium sensor protein calmodulin, which is bound to a primary IQ motif in the C-terminus of L-type channels to promotes rapid inactivation kinetics in the presence of increasing intracellular calcium ions (Brehm & Eckert, 1978; DeMaria et al., 2001; Lee et al., 2000; Lee et al., 2000; Peterson et al., 1999).

We have identified an L-type Ca_v1 channel homolog in the simplest known organism to have one (Fig. 1.3), that is, the choanoflagellate, *Salpingoeca rosetta*, and evaluate its functional properties expressed in HEK-293T cells. The studies of an extant relative of the earliest branching L-type calcium channel will provide insights into the evolution of calcium channels, first appearing animals before multicellularity.

1.14 Ancillary subunits

HVA calcium channels (L-type, N-/P-/Q-/R- type channels), and Na_v1 channels, require the co-expression of accessory protein subunits in order to be functionally expressed at the cellular membrane and exhibit proper gating kinetics (Buraei & Yang, 2010; Gerster et al., 1999; Opatowsky et al., 2004; Van Petegem et al., 2004). Accessory β-subunits in Na_v1 sodium channels are not related genes in mammals and invertebrates, and β-subunits of sodium channels appear to be completely lacking in the Na_v2 channels of invertebrates.

The calcium channel accessory β-subunits on the other hand, are homologous subunits in both invertebrates and mammals. Invertebrates have a singleton gene for beta subunits, with four genes (β_1-β_4) in mammals. They are intracellularly-bound proteins closely resembling the MAGUK (membrane-associated guanylate kinase) family of proteins, appearing to act as intracellular protein scaffold proteins at the cellular membrane (Van Petegem et al., 2004). Experimental evidence indicates that without co-expression of β subunits, core α-subunits show diffuse localization within the cell likely associated with the endoplasmic reticulum, but in the presence of β-subunits there is enhanced membrane expression of both proteins (Gerster et al., 1999; Weissgerber et al., 2006). β subunits are also known to prevent ubiquitination and proteosomal degradation of calcium channels, to also enhance expression of calcium channels (Altier et al., 2010).

β subunits comprise two highly conserved core regions, a Src3 homologous (SH3) domain and a guanylate kinase (GK) domain, connected by a weakly conserved HOOK domain and flanked by variable N- and C- termini (Buraei & Yang, 2010). The association of β subunit with the core α subunit of the ion channel is mediated through the interaction of the α subunits 'α-interaction domain' (AID), a highly conserved 16 residue region within the I-II linker of HVCCs, and the β subunit 'β-interaction domain' (BID), also known as the AID-binding pocket (ABP) (Buraei & Yang, 2010; Van Petegem et al., 2004). The exact mechanism of how this interaction results in the up-regulation of functional α_1-subunits is not completely understood. One theory has hypothesized the I-II linker of the $Ca_v1.2$ channel contains a 'signal switch' mechanism that triggers ER retention or export (Fang & Colecraft, 2011). It is proposed that the I-II linker possesses an ER *export* signal which is masked by the ER *retention* signal of the other linkers, as well as the N- and C- termini of the channel. The β subunit interactions are proposed to cause enough of a conformational change to allow the ER *export* signal to dominate and cause trafficking of the channel to the cellular membrane (Fang & Colecraft, 2011). Additionally, β subunit association prevents proteosomal degradation, further enhancing the cellular density of calcium channels. Alongside their influences on expression of calcium channels, β subunits modulate channel gating properties including activation and inactivation kinetics, and voltage-sensitivities. All calcium channel β subunit appear to shift both the midpoint of channel activation and inactivation to a more hyperpolarized potentials, causing changes in calcium-dependent inactivation (CDI) and voltage-dependent inactivation (VDI), and increasing open

state probability of a channel and therefore resulting in potentially larger transients (Buraei & Yang, 2010; Dzhura & Neely, 2003; Murakami et al., 2002; Weissgerber et al., 2006). Different calcium channel β subunit isoforms also speed up or slow down the kinetics of inactivation of calcium channels, and this is the case for mammalian and invertebrate calcium channel beta subunits (Dawson et al., 2014).

Alongside the various β subunits high voltage activated calcium channels require the co-expression of a primarily extracellular $\alpha_2\delta$ subunit. The $\alpha_2\delta$ subunit is a highly glycosolated protein composed of an α_2 subunit and a δ subunit that are linked via disulphide bonds (Canti et al., 2003), and generated from the same mRNA transcript. The N-terminal region and α_2 portion of the protein appear to be extracellular, while the C-terminal region is more hydrophobic and likely glycosylphosphatidylinositol (GPI) anchored to the membrane through the delta subunit (Brickley et al., 1995; Canti et al., 2003; Dolphin et al., 1999; Dolphin, 2012; Wiser et al., 1996). The primary role of the α_2 and δ subunits are in promoting membrane expression of calcium channels and has a more minor effect on the biophysical properties of calcium channels (Canti et al., 2003; Hendrich et al., 2008; Marais et al., 2001; Wiser et al., 1996).

We have identified both an $\alpha_2\delta$ and β subunit *Salpingoeca rosetta*. There have been many studies that suggest that auxiliary alpha2-delta and beta subunits of calcium channels have functions outside of calcium channels. The omni-presence of the calcium channel $\alpha_2\delta$ and β subunit gene in *Salpingoeca rosetta* and other organisms that also possess a Ca_v1 and/or Ca_v2 calcium channel, is evidence of the co-evolution of calcium channels and their accessory subunits during the early evolution of calcium channels in eukaryotes.

1.15 Calmodulin regulation

Calmodulin (CaM) is a bi-lobed molecule containing two calcium-binding pairs of EF-hand motifs connected via a flexible linker. Calmodulin was identified to interact with calcium to increase inactivation kinetics of calcium channels first in the single cell protist, *Paramecium* (Brehm & Eckert, 1978; Kovalevskaya et al., 2013). CaM requires the presence of Ca^{2+} to become "activated" which causes a conformational change from a compact folded state (apo-CaM) to an open conformation allowing exposure of its interaction site with its target proteins

through recognition of a melittin amino acid pattern within the calmodulin binding site (Ben-Johny & Yue, 2014; Jarrett & Madhavan, 1991; Kovalevskaya et al., 2013). This configuration involves the placement of two clusters of basic amino acids residues adjacent to hydrophobic residues and operates via interaction with both N- and C-termini of target protein molecules (Ben-Johny & Yue, 2014; Jarrett & Madhavan, 1991). Voltage-gated calcium channels possess several CaM interaction elements as well as conservation of N-terminus and C-terminus effector elements. N-terminal modulation occurs via interaction with an N-terminal Spatial Ca^{2+} Transforming Element (NSCaTE) site, while C-terminal regulatory elements include two EF hands, an IQ (isoleucine-glutamine) motif (some channels possess an 'IM' – methionine – motif) and a Calmodulin Binding Domain (CBD) (Ben-Johny & Yue, 2014; DeMaria et al., 2001; Dick et al., 2008; Jarrett & Madhavan, 1991; Wong, et al., 2000; Peterson et al., 1999). The presence of N- and C-terminal calcium binding motifs such as an NSCaTE and carboxyl terminal EF hand motif, respectively, involved in bridging a tethered and 'resident' CaM molecule present the possibility of generating a rapid inactivation via calcium-calmodulin interaction characteristic of calcium channels (Dick et al., 2008; Peterson et al., 1999). NSCaTE interaction is not present in all native high voltage-activated calcium channels (i.e. $Ca_v2.2$) (Dick et al., 2008) however when present has the ability to interact with the CaM N-lobe and shift global CaM modulation to local modulation that most commonly result in attenuation of calcium-dependent inactivation (CDI) and reduced excitation sensitivity of the channel (Ben-Johny & Yue, 2014; Dick et al., 2008; Saimi & Kung, 1994). Our finding that the L-type calcium channel of one of the simplest eukaryotic organisms to have an L-type calcium channel, *Salpingoeca rosetta*, possesses a mostly conserved calmodulin interaction elements. A C-terminus which includes an IQ-like motif where calmodulin is expected to associate, and an N-terminus with a potential NSCaTE motif. The finding of potential regulation of L-type calcium channels in choanoflagellate *Salpingoeca rosetta*, suggests that calcium regulation of L-type calcium channels by calmodulin evolved with the appearance of the first calcium channels in eukaryotic ancestors.

1.16 Proposed functions of sodium and calcium channels in single celled organisms

Sodium-selective Na_v1 channels only appear in multicellular organisms, which also have a nervous system. The function Na_v1 channels is involved in generating fast action potential spikes for neuron-to-neuron communication, involving sodium ion influx and not calcium ion influx, which is toxic to cells at high intracellular levels. Calcium channels have a primary role in linking electrical signals to calcium-dependent intra-cellular pathways that we normally associate with multicellular organisms, like the contraction of heart and skeletal muscle, synaptic transmission in nervous systems and secretion of hormones. The finding of the presence of sodium (Na_v2) and calcium (Ca_v1) channels in single celled organisms raises the question of what Na_v2 channels and Ca_v1 channels are doing in a single cell organism.

One theory proposes that the control of ionic flux across cellular membranes evolved as an "emergency response" to cellular damage. It may also be a trigger for mediating flagellar beating and amoeboid movement in a single cell organism (Brunet & Arendt, 2016). It is also known that bacteria can communicate amongst each other in a manner that is analogous to nerve-nerve communication via action potential spikes. Bacteria communicate with other bacteria when nutrient source, glutamate becomes low, by changing the membrane potential in the extracellular biofilm by potassium channel flux-inducing waves (Beagle & Lockless, 2015; Prindle et al., 2015)

Salpingoeca rosetta can be considered a reduced model for understanding the control of cellular repair, movement and inter-organismal communication by means of calcium and sodium channels. *Salpingoeca rosetta* exists in single cell fast and slow "swimmer", a sedentary "thecate" stage, and colonial "rosetta" stages triggered by co-factors released by Bacteriodes bacteria, which is commensal with *Salpingoeca rosetta*. The presence of only a single gene representative of these channel types more ancestral to the channels currently known (Fig. 1.4) provides an opportunity to gain insights into what was the impetus to create these sodium and calcium channel classes in the first eukaryotes. Through PCR amplification, molecular cloning, and electrophysiological analyses of expressed channel plasmids in HEK293T cells we have been able to characterise the Ca_v1 L-type calcium channel and Na_v2 sodium channel of *Salpingoeca rosetta*. The Ca_v1 channel is a highly calcium-selective and rapid calcium channel that lacks prominent calcium-dependent inactivation characteristics. The Na_v2 channel is a

"slow" sodium channel that is non-selective for extracellular cations allowing the passage of calcium [Ca^{2+}], sodium [Na^{+}], and barium [Ba^{2+}]. Altering the native Na_v2 selectivity filter to mimic vertebrate homologs (DEEA → DEKA) results in a channel highly selective for monovalent ions.

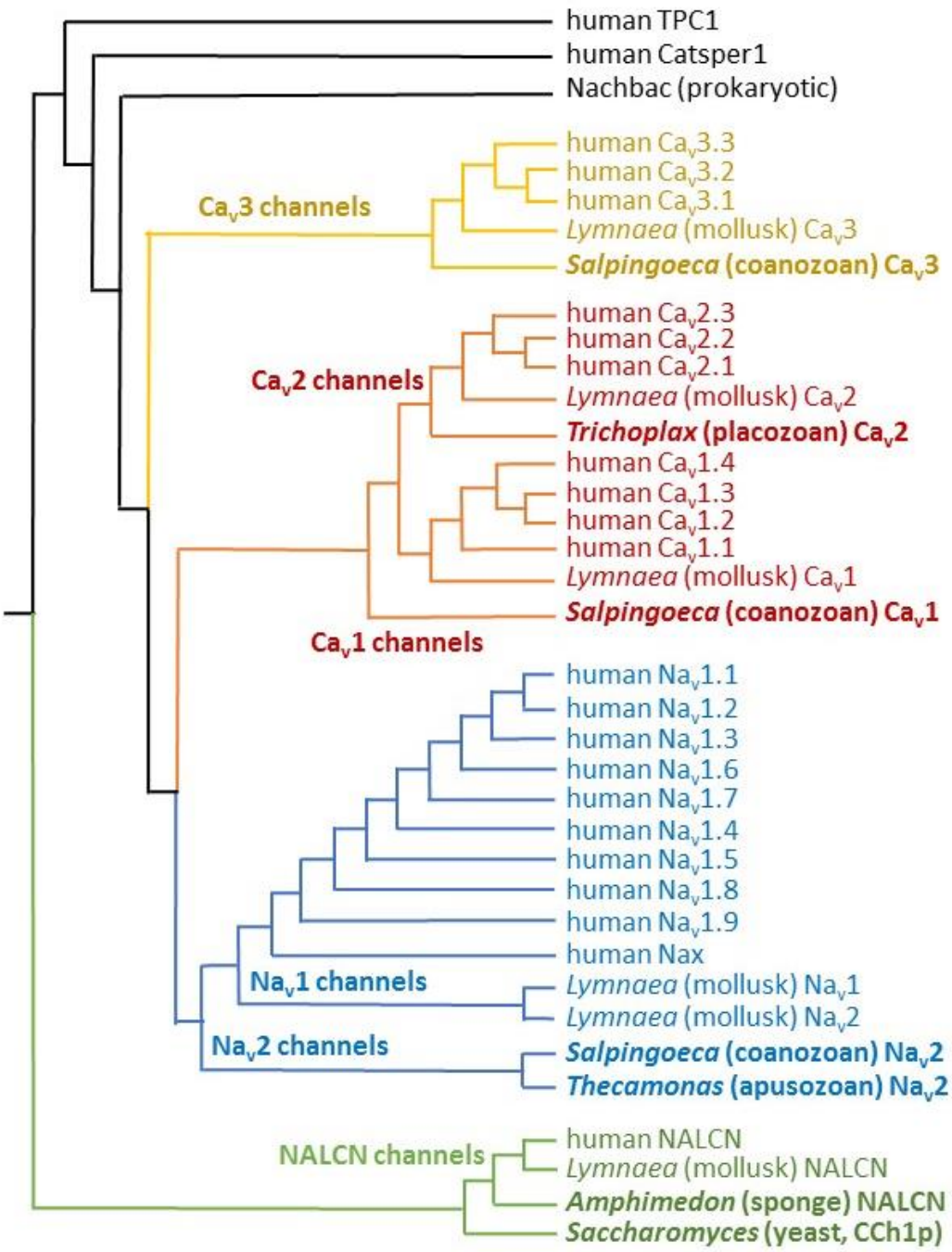

Figure 1.4 Phylogenetic alignment of *Salpingoeca rosetta* cation channels

A phylogenetic tree illustrating the position of the voltage-gated ion channels (Na_v2, Ca_v1, and Ca_v3) of Salpingoeca rosetta in relation to other vertebrate and invertebrate homologs. TPC: two-pore channel, Catsper: sperm-specific calcium channel, Nachbac: bacterial sodium channel.

Chapter 2

Materials & Methods

2.1 General cloning methods

2.1.1 mRNA treatment

The calcium and sodium channels introduced in this thesis were isolated via polymerase chain reaction (PCR) using complementary DNA (cDNA) prepared from messenger RNA (mRNA) kindly provided by the Nicole King Laboratory (University of California, Berkeley campus). Pre-treatment of mRNA was carried out to remove any residual contaminating genomic DNA sequences. 8µL mRNA sample, 1µL DNAse buffer and 1µL DNAse I (Thermo-Fisher, #AM2222) were added to a 0.2mL microcentrifuge tube and incubate at 37˚C for 30 minutes. 1µL 50mM EDTA was then added and temperature was increased to 70˚C for 15 minutes to inactivate the DNase enzyme. The reaction was then stored in -80˚C until ready for cDNA preparation.

2.1.2 cDNA preparation

cDNA was produced using the SuperScript III Reverse Transcriptase (ThermoFisher, #18080044). 5.5µL mRNA, 5.5µL milli-Q water, 1µL of 1µM random hexamer primer (ThermoFisher, #N8080127) and 1µL of 10mM dNTP (ThermoFisher, #18427013) were combined in a 0.2mL microcentrifuge tube. Mixture was then heated to 65˚C for 6 minutes to relax secondary mRNA structures, followed by incubation at 25˚C for 4 minutes. At this point, 1µL of 0.1M DTT, 4µL of 5x First Strand buffer (ThermoFisher, #18080044) and 1µL of RiboLock RNase Inhibitor (ThermoFisher, #EO0381) were added and incubated at 25˚C for a further 10 minutes. Finally, 1µL SuperScript III RT was added and total reaction incubated at 42˚C for 60 minutes, followed by heat inactivation of the reverse transcriptase at 65˚C for 15 minutes. To concentrate cDNA product and remove extraneous salts and proteins, 2µL of molecular grade glycogen (ThermoFisher, #R0561), 30µL of 10M ammonium acetate and

100µL of 100% molecular grade ethanol were added to tube and allowed to incubate overnight at -20˚C. The next day the pelleted product was centrifuged at 4˚C for 30 minutes, followed by 2 wash spins with cold 70% ethanol. After brief air-drying, 20µL of autoclaved milli-Q water was added to resuspend the pellet and final product was stored at -20˚C.

2.1.3 Nested polymerase chain reaction

PCR primers were designed by Dr. J. David Spafford and supplied by Eurofins Genomics (Table 4-6). Primers were designed based on available *Salpingoeca rosetta* channel sequences from genome sequences (PRJNA37927, PRJNA193541, PRJNA222515) and transcriptome (PRJNA62005) sequences deposited from the Broad Institute (MIT, Massachusetts) and Dr. Nicole King (University of California, Berkeley). Primers were resuspended in milli-Q water as per provided instructions to create a stock solution, a 1/10 dilution was made in 1.5mL microcentrifuge tubes as working stocks of each primer. Prior to addition into master PCR mixture each working primer stock was quantified using the Nanodrop 1000 spectrophotometer to ensure that quantity of each added primer were equal and ranged from 120 – 140ng per 50µL reaction. In some instances, primers were designed to span intron splice sites (intron-spanning primers) when it was noticed that PCR products were subject to genomic contamination. Primers were designed to isolate the coding sequence of each channel in several smaller fragments. SroNav2 and SroCav1 coding sequences were divided into 4 and 5 fragments, respectively.

All components of PCR reaction were combined in a 0.2mL microcentrifuge tube on ice. The components were added in the following order; milli-Q water, 5µL 10x PCR buffer (Aligent, #600250), 1µL of 10mM dNTP mix (ThermoFisher, #18427013), 1µL 50mM $MgSO_4$, 2.5µL DMSO, 2µL cDNA template, 120-140ng of each forward-reverse primer pair, 1µL PfuTurbo AD DNA Polymerase (Aligent, #600250). A nested PCR protocol was conducted using a set of outer flanking primers to generate an initial product. A second PCR reaction using the product of the first PCR reaction (diluted 1000 fold) as template amplfied with an nested PCR primer set to the outer flanking set. Cycling parameters for outer primer pairs were as follows: initial denaturation at 95˚C for 2.5 minutes, temperature increase to 97˚C for 30 seconds, followed by 10 cycles of denaturation at 95˚C, primer annealing (T_m – 7) for 15 seconds

and strand extension at 68˚C at a rate of 2 minutes per kilobase. After these initial 10 cycles, per cycle denaturation was increased to 20 seconds, primer annealing duration was increased to 20 seconds, followed by extension duration increase to 2 minutes and 10 seconds per kilobase; these cycling parameters were carried out for an additional 20 cycles. Final extensions were performed at 68˚C for 5 – 10 minutes. Inner nested PCR was performed using standard PCR protocols; 2.5-minute denaturation at 95˚C, temperature increase to 97˚C for 30 seconds, followed by 30-35 cycles of initial denaturation at 95˚C for 30 seconds, primer annealing at T_m-7 for 30 seconds, strand extension at 68˚C for 1 minute per kilobase (Fig. 1). Final PCR reactions were then screened by taking a 5µL sample on a 1% agarose gel. Successfully amplified products were then run on a subsequent 1% agarose gel and extracted.

2.1.4 DNA agarose gel extraction

All agarose gels were made by combining 75mL of TAE buffer (40mM Tris-acetate, 1mM Ethylenediaminetetraacetic acid, 0.11% glacial acetic acid) with 0.75g Agarose A (BioBasic, D0012). A microwave was used to heat and dissolve the agarose into solution, and then the flask of melted agarose was allowed to cool on a countertop prior to being poured into a gel cast. Gel cast was taped of using green painters tape to block open ends and a gel comb was inserted into appropriate slot of cast to create gel lanes. Liquid TAE-agarose mixture was poured into taped cast once mixture was cool to touch based on contact to inner forearm. Gel was allowed to solidify for 20-30 minutes at room temperature, after which tape and gel comb were carefully removed. Solid gel and surrounding cast were then lowered into an electrophoresis chamber containing TAE as a running buffer and with lanes positioned at the negative terminal. TAE buffer was added until a thin layer of liquid lay over top of the gel. A 6x loading dye was then diluted in each sample and samples were loaded into wells of prepared gel. A current of 100mV was applied across the gel and allowed to run for ~30-40 minutes, until migration of loading dye was deemed sufficient. Completed gels were then visualized using AlphaImager software (AlphaInnotech) on a PC computer connected to an AlphaImager HP Gel Documentation system into which the gel was placed and documented under UV light illumination.

When not using commercially available pre-cut TOPO or pGEMT-Easy vectors, PCR products were cloned in vectors by ligation of restriction enzyme excised fragments. Restriction endonuclease digested PCR and cloning plasmids were run and isolated on a 1% agarose gel, excised and extracted using the QIAquick Gel Extraction Kit (Qiagen, #28706) with some modifications. Binding buffer was added to the excised gel slice at a determined volume of 1µL per 1µg of gel in a 1.5mL microcentrifuge tube. Tube and contents were then heated to 55˚C with shaking at 750rpm to the melt agarose. Once melted, the mixture was added to the provided columns in 700µL aliquots (volumes greater than 700µL were centrifuged in same column in series). Columns were centrifuged at 5,000g for 2 minutes, the centrifuged mixture in lower collection tube was added to the upper column and spun again; this was repeated for a total of 4 spins. After the final spin, 500µL of binding buffer was added to column and spun at 10,000g for 1 minute and flow-through contents were discarded. 700µL of wash solution containing 100% molecular grade ethanol (4:1, EtOH: buffer) was added and spun at 10,000g for 1 minute. Following wash, upper column was transferred to sterile 1.5mL microcentrifuge tube and spun at 16,100g for 2 minutes to remove residual ethanol. To elute DNA product, 3 rounds of 67µL of milli-Q water heated to 85˚C was added to the column, incubated for 1 minute at room temperature and spun at 16,100g for 1.5 minutes. DNA was then concentrated by adding 2.5µL molecular grade glycogen (ThermoFisher, #R0561), 50µL of 10M ammonium acetate, and 700µL of molecular grade 100% ethanol. Tubes were incubated at -20˚C for a minimum of 2 hours, at which point they were centrifuged for 30 minutes at 4˚C to pellet product, washed with 200µL ice cold 70% ethanol, briefly air-dried and resuspended in 20µL autoclaved milli-Q water.

2.1.5 TOPO cloning and sequencing of channel fragments

For large PCR fragments freshly isolated from *Salpingoeca* cDNA template, we cloned their blunt-end PCR products into Zero Blunt TOPO PCR Cloning kit (ThermoFisher, #450245). All components were combined in a 0.2mL microcentrifuge tube; 4.5µL of purified PCR product, 1µL of provided salt buffer solution, 0.5µL TOPO vector. Reaction was allowed to incubate at room temperature for a minimum 25 minutes, at which point it was diluted 4-fold with sterile milli-Q water to be transformed into DH5-alpha or STBL2 *Escherichia coli* strain via

electroporation. SroNav2 and SroCav1 channel fragments were sequenced directly off the TOPO vector using commercially available M13 forward (-20: 5'GTAAAACGACGGCCAGT'3) and M13 reverse (5'CAGGAAACAGCTATGAC'3) primers (Table 4). Sequencing was outsourced to The Centre for Applied Genomics (TCAG) at The Hospital for Sick Children (Toronto, Ontario). Consensus sequences were created by identifying three independently sequenced fragments per nucleotide position. Analysis and identifying consensus sequences were carried out by Dr. J. David Spafford.

2.1.6 A-tailing and pGEM-T Easy cloning of channel fragments

The N-terminal sequence of $SroCa_v1$ was cloned into pGEM-T Easy (Promega, A1360) vector for sequencing. Following PCR amplification with Pfu Turbo AD DNA polymerase (Aligent, #600250), the PCR product was isolated via agarose gel electrophoresis and recovered in solution using gel extraction technique. Due to the 3' to 5' exonuclease activity of Pfu Turbo AD which produces blunt-ended products, the isolated channel fragment was modified by the addition of deoxyadenine nucleotide from dATP on each blunt end using Taq polymerase (ThermoFisher, #18038018). To add an A tail to the blunt ended PCR product, the following components were combined in a 0.2mL microcentrifuge tube: 7µL of purified PCR product, 1µL of 100mM dATP (ThermoFisher, R1041), 1µL 10X Taq buffer without $MgCl_2$, 1µL of 25mM $MgCl_2$ ThermoFisher, R0971), total reaction volume of 10µL. Reaction was incubated at 72˚C for 30 minutes. Following incubation, product was ready to use in ligation with pGEM-T Easy vector. Ligation was composed by adding in a 0.2mL microcentrifuge tube: 0.5µL of pGEM-T Easy vector (@50ng/µL), 5µL of A-tailed PCR product, 2.5µL of 10X ligation buffer, 1µL of T4 DNA ligase (BioBasic, B1125). Ligation was carried out overnight at 16^{o} C.

2.1.7 Preparing electro-competent E. coli cells

All plasmid constructs were transformed by electroporation with prepared electrocompetent cells and grown as bacterial cultures that were purified in a standard plasmid mini-prep protocol. To make electrocompetent cells, frozen aliquots (ThermoFisher; Stbl4 - #11635018, TOP10 - C404050) were streaked onto Luria Bertani (LB) agar plates without

antibiotic and grown overnight at 37˚C. Single, well-isolated colonies were then used to inoculate 10mL of Super Broth (SB) without antibiotic, which was then incubated overnight at 37˚C in a shaking incubator rotating at 300rpm. The following day the 10mL Super Broth culture was divided and added to two 250mL fresh Super Broth aliquots without antibiotic and incubated at 37˚C in a shaking incubator until bacterial growth density reached an OD_{600} of 0.03 – 0.06 as measured by a Nanodrop spectrophotometer. Cells were then chilled on ice for 20 minutes then transferred to chilled centrifuge bottles and spun for 15 minutes at 4000g (4˚C) to pellet cells (Beckman Coulter Alegra 25R). Supernatant was removed and cells were then washed twice with 250mL of a chilled, filtered 10% glycerol solution by resuspending the cells and spinning the bottles for 15 minutes at 4000g (4˚C) - supernatant was removed after each wash. After the second wash, cells were resuspended in 20mL of chilled 10% glycerol and transferred to a 50mL falcon tube, then spun for 15 minutes at 4000g (4˚C). Supernatant was then discarded and cells were then resuspended in 2-4mL of chilled 10% glycerol until cell density was measured to be 0.375 at an OD_{600}, as measured by Nanodrop spectrophotometer. Once desired density was reached, cell aliquots of 40-80µL were made in 0.2mL microcentrifuge tubes that were then dropped into liquid nitrogen to flash freeze. Cells were then kept at -80˚C until needed for plasmid transformation by electroporation.

2.1.8 Bacterial transformation

Bacterial transformations of plasmid constructs were carried out via the electroporation method of transformation, with the parameters in electroporation voltage and time optimized for *Escherichia coli* (*E. coli*). Frozen aliquots of competent *E. coli* stored in -80˚C were allowed to thaw on ice for 5 minutes, after which 1-6µL of plasmid containing solution were added to cells and allowed to incubate further on ice for 30 minutes. Fresh 1mL of Super broth (SB) media was warmed to 37˚C in a 1.5mL microcentrifuge tube. After 30 minutes, cell-plasmid mixture was transferred to an ice cold 0.2cm electroporation cuvette (ThermoFisher, P45050) and transformed using an Eppendorf 2510 electroporator (Sigma, #618969) (TOP10 strain of *E. coli* shocked with voltage of 1120V for TOP10 cells, (while all other strains were transformed with 1200V). Immediately following electric shock, the cells were placed on ice, then 1mL of warm media was added to cells and transferred to a 1.5mL microcentrifuge tube to allow for recovery

on a heat block at 37˚C with shaking at 500rpm for 1 hour. After one hour, cells were spun down at 4000g for 3 minutes, 850µL of supernatant was removed and discarded, cells resuspended in remaining media and plated onto a petri dish of Luria-Bertani (LB) agar with the proper antibiotic. Plates were parafilmed, inverted and incubated overnight at 37˚C. Single, isolated colonies were chosen to grow up and screened for positive recombinants containing the expected plasmid.

2.1.9 Mini-prep plasmid isolation

Single, well-isolated colonies from overnight LB agar plates were grown and amplified overnight in 10mL SB media with proper antibiotic. Cells were then spun in 2mL aliquots in 2mL microcentrifuge tubes at 4500g for 1.5 minutes. Pellet was resuspended in 270µL resuspension solution (25mM Tris, 10mM EDTA, 50mM glucose), followed by addition of 540µL of lysis buffer (0.2M NaOH, 1% SDS) and 405µL neutralization solution (3M K^+, 5M acetate). Tubes was inverted, rotated and then vortexed to distribute solutions and break down cellular membranes. Tubes were then spun at 5000g for 3 minutes to pellet cell debris and large chromosomal DNA, supernatant was transferred to fresh 2mL microcentrifuge tube and 800µL of 2-propanol was added and incubated at -20˚C for minimum 1 hour to precipitate plasmid. Tubes were then spun at 16,100g for 30 minutes, the supernatant was discarded and tubes briefly air-dried before resuspending in 200µL milli-Q water. 400µL of 5M LiCl was added to tubes, incubated on ice for minimum 20 minutes then spun at 16,100g for 10 minutes, the supernatant was transferred to fresh 1.5mL tube and 500µL of 2-propanol was added to tubes, and incubated at -20˚C for minimum 1 hour to precipitate DNA. Tubes were then spun for 30 minutes at 16,100g (4˚C). The supernatant was discarded, and the resulting pellet was resuspended in 400µL milli-Q water. To remove residual RNA, 2µL heat-treated RNAse A was added to each tube and incubated at 37˚C for 45-60 minutes. Following sufficient incubation, equal amount (400µL) of 50:50 phenol:chloroform was added to each tube, shaken and vortexed, then spun for 5 minutes at 16,100g to separate phases. The upper aqueous phase containing the plasmid DNA was then transferred to fresh 1.5mL microcentrifuge tube and the lower remaining organic phase was discarded along with the tube. The removed upper phase was then washed with the addition of an equal amount pure chloroform (400µL), tube was then shaken and vortexed, followed by

centrifugation at 16,100g for 5 minutes to separate phases. The upper aqueous layer was transferred to fresh 1.5mL microcentrifuge tube, to which 90µL 10M ammonium acetate and 1mL 100% molecular grade ethanol was added and allowed to incubate at -20˚C overnight. Tubes were spun for 30 minutes at 16,100g (4˚C) to pellet DNA, supernatant was discarded. The pellet was then washed with 450µL ice cold 70% ethanol, supernatant was discarded and pellet allowed to air-dry for 5 minutes before being suspended in 30-50µL sterile Milli-Q sterile water.

2.1.10 Restriction Digests

Restriction enzymes were obtained from New England Biolabs and were used to clone ion channel fragments into the mammalian expression vector pIRES2-eGFP (pIRES2-dsRED for SroCav1 β-subunit). All reactions contained 10% v/v of 10x NEB reaction buffer, ≤5% v/v total enzyme volume, variable plasmid amount, and the remaining volume of reaction was filled with Milli-Q water.

To determine successful acquisition of full length SroNa$_v$2 channel construct, plasmids were digested twice, in parallel, with (1) 2µL NEB Cutsmart buffer (B7204S), 2µL mini-prep isolated plasmid, 1µL SacII enzyme (R0157S), with expected banding pattern of 2100 bp and 9500 bp; (2) 2µL NEB buffer 3.1 (B7203S), 2µL mini-prep isolated plasmid, 1µL BglII (R0144S) and 1µL HindIII (R0104S) enzymes, with an expected banding pattern of 1150 bp,

2.1.11 Ligation

Cloning of channel fragments into pIRES2-eGFP with adapters and SroCa$_v$1 N-terminal sequence into pGEM-T Easy vector was done using T4 DNA ligase (BioBasic, B1125). Concentrations of prepared inserts and vector backbones were determined with a Nanodrop spectrophotometer. A ratio of 3:1 (insert:vector) was used in most cases (5:1 and 6:1 were also used) where vector concentration was set at 50ng per reaction and insert concentration was determined based on size ratio using the following equation:

$$3 \times \left(\frac{insert\ size\ (bp)}{vector\ size\ (bp)}\right) \times 50ng\ = ng\ of\ insert$$

From this, x-µL of insert and y-µL of vector were determined and combined with 2.5µL of buffer, and milli-Q water to bring total reaction volume to 25µL in a 0.2mL microcentrifuge tube. Reaction was then incubated at 16˚C for 6.5 hours followed by a decrease in temperature at a rate of 1˚C per 30 minutes to a final temperature of 4˚C where it was held until bacterial transformation.

2.2 Mammalian cell culture

Human embryonic kidney – 293T (HEK-293T) cells were cultured and maintained in Dulbecco's Modified Eagle Medium (DMEM) (Sigma, D5796), supplemented with 10% v/v fetal bovine serum solution (Sigma, F1051), 1% v/v sodium pyruvate (Sigma, S8636), and 250mg/mL of penicillin/streptomycin (Sigma, P4458). Media was pre-warmed to 37˚C in a water bath prior to each use. All HEK-293T cell work and manipulation was done in a laminar flow hood. Fetal bovine serum (FBS) was heat-inactivated in a 56˚C water bath for 30 minutes with manual shaking at 5 minute intervals, prior to being divided into aliquots and frozen until ready to use.

2.2.1 Thawing HEK cells

HEK-293T cells were received from ATCC and aliquots were stored in liquid nitrogen for long-term storage. A new cell aliquot was thawed for use after every 20-25 passages. Prior to thawing a cell aliquot, prepared DMEM was warmed to 37˚C in water bath, at which point 4mL of media was added to new, sterile 25cm^2 tissue culture flask (Cell Star, #690-071). A single tube aliquot was removed from liquid nitrogen storage and submerged in 37˚C water bath to quickly thaw. Once thawed, 1mL of warm media was added to tube and mixed with the pipette before being transferred to prepared tissue culture flask. Flask was then placed into a water-jacked 37˚C incubator with circulating 5% CO_2 for 3-4 hours to allow cells to adhere. After this incubation period, media was removed and replaced with 6mL of warm fresh media and returned to incubator until cells reached confluency.

2.2.2 Cell culture maintenance

HEK-293T cell cultures were maintained by allowing culture to grow to ~70-100% confluency in 25cm^2 tissue culture flask at 37˚C. Cells were passaged once confluent by being split to various ratios (ie. 1:8, 1:12, 1:16, 1:20). To passage (split), media was aspirated by inverting flask and removing media, 1mL of 0.25% of trypsin-EDTA solution (Sigma, T4049) was added to opposite side of cell monolayer. Flask was then rotated to neutral position and rocked back and forth to distribute trypsin across the monolayer. The Flask was once again inverted and trypsin solution was removed. Another 500µL of trypsin solution was added to flask and allowed to incubate in neutral position for 3-5 minutes at 37˚C. Following sufficient incubation, 7mL of warm media was added to flask to inactivate trypsin, and cells were resuspended by pipette mixing up and down. Cells were then divided into desired ratios labelled with subsequent passage number. Cells were split to a ratio of 1:4 (cells:media) and incubated for minimum 4 hours at 37˚C prior to transfection with a plasmid construct.

2.2.3 Transient transfection of ion channel plasmid constructs

To allow for transfection, HEK-293T cells were split to a ratio of 1:4 earlier the same day. A standard calcium phosphate precipitate transfection protocol was utilized (Senatore et al., 2011). Plasmid concentrations were standardized to 1µg/mL of tissue culture media, for a total of 6µg in a 600µL transfection mixture. Standard protocol requires two sterile 1.5mL microcentrifuge tubes. Microcentrifuge tube #1 contains 6µg of desired plasmid, 30µL of 2.5M $CaCl_2$ (filtered through a 0.2µm cellulose filter (ThermoFisher, #726-2520)), and remaining volume was made up with sterile Milli-Q water. This mixture was then added drop-wise into microcentrifuge tube #2 containing 300µL of a HEPES-buffered saline solution (containing 280mM NaCl, 50mM HEPES, and 1.5mM Na_2PO_4-$7H_2O$; filtered through a 0.2µm cellulose filter (ThermoFisher, #726-2520)), was then mixed and allowed to incubate for 20-30 minutes at room temperature. After this short incubation, transfection solution was then added to HEK cell flask and placed in 37˚C incubator for 16-20 hours.

The following day, the transfection was washed with warmed media in a fashion similar to passaging the cell line. Culture flask was inverted and media removed via aspiration, warm

media was then added to the flask opposite the layer of HEK cells, flask was rotated back to a neutral position and gently rocked back and forth several times before once again removing media. This process was repeated for a total of 3 "washes", after which a final 6mL of warm media was added to the flask and replaced in the 37˚C incubator. Cells were left in 37˚C incubator for 1-3 hours to allow adherence to flask surface, after which the flask was transferred to an identical incubator with an ambient temperature of 28˚C until ready to record.

2.2.4 Poly-L-Lysine coated coverslips

In order to record HEK cells transfected with the $SroCa_v1$ channel, the cultured HEK cells needed to be plated several days in advance on poly-L-lysine coated coverslips. To coat coverslips, a 0.01% poly-lysine solution is prepared from a 0.1% stock solution (Sigma, P8920) and filter sterilized. Circular glass coverslips (Fisher Scientific, #12-545-80) were placed in a 60mm petri dish (Corning Life Sciences, #430166), washed with 100% molecular grade ethanol and allowed to air-dry at room temperature. 5mL of working poly-l-lysine solution was then added to coverslips in the dish and allowed to incubate at room temperature for 30-45 minutes. Following incubation, poly-L-lysine solution was removed via aspiration, and coverslips were washed by adding 5mL of sterile milli-Q water, removing again via aspiration. Coverslips in the petri dish were then placed into a 55˚C oven to dry for approximately 2 hours at which point they could be used to plate transfected HEK cells or placed at 4˚C until needed.

2.2.5 Plating of transfected HEK cells

In order to perform whole-cell patch clamp electrophysiology transfected HEK cells need to be plated onto glass coverslips. Cell plating follows a modified passage protocol and cells were plated on uncoated, or poly-L-lysine coated for $SroCa_v1$, coverslips. Cell media was removed and cells were trypsinized in the same manner previously outlined (see 2.2.2) for passaging. Following 3-5 minute incubation at 37˚C, 7-10mL of fresh media was added to the flask containing cells. Cells were mixed by pipette mixing up and down, and 5mL of these cells were added to a 60mm petri dish (Corning Life Sciences, #430166) containing coverslips. Petri dish was then incubated at 37˚C for 3-5 hours to allow cells to adhere to coverslips, after which

point the cells were ready to be recorded. For SroCa$_v$1 cells were plated 3-days post-transfection, and after 4 hours at 37˚C to allow adherence to coverslips were moved to 28˚C for several days until ready to record.

2.3 Electrophysiology recordings

Coverslips of attached cells were transferred from DMEM containing petri dish to a 35mm petri dish (Sarstedt, #83.3900) containing extracellular ionic recording solution. Ground electrodes were composed of 1.25% agarose in 3M cesium chloride (CsCl) filled with 3M CsCl. Patch pipettes were produced by pulling thin-walled borosilicate glass capillaries using a Sutter-1000 pipette puller with a trough-shaped platinum filament. Pipette tips were then heat polished using a microforge (Narishige, MF-830).

All whole cell patch clamp recordings were carried out at room temperature. Recording were carried out using an Axopatch 200B amplifier that was sampled through a Digidata 1440 A/D converter outputted to a PC computer, controlled through pClamp 10 software (Molecular Devices). Pipette resistance was kept to between 2-6 MΩ, pipettes with higher or lower resistance were discarded. During patch access, cells with an access resistance of <12 MΩ, and a leak of less than 10% of peak current size were kept and used for analysis. Leak subtraction was done offline in post analyses, and background noise was smoothed with a 1000Hz Gaussian filter using Clampfit software (Molecular Devices). Analysis was carried out using Clampfit software, Data was tabulated within Microsoft Excel, and illustrated through OriginLab 9.1.

2.3.1 Electrophysiology solutions

Solutions for recording SroNav2 currents and SroCav1 currents were adopted from solutions previously used by former graduate students in the laboratory, Wendy Guan (2014) and Adriano Senatore (2011), respectively.

SroNav2 external kinetic bath solution was composed of 2mM calcium chloride ($CaCl_2$), 160mM tetraethylammonium chloride (TEA-Cl), 10mM 4-(2-hydroxyethyl)-1-piperazineethanesulfonic acid (HEPES); solution pH was adjusted to 7.4 using TEA-OH.

Internal pipette solution contained 110mM cesium chloride (CsCl), 10mM ethylene glycol tetraacetic acid (EGTA), and 10mM HEPES. Solution pH was adjusted to 7.2 and filtered through 0.2µm cellulose filter.

SroCav1 external kinetic bath solution was composed of 20mM $CaCl_2$, 40mM TEA-Cl, 1mM magnesium chloride ($MgCl_2$), 10mM glucose, 10mM HEPES, 65mM CsCl. Solution pH was adjusted to 7.2.

Internal pipette solution was consisted of 108mM cesium methanosulfonate (CsMSF), 4mM $MgCl_2$, 10mM EGTA, 9mM HEPES, 3mM MgATP, 0.6mM Li-GTP. Solution pH was adjusted to 7.2 and filtered through 0.2µm cellulose syringe filter.

Table 2.1. $SroNa_v2$, $SroCa_v1$ kinetic solutions

	$SroNa_v2$		$SroCa_v1$	
(mM)	Internal	External	Internal	External
$[Ca^{2+}]$	-	2	-	20
TEA-Cl	-	160	-	40
HEPES	10	10	9	10
EGTA	10	-	10	-
CsCl	110	-	-	65
$MgCl_2$	-	-	4	1
Glucose	-	-	-	10
Li-GTP	-	-	0.6	-
Mg-ATP	-	-	3	-
Cs-MSF	-	-	108	-

$SroNa_v2$ solutions adopted from Wendy Guan (2014). $SroCa_v1$ solution adopted from Adriano Senatore (Senatore et al., 2011).

pH to 7.2-7.3 (External: TEA-OH; Internal CsOH)

Table 2.2. Na-NMDG experiment solutions

External ionic composition (mM)

$CaCl_2$	NaCl	NMDG	HEPES	TEA-Cl
2	135	-	10	25
2	-	135	10	25

Internal ionic composition (mM)

CsCl	Li-GTP	Mg-ATP	HEPES	EGTA
110	0.6	3	10	10

Adopted from Wendy Guan (2014).

pH to 7.2-7.3 (External: TEA-OH; Internal CsOH)

Table 2.3. Bi-ionic condition solutions

External ionic composition (mM)

$CaCl_2$	HEPES	TEA-Cl
4	155	10

Internal ionic composition (mM)

	CsCl	NaCl	LiCl	KCl	EGTA	TEA-Cl	HEPES
1	100	-	-	-	10	10	10
2	-	100	-	-	10	10	10
3	-	-	100	-	10	10	10
4	-	-	-	100	10	10	10

Adopted from Wendy Guan (2014).

pH to 7.2-7.3 (External: TEA-OH; Internal XOH, $X=Cs^+$, Na^+, Li^+, K^+)

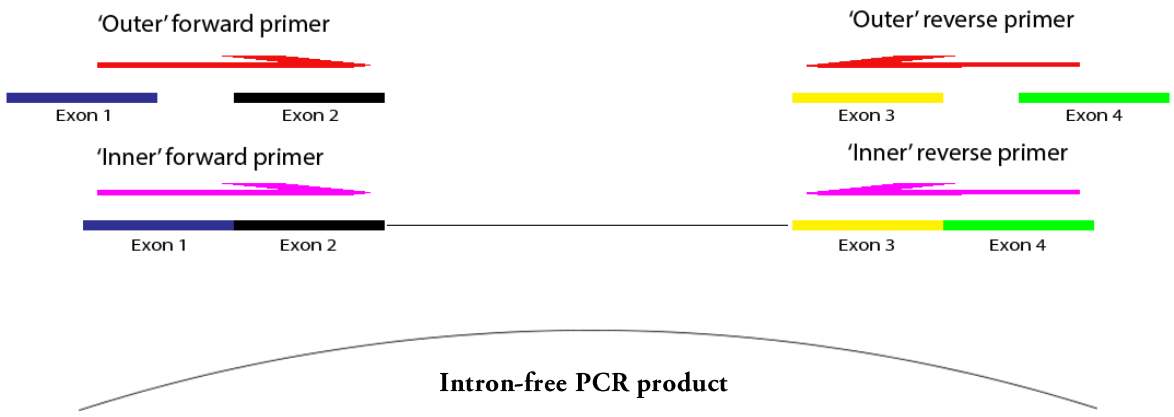

Figure 2.1: Polymerase chain reaction strategy employing intron-spanning primer sets

Table 2.4: Primers used in nested PCR cloning of SroCa$_v$1 α_1 subunit

Cloning of SroCav1 α subunit				
Name	**Sequence**	**Length**	**Tm (°C)**	**GC %**
SroCav1SalFseIF1	CAGCAACTGTGAAAACACACG	21	55.1	47.6
SroCav1BsmBIb1	GGATGGACAACAGGATCGAG	20	55.1	55
SroCav1SalIFseIF2	GTCGACGGCCGGCCACCATGACCAACG ATGACCTGAGC	38	72.7	65.8
SroCav1BsmBIb2	CACGGATGTGATGAGACGAA	20	54.6	50
SroCav1BsmBIf1	CTTTATCATCGTCGCAGTCG	20	53.4	50
SroCav1SgrAIb1	CCAGCTTCACCAGCATCTC	19	55.9	57.9
SroCav1BsmBIf2	GGAGCAATCTGGCAGCAG	18	56.6	61.1
SroCav1SgrAIb2	AGTACAAACAGGCCCACAAA	20	54.7	45
SroCav1SgrAIf1	AACCTCGTGGTGACGTTCAT	20	56.6	50
SroCav1PpuMIb1	ATGTCCGCTGTTTCCAAATC	20	53.5	45
SroCav1SgrAIf2	CTGGTGAACACTGTGCTGCT	20	58	55
SroCav1PpuMIb2	TCAAGATTGACGGGGTCCT	19	55.8	52.6
SroCav1PpuMIf1	CAACCGGTTTGAGTCTGTGA	20	55.1	50
SroCav1SacIIb1	ATCAGAGCAGCAACATACGG	20	55	50
SroCav1PpuMIf2	GCAGCGCTCTTCTTGCTG	18	57.2	61.1
SroCav1SacIb2	ATTTCGCAAACGTCCACAG	19	53.8	47.4
SroCav1SacIIf1	GGGATAGCGGTGTCAACATT	20	55.1	50
SroCav1XmaIb1	ACGAAAACGAAGGGTTCCAT	20	54.7	45
SroCav1SacIIf2	CTTGTGAGCCGCGGTAAG	18	56.3	61.1
SroCav1XmaIb2	CCCGGGTTAGAAAGCATGTTCCACCAG	27	63	55.6

Table 2.5: Primers used in nested PCR cloning of SroCa$_v$1 β subunit

Cloning of SroCav1 β subunit				
Name	**Sequence**	**Length**	**Tm (°C)**	**GC %**
SroCavbetaF1	GCCAACGACAACGAACAAA	19	54.2	47.4
SroCavbetaB1	CATCATCATCATCATCGCATC	21	51.5	42.9
SroCavbetaF2-XhoI	GGAACTCGAGACCATGATGCAGCGAAGCCGCCGG	34	70.9	64.7
SroCavbetaB2-XmaI	CCATGCCCGGGCTACACGGGGTGCAGCATGCG	32	74.1	71.9
Srocavbetaintron B3	CCACTTCTGGGGACTAGGGA	20	58	60
Srocavbetaintron F3	TCCCTAGTCCCCAGAAGTGG	20	58	60
SroCavbetaF5	CGACAACGAACAAACATGATGC	22	55.2	45.5
SroCavbetaB6	GGACCAAAGAAGACGAGGGG	20	57.6	60
SroCavbetaF7	CCCCTCGTCTTCTTTGGTCC	20	57.6	60
SroCavbetaB8	ATCATCGCATCTACACGGGG	20	56.9	55

Table 2.6: Primers used in nested PCR cloning of SroNa$_v$2 α_1 subunit

Cloning of SroNav2 α subunit				
Name	**Sequence**	**Length**	**Tm (°C)**	**GC %**
SroNav2SpeIF1	TTGTTGCAGTTGTCCCTCTG	20	55.4	50
SroNav2PvuIB1	GTTGTCCAGGAGCCAGTAGC	20	57.9	60
SroNav2ISpeIF2	ACTAGTCCACCATGTCGGCCAGCCCTG ACACTCGT	35	70.5	60
SroNav2PvuIB2	GAGTTGAGCAAGGCGTCAC	19	56.5	57.9
SroNav2PvuIF1	TCTGCGTCTTCTCCATCCTC	20	56.3	55
SroNav2SacIB1	AGAGCGTGCAACATCTCTCC	20	57.3	55
SroNav2PvuIF2	GAACCTGCGATCGGTGAC	18	56	61.1
SroNav2SacIB2	GAGCTCGCCACTATCATCACTG	22	57.4	54.5
SroNav2SacIF1	TTCCTTCTCCAGCAGTCAGC	20	57	55
SroNav2BspEIB1	AAGGATGCCCAGCTCAAAC	19	55.6	52.6
SroNav2SacIF2	GAGCTCGGCAAAGATGCTG	19	56.6	57.9
SroNav2BspEIB2	ACCAGGCGAAACACAAACTT	20	55.4	45
SroNav2BspEIF1	AACCGCAAGCCTGTGAAG	18	56	55.6
SroNav2XmaIB1	AGCGGATGGTTGTCTGAAGT	20	56.5	50
SroNav2BspEIF2	AAGGTGGAGCCCAAGTCAC	19	57.5	57.9
SroNav2XmaIB2	CCCGGGCTACAAAGTTGTTGCTTGGAT G	28	63.4	53.6

Table 2.7: Primers used for sequencing of subunit fragments in TOPO and pGem-T

Sequencing primers				
Name	**Sequence**	**Length**	**Tm (°C)**	**GC%**
M13 Forward (-20)	GTAAAACGACGGCCAG	16	50.7	56.2
M13 Reverse	CAGGAAACAGTATGAC	16	43.2	43.8
T7	TAATACGACTCACTATAGGG	20	47.5	40
SP6	ATTTAGGTGACACTATAG	18	42.1	33.3
Synthetic oligonucleotide for insertion into pIRES2-eGFP				
SroNav2	TCGACGGCCGGCCCCTGCGATCGTGGCGAGCTCCCGGCATCCGGAAGTTC			
SroCav1/SroCav1 β subunit	TCGACGGCCGGCCGGCTTCGTCTCATCACATCGGACGCCGGCGACCGAGGACCCCGTCCCGCGGTCGTC			

SroCav1 gene synthesis (SgrAI-SgrAI: 470bp)
CGCCGGTGCTGATGGGAATGACGGCGACGACGACGATGACGACATTGACGATGACGCGACCACCGTGCTGGTCCTCGGCCTCTCCCTACCCAGCGGCAATCGAGACTTTGTTGAAGCGGAGCCAACAGAGCCCATCAGCAACATCCGCACGCGCATTATGCAGAAGTTTGCTGAGCAGGGCGAGGACAGGGACAAGCTGATGTCGTTTGTGCTGGCGCATCCGCACGACGGCCACATTCTTGATGAGACACGCACGCTCGGGGAACAAGGCGTCCAAGTGAAGTCACTGCGGGAGTACAACGAAATCCTCACGATGTCGCAGCACAATCAGCACGAACTGTTGAAGCCGGCGACAGTGCAGATGCTCTCAAAATTGGGCGCCGTTGTCAAGTCGCGCTGGTTCAACCTCGTGGTGACGTTCATGGTGCTGGTGAACACTGTGCTGCTCGCCGTCCAGACGGACGCCGGCG

Figure 2.2. Synthetic oligonucleotide for SroCa$_v$1

Synthetic oligonucleotide provided by BioBasic Inc. (Markham, ON, CA) to complete cloning of SroCa$_v$1.

Chapter 3
Results

3.1 Isolation of channel gene coding sequences

PCR amplification of the genes encoding for the α_1 subunit of SroNa$_v$2 and α_1 subunit and β subunit of SroCa$_v$1 proved to be difficult due to various spurious intron sequences being amplified. A significant amount of PCR amplification resulted in larger than expected products which were found to be a result of introns not being removed from the coding sequence. To counter this, intron-spanning primers were created which would only anneal to adjacent exon sequences in which the contaminating intro was excised. Consensus sequence data was compiled by Dr. David Spafford to confirm correct coding sequence. In each consensus, a minimum of 3 independently amplified PCR products sequenced at The Center for Applied Genomics (TCAG) at Sick Kids Hospital (Toronto) were aligned using Sequencher5.1 software (GeneCodes Corp.).

The two fully isolated channel α_1-subunits had no alternative splice variants. For both SroNa$_v$2 and SroCa$_v$1 α_1-subunits previously unidentified sequences (Fig. 3A,B) were found to be exon coding sequence. To confirm, the sections of each respective channel were PCR amplified with additional primer sets, including intron-spanning primers. Fragments were then identified at TCAG to confirm amino acid sequence, from which a consensus was built with a minimum of three independent clones.

A

Previously identified intron of SroNa$_v$2

5'-
CACTTCCAGCAGCACTTCCAGCAGCAGCACAGCTCAGAGTATACGTGTGAATGGTATTGGC
ACGCGTGGCAAAGCAAGCAGGCAGCCAGTCTCGACAGAGCAGCGGCTGCAGAGCATGGAG
ACGATCAAGGCAACGAAAGCCGGTTCGAGGAATGTCATCAAGCACGTGTGGAGTGAAGACG
GCGCTGACCCCACAAGCACCAGTGTTGTCGACTCAGATGCGCGCGCGCACAGGGGCGCTGG
TGATGTGGTGCTCGTTCCAAGTTGAGAGCACCATCACCGTTTGGACACGATGCTGCACGCA
CCGGTGTGATGGCGGTGAACGAGGGCTTCCTCAGGGTGGGCGCCAACCAGGCAGCCCTTCT
GTCGAGCCCAAAGGCCAAGTTTGGTGCAGACAGCAACGACGACAGTGATGAGGACGTCGAT
CATGACATGACAGGGAGATGGGCAGTCCACAGGCACGGGGGTGGCAAGAGCAATGAGAGT
AGCGACGACGACACAATCTCAAGAGCATCGTCTCTGCCACAGAAGAGGATGCAAGGCAAGC
AGGTGACGCTGGTTGAGGAGCCAACTGTCGTGCCACACCAACAACGGCTTGGGACACGGAC
AGCGAGCGTGGCACCGTGGATACTGTTGCGATGCTAG
CTGGGGACGGAGCCGCTGCTGTGATGCCGCGATACCGCCGCCG-3'

B

Previously unidentified SroCa$_v$1 coding sequence

5'-
GCTGTGTCTTGCTGGATCGTCGCCAAACTCCAACATCACCGCGTTCGACCACGCAGGGATT
GCCATTCTTGCCGTCTTCCAGTCAATCACACTCGAGGGATGGACTGATATCCTCTACAACGT
GGACGATGCTGTTGGTTACAAGAACATCAACTGGCTGTTCTTTGTGTCTCTGGTGATTGTGG
GCGCATTCTTCGTCATCAACCTCGTCCTCGGTGTTCTCAGCGGGCAGTTCACCCGCGAGGGT
GACCGCATGAAGGCGTCTGTGAAGTTTCTTCGCGCGCGGCGCAAAGAACAGCACCGCTTCC
AAGTCGCCGGGTACAGGGACTGGCTCTCAACAGCGCGCACGCTGCAGCCGAATGAGCCGTG
GCAGTCGGAGCTCCCAGACCACATGGTGCTCTACCACCGCGACAAGTTTCTCAAGTTTGATG
CGGCGGAGAGCATGGCAGAGCACGAGCAGAACTTCTTCAACAGCAGCGCCGGTGCTGATGG
GAATGACGGCGACGACGACGATGACGACATTGACGATGACGCGACCACCGTGCTGGTCCTC
GGCC TCTCCCTACCCAGCGGCAATCG**AGACTTTGTTGAAGCGGAGCC-3'**

Figure 3.1. Newly identified coding sequence in SroNa$_v$2 and SroCa$_v$1

(A) Coding sequence previously identified as intron sequence was found as part of Domain III of SroNa$_v$2. (B) Previously unidentified coding sequence was found at the N-terminus of the SroCa$_v$1 channel.

SroNa$_v$2 shares only 33% - 51% sequence similarity among the channels examined. The fully expressed channel has an open reading frame of 5502 base pairs (bp) long transcript, producing a protein of 1834 amino acids (AA). The full coding sequence of SroNa$_v$2 was aligned with vertebrate Na$_v$ and invertebrate channel homologs that have either been functionally characterized or have been proposed as basal proteins but remain categorized as putative proteins as per GenBank (NCBI) (Fig. 3.2A).

A cladogram was generated (Jalview) based on neighbouring % identity scores (Fig. 3.2B). Based purely on the selected sodium channel gene coding sequence, SroNa$_v$2 branches basally to all vertebrate homologs and closely with Na$_v$2 channels from *Drosophila melanogaster* and *Blattella germanica*. The *Trichoplax adhaerens* Na$_v$ channel has not been isolated or functionally analysed to confirm identity and remains a putative channel based on transcriptome data entry.

SroNa$_v$2 possess the DEEA selectivity filter configuration in agreeance with other invertebrate channels, with the differentiating factor from Na$_v$1 homologs being the lysine (K) residue in primarily in Domain III but also Domain II in the case of *Cyanea capillata* (jellyfish) (Figure 3.3A). In the III-IV linker, the residues of the IFM-motif (boxed) are replaced by VLL (valine-leucine-leucine) (Fig 3.3B). Furthermore, the proposed docking site alanine (A) residue of Domain III is substituted with a serine (S). These likely play a role in the slow inactivation seen in SroNa$_v$2 (Fig. 3.10C) and other Na$_v$2 channel homologs from other invertebrates.

SroCa$_v$1 shares 45% - 58% sequence similarity among the channels examined. The fully expressed channel produces an open reading frame of 4998 bp, producing a protein of 1666 AA. SroCa$_v$1 sequence was aligned with vertebrate HVA calcium channels, including all human homologs, as well as invertebrate channels that have been experimentally confirmed and functionally characterized (Fig. 3.4A) Invertebrate channels include those that remain as putative proteins as per GenBank (NCBI). A cladogram was then created based neighbouring % identity scores of calcium channel gene CDS (Fig. 3.4A). SroCa$_v$1 branches basally to all vertebrate channels but at a later node than all other invertebrate channels (except *Lynmaea stagnalis*). This could reflect the similarity and degree of conservation between the *S. rosetta* and human homologs.

SroCa$_v$1 appears to be the only channel to possess an 'EDEE' selectivity filter, while all other HVA calcium channels possess an 'EEEE' filter (Fig. 3.5A). Comparison of the calcium-calmodulin (CaM) binding domain (Fig. 3.5B) which contains the critical IQ-motif for CaM binding reveals that SroCa$_v$1 is the only channel to possess an 'LQ'. Interestingly, this does not seem to affect channel inactivation with calcium as the charge carrier (Fig. 3.13).

During cloning of SroCa$_v$1 it was discovered that *S. rosetta* possessed the gene for an auxiliary β-subunit to SroCa$_v$1. This subunit was isolated and cloned into the mammalian expression vector pIRES2-dsRED. The gene CDS is aligned in Figure 3.7A. SroCa$_v$β shares only 24-26% sequence similarity with other vertebrate and invertebrate β-subunits examined and based on neighbouring % identity scores places basely to all other β-subunits. It is essential to successful expression of SroCa$_v$1.

A

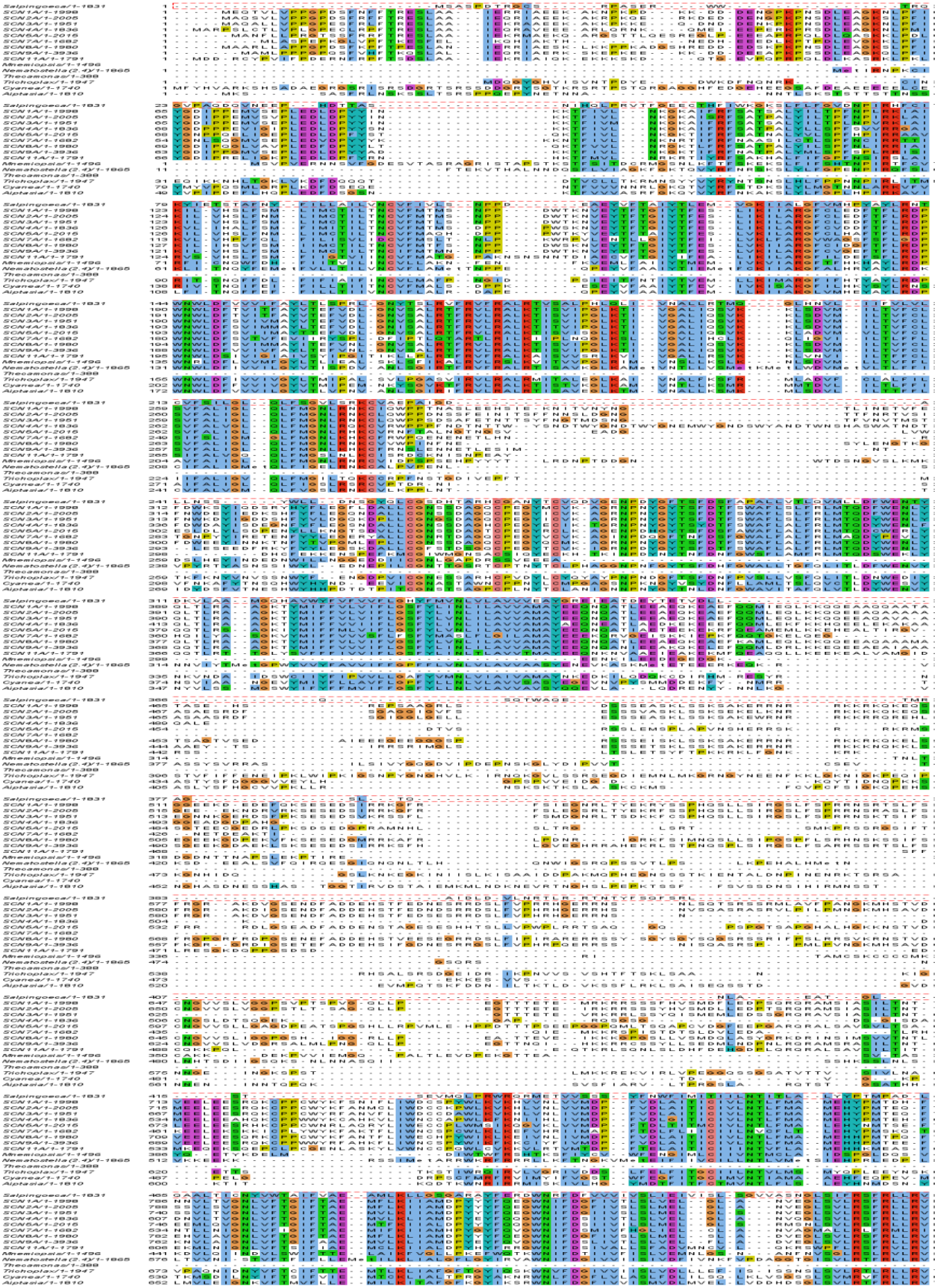

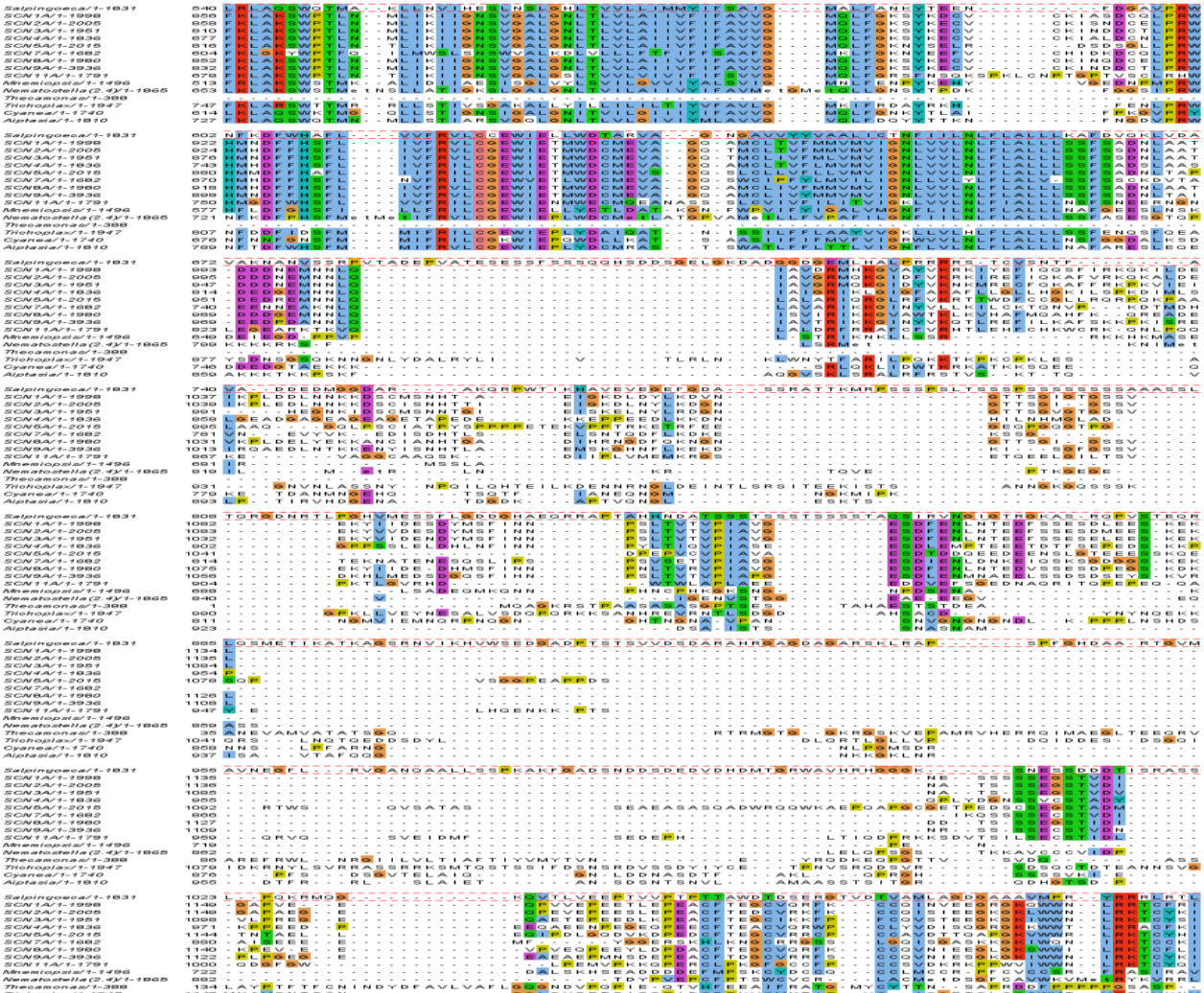

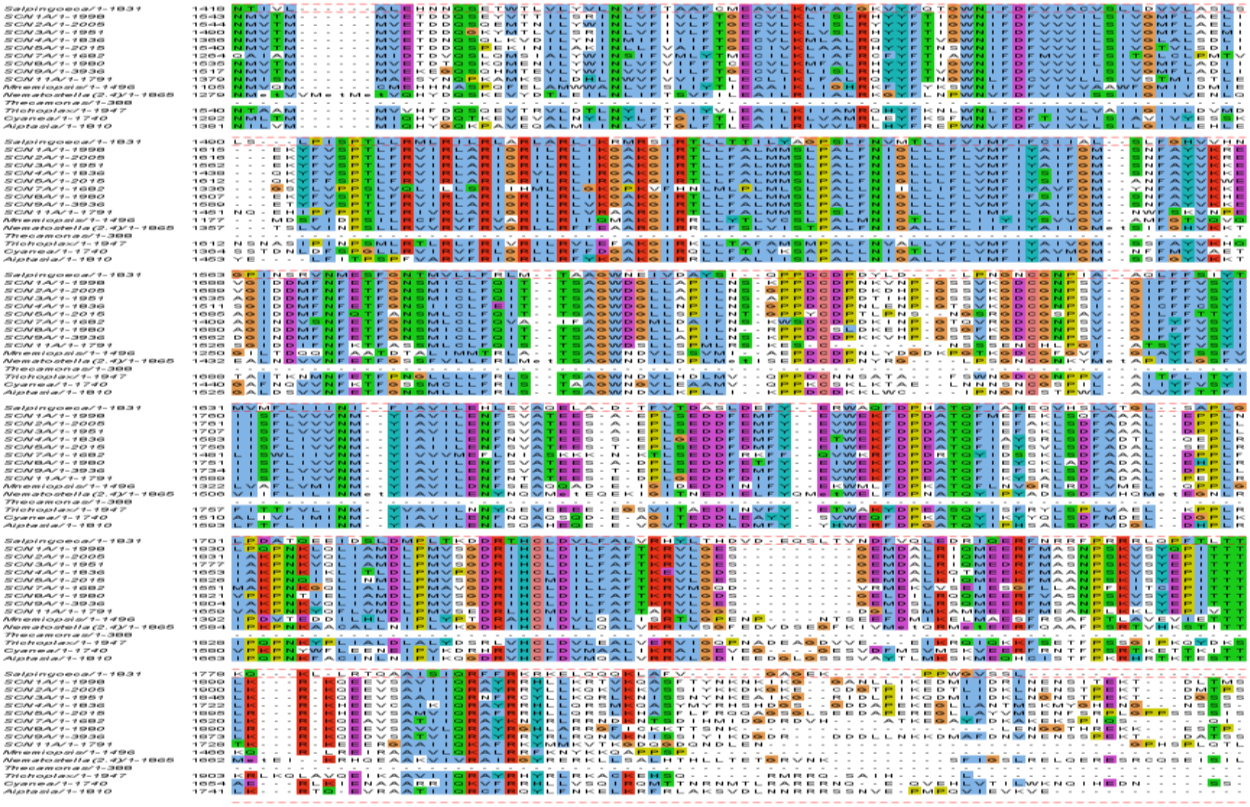

B

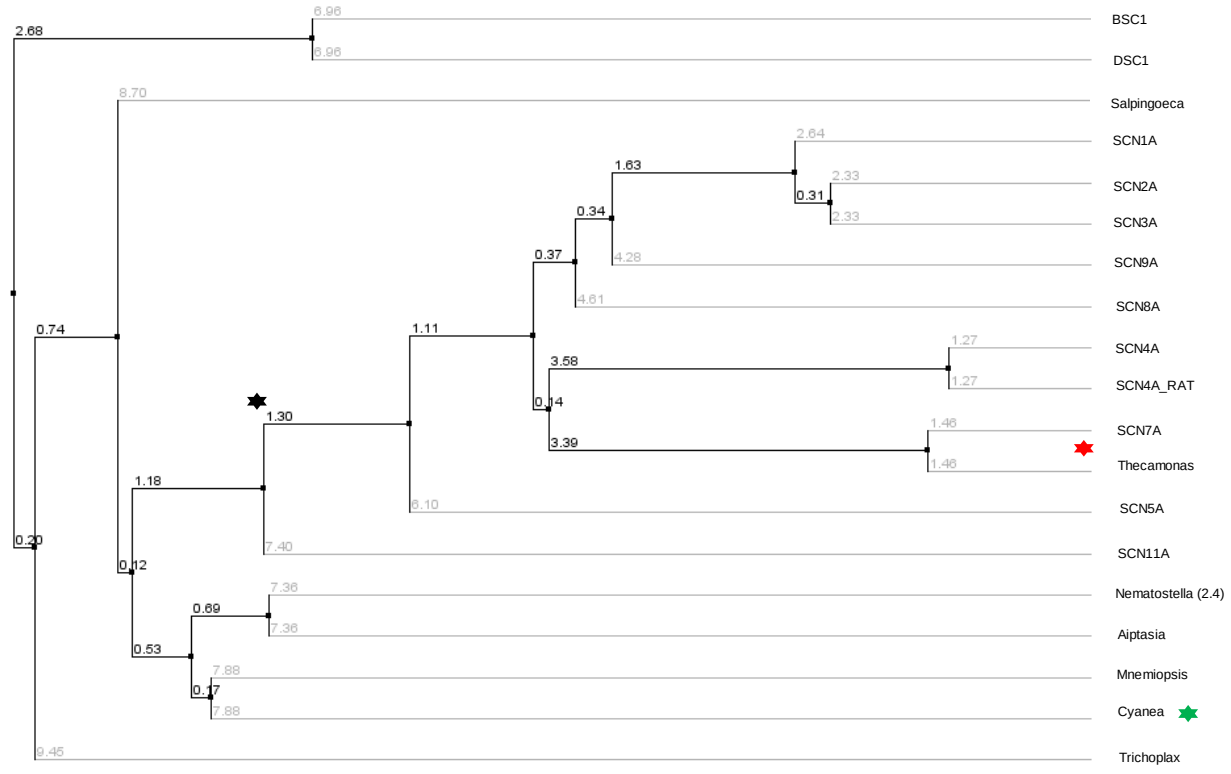
6.96
2.68
6.96
BSC1
DSC1
8.70
Salpingoeca
2.64
SCN1A
1.63
2.33
SCN2A
0.31
2.33
SCN3A
0.34
0.37
4.28
SCN9A
4.61
SCN8A
0.74
1.11
1.27
SCN4A
3.58
1.27
SCN4A_RAT
0.14
1.30
1.46
SCN7A
3.39
1.46
Thecamonas
1.18
6.10
SCN5A
0.20
7.40
SCN11A
0.12
7.36
Nematostella (2.4)
0.69
7.36
Aiptasia
0.53
7.88
Mnemiopsis
0.17
7.88
Cyanea
9.45
Trichoplax

Figure 3.2. SroNa$_v$2 Sequence alignment and neighbour % identity cladogram

A) Amino acid alignment of Na$_v$1 (Homo sapiens) and Na$_v$2 (invertebrate) sodium channel homolog. Input sequences on left (top to bottom): *Salpingoeca rosetta*; SCN1A [Homo sapiens]; SCN2A [Homo sapiens]; SCN1A [Homo sapiens]; SCN4A [Homo sapiens]; SCN5A [Homo sapiens]; SCN6A [Homo sapiens]; SCN7A [Homo sapiens]; SCN8A [Homo sapiens]; SCN9A [Homo sapiens]; SCN11A [Homo sapiens]; *Mnemiopsis leidyi*; *Thecamonas trahens*; *Nematostella vectensis*; *Trichoplax adhaerens*; *Cyanea capillata*; *Aiptasia pallida* . Sequence similarity is indicated by colour blocks. Salpingoeca rosetta Na$_v$2 (highlighted by red box) exhibits a high degree of similarity to other recognized Na$_v$1 and Na$_v$2 channels. Extraneous 3' sequence trimmed. (B) Phylogenetic tree generated based on '% sequence similarity scores of Na$_v$1/2 channels. Branch numbers indicate distance scores based on % neighbour identity. Black star represents emergence of Lysine-K residue in selectivity filter. Red star channels lack Lysine-K. Green star indicates Na$_v$1-DKEA channel in jellyfish. Alignment done using Clustal Omega and Jalview, phylogenetic tree produced using Jalview.

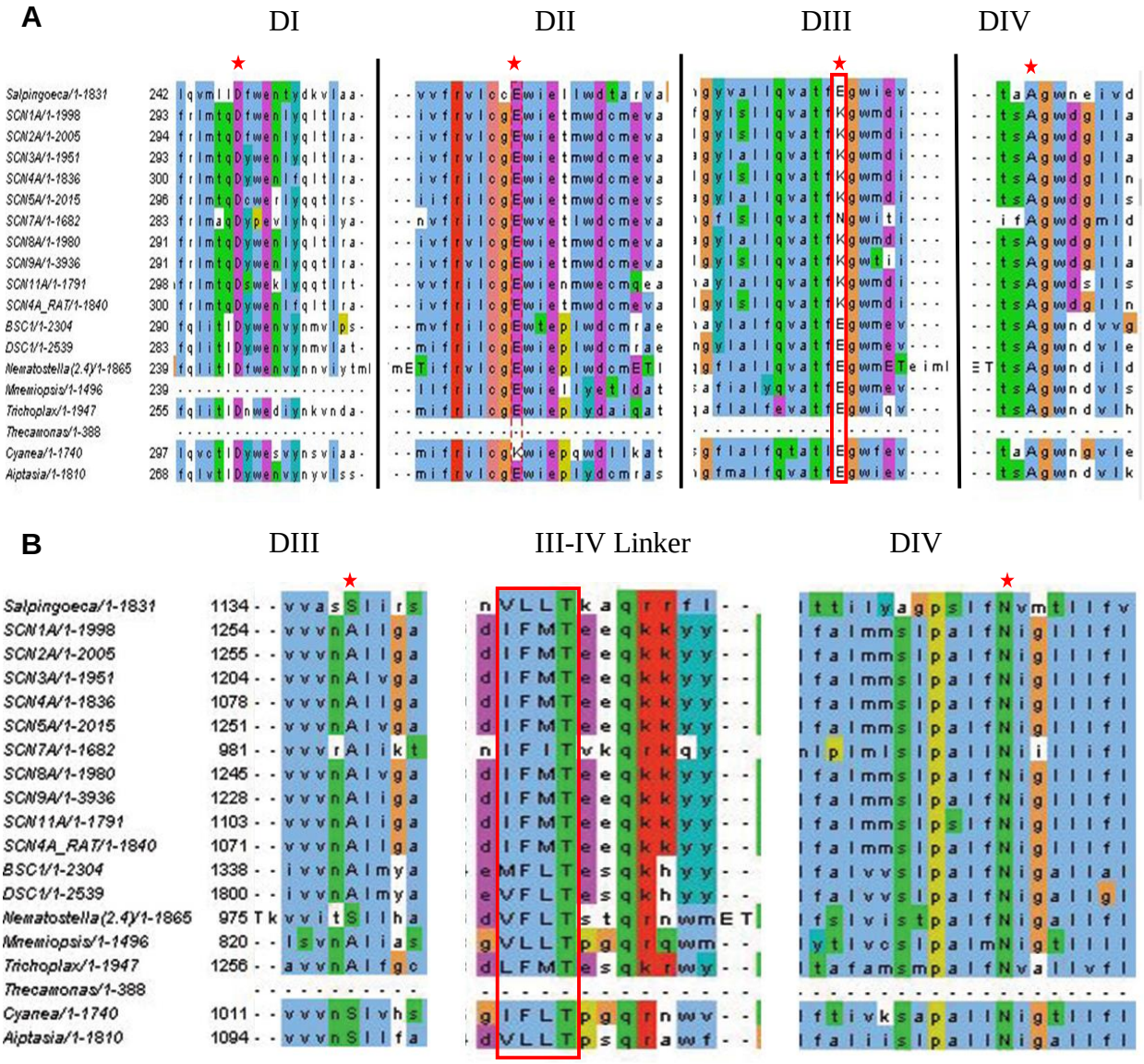

Figure 3.3. Selectivity and inactivation features of SroNa$_v$2

(A) Expanded view of selectivity filter (star) and neighbouring residues of each Domain in SroNa$_v$2. Red box in Domain III highlights major substitution between vertebrate lysine (K) to invertebrate glutamate (E). (B) Expanded view of docking site residues on the S4-S5 linkers of Domain III & IV (stars) and IFM-motif (boxed) responsible for fast inactivation kinetics in Na$_v$1 channels.

A

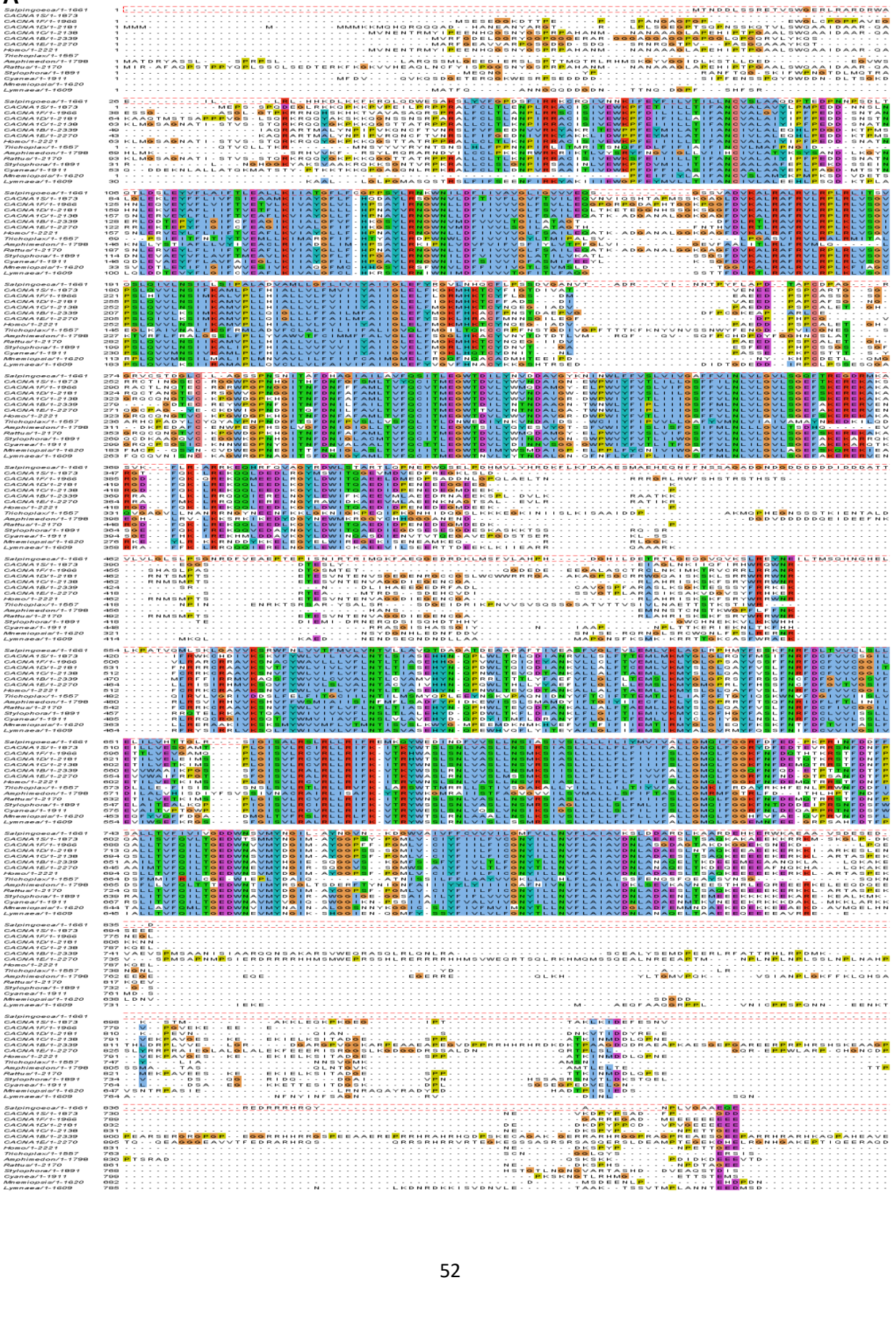

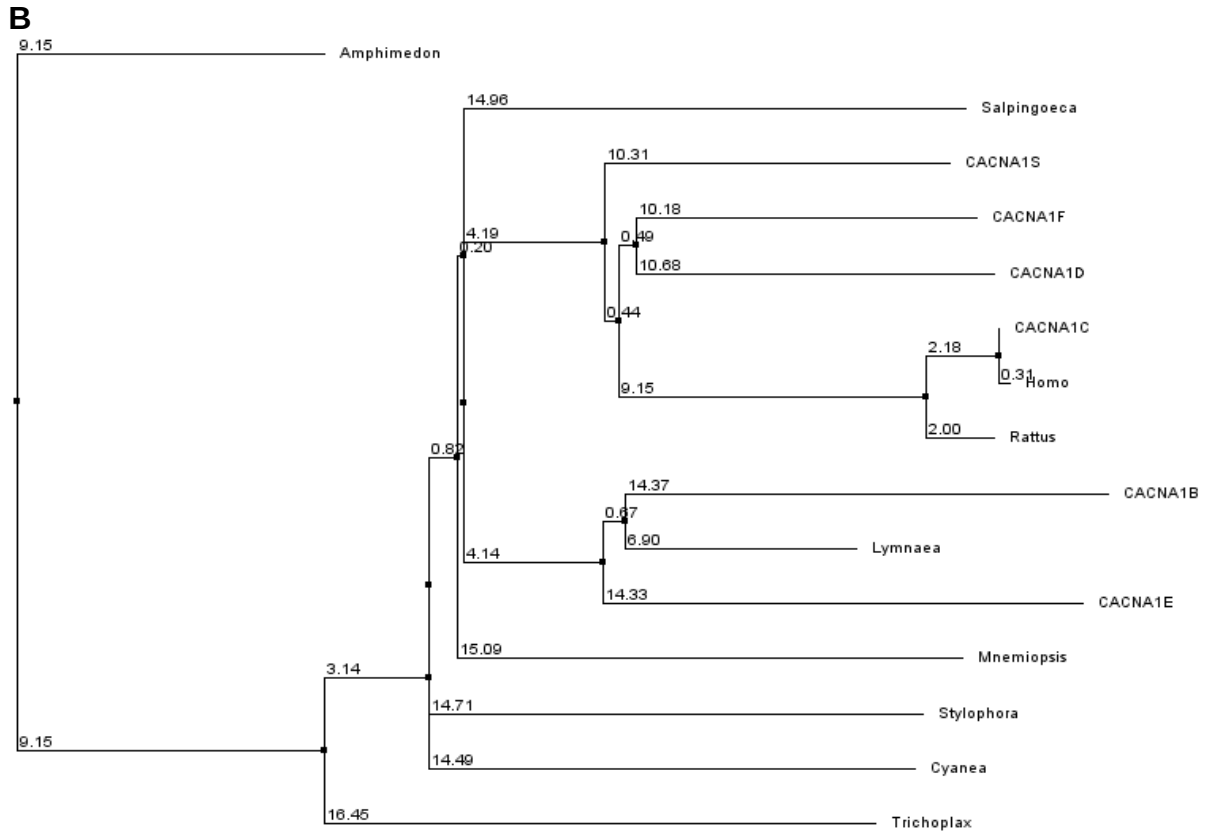

Figure 3.4. SroCa$_v$1 Sequence alignment and neighbour % identity cladogram

(A) Amino acid alignment of Ca$_v$1 L-type calcium channel homologs. Input sequences on left (top to bottom): *Salpingoeca rosetta*; CACNA1S [Homo sapiens]; CACNA1F [Homo sapiens]; CACNA1D [Homo sapiens]; CACNA1C [Homo sapiens]; CACNA1E [Homo sapiens]; CACNA1B [Homo sapiens]; CACNA1A [Homo sapiens]; *Trichoplax adhaerens*; *Amphimedon queenslandica*; *Rattus norvegicus*; *Stylophora pistillata*; *Mnemiopsis leidyi*; *Cyanea capillata*; *Lymnaea stagnalis*. Sequence similarity is indicated by colour blocks. *Salpingoeca rosetta* Ca$_v$1 channel (highlighted in red) shows a high degree of similarity to identified homolog L-type calcium channels in higher vertebrates and invertebrates. Extraneous 3' sequence trimmed. (B) Phylogenetic tree generated using Ca$_v$1 channel sequence based on '% sequence identity'. Alignment done using Clustal Omega and Jalview, phylogenetic tree produced using Jalview.

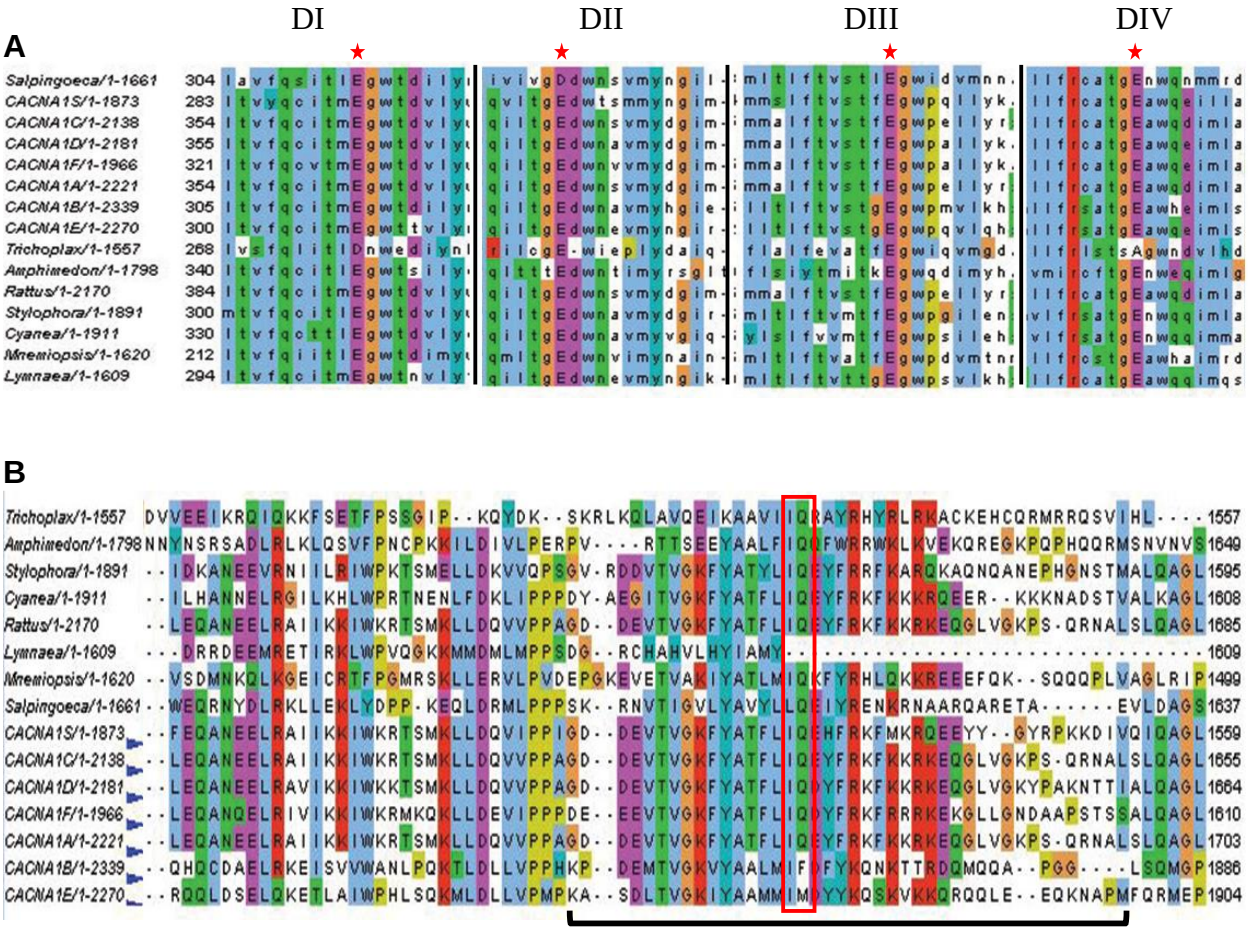

Figure 3.5. Selectivity filter and calcium-calmodulin docking site of SroCa$_v$1

(A) Expanded view of aligned selectivity filter residues (star) within Domains I-IV. (B) Calcium-calmodulin (CaM) binding site (black bracket) at C-terminus of HVA calcium channel. Highlighted (red box) indicates key residues of the IQ-motif responsible for CaM binding. Alignments done using ClustalOmega and Jalview.

A

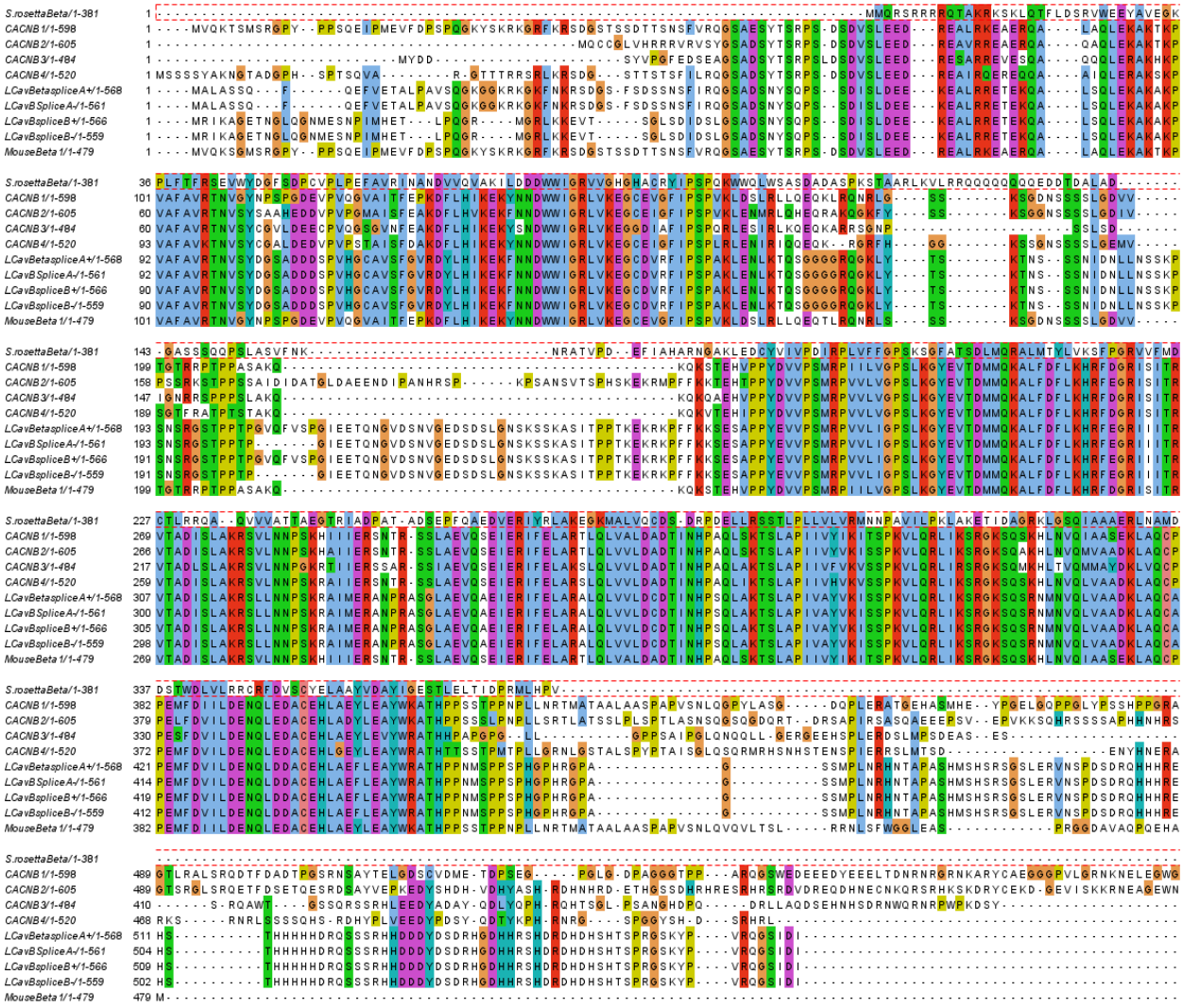
S.rosettaBeta/1-381
CACNB1/1-598
CACNB2/1-605
CACNB3/1-484
CACNB4/1-520
LCavBetaspliceA+/1-568
LCavBSpliceA+/1-561
LCavBspliceB+/1-566
LCavBspliceB+/1-559
MouseBeta 1/1-479

B

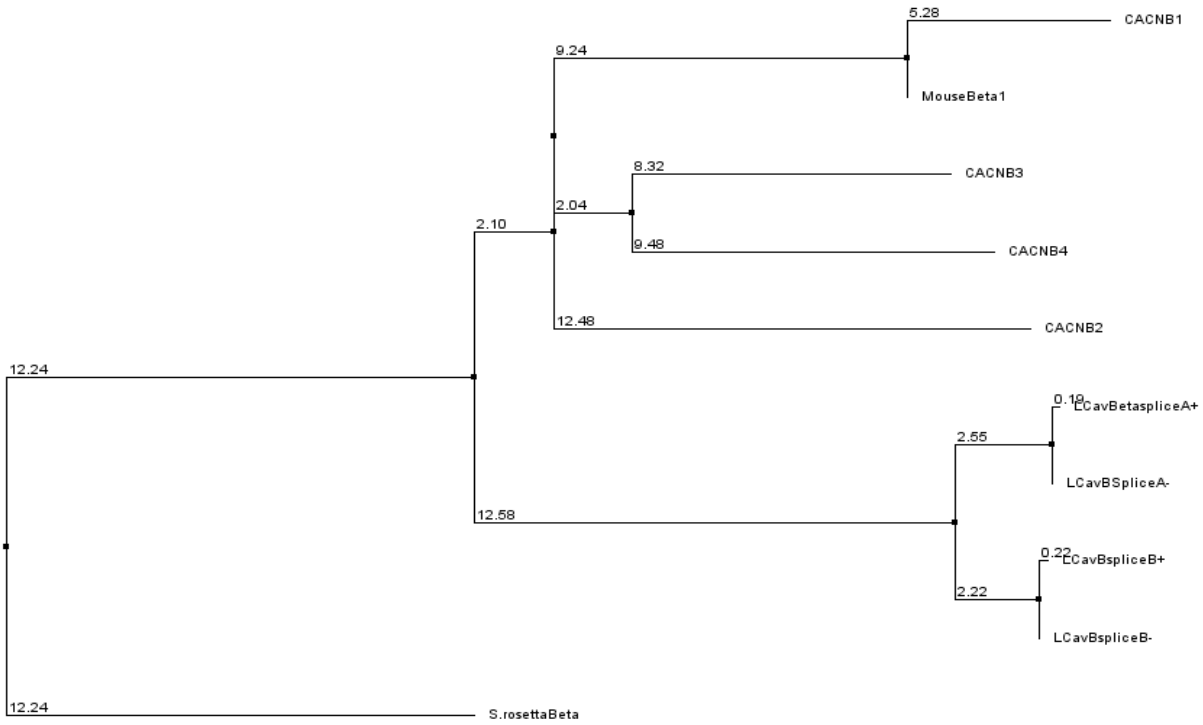

Figure 3.6. SroCa$_v$β alignment and cladogram

(A) Alignment of isolated SroCa$_v$β subunit against vertebrate homologs and invertebrate homologs from *Lymnaea stagnalis*, including all splice variants. (B) Phylogenetic tree produced based on neighbouring % identity scores (Jalview).

3.2 HEK cell expression

SroNa$_v$2 exhibits striking levels of expression observed in HEK-293T cells by using the standard calcium phosphate transient transfection strategy. Channel currents are observable in as little as 12 hours after transfection and remain at significant current measurements for approximately 72-hours post-transfection, at which point peak current produced by SroNa$_v$2 increased significantly in 2mM extracellular calcium. Also, HEK cell membranes exhibited decreased integrity as seen by significant current leakage, unstable membrane potential, and cell death during patch clamp protocols. Visually, cells would appear shriveled or appeared to lose the distinct outline of a cellular membrane. While expressing SroNa$_v$2, HEK cells were found to be highly unstable when resting membrane potentials were maintained below -100mV during whole-cell patch. Only cells expressing the channel 12-14 hours after transfection could be used to obtain steady state inactivation data where membrane potential needed to be set at -130mV. After this time the patch holding potential had to be adjusted to more depolarized potentials ([-110mV] – [-90mV]). This phenomenon was not seen when expressing the SroCa$_v$1 channel where cells could be held indefinitely at -110mV. The precise reason(s) behind the cellular instability was not investigated but currently remains unknown.

SroCa$_v$1 currents were observable 7-days post-transfection and were recordable for approximately 48 hours. HEK cells maintained for >9-days post-transfection exhibited signs of senescence similar to SroNa$_v$2. Increased leak current, cellular death during patch clamp recording and loss of a distinct cell membrane restricted experimentation to a 48-hour window. Additionally, SroCa$_v$1 expression required co-expression with the SroCa$_v$1 β subunit and human $\alpha_2\delta$ subunit. Expression attempted without the SroCa$_v$1 β subunit resulted in no observable current up to 14-days post-transfection. Human β-subunit (β_1, β_2, and β_3) co-expression was also attempted in various combinations but no observable currents were seen up to 14-days post-transfection. Combinations of human β-subunits with the *Salpingoeca* β-subunit were also tested but no differences in kinetics compared to expression of only SroCa$_v$β were seen.

Interestingly, under mercury lamp excitation HEK cells transfected with SroCa$_v$1 α_1 channel construct but without SroCa$_v$1 β-subunit continued to fluoresce green starting at 3-days post-transfection. This could only confirm successful transfection of cell aliquot and did not reflect channel expression.

3.3 Activity of SroNa$_v$2

SroNa$_v$2 appears to be permeable to calcium ions as measurable currents were seen in 2mM calcium (extracellular). Interestingly, substituting barium in place of calcium as the primary charge carrier resulted in approximately 30% decrease in peak current amplitude at equal molar concentrations (Fig. 3.7B). An anomalous effect between calcium and barium was not tested. We cannot conclude whether SroNa$_v$2 is impermeable to barium and the seen decrease in current size is from barium pore block thereby restricting the conducting calcium ions, or the channel pore affinity for barium is lower.

SroNa$_v$2 peak currents were elicited at depolarising steps to -10mV in 2mM Ca^{2+} (Fig.3.8B) with $V_{1/2}$ achieved at approximately -31mV (Fig. 3.9B). SroNa$_v$2 is a "slow" sodium channel as time to peak data indicates approximately 15.5ms (±3.62ms) to maximal current. It also appears to require >300ms for complete current decay (Fig. 3.8C). Recovery from inactivation of the channel is dependant on patch holding potential but requires at minimum 13 seconds (holding potential [-90mV]) to achieve full recovery (Fig. 3.9G, H). The most interesting feature comes from steady state inactivation data indicating that SroNa$_v$2 is 90% inactivated at a holding potential of -90mV (Fig. 3.9C, D). Full recruitment of channels is achieved with a holding potential of [-120mV] to [-130mV], with half inactivation achieved at a potential of -103mV. This implies that in several physiological contexts where other sodium channel homologs are expressed (muscle, myocardial, neuronal cell) SroNa$_v$2 is likely to be in an inactivated state. The activation and activation curves of SroNa$_v$2 do not overlap and there is no window current possible.

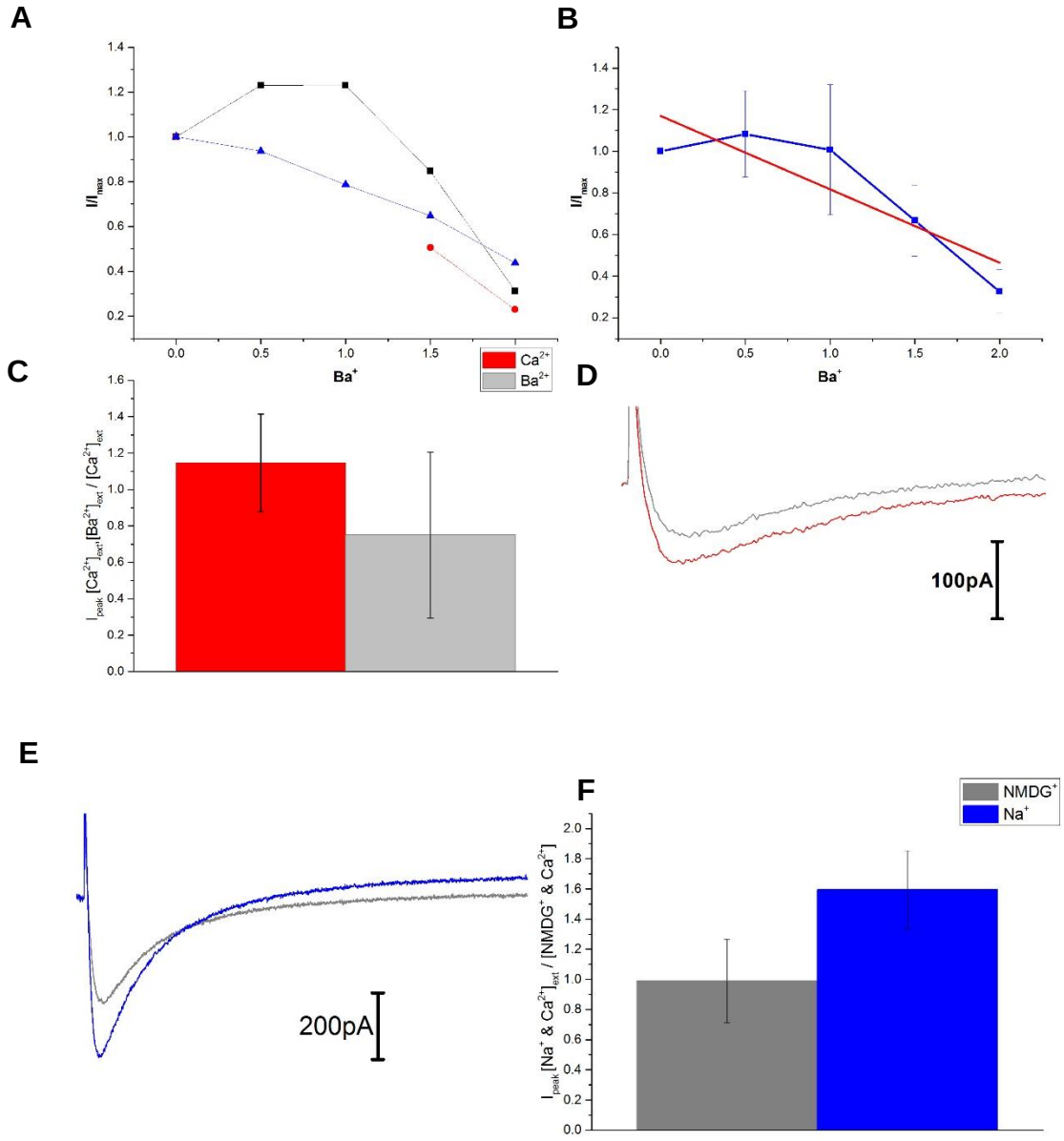

Figure 3.7. SroNa$_v$2 extracellular ion permeability

(A, B) Normalized barium perfusion data indicating a decrease in inward current with increased barium concentrations. (C) Bar graph showing decrease in average peak current for barium perfusion experiments. Error bars represent standard deviation (D) Sample trace showing relationship of Ca^{2+} [red] conductance against Ba^{2+} [grey] through SroNa$_v$2. No change in kinetics, inactivation decay or speed are seen. (E) Sample representative trace recording of Ca^{2+}+$NMDG^+$ (grey) and Ca^{2+}+Na^+ (blue) to illustrate increase in current at peak conductance voltage. (F) Bar graph showing the average increase in current size at peak conductance voltage of Na^+ against impermeable $NMDG^+$. Error bars represent standard deviation.

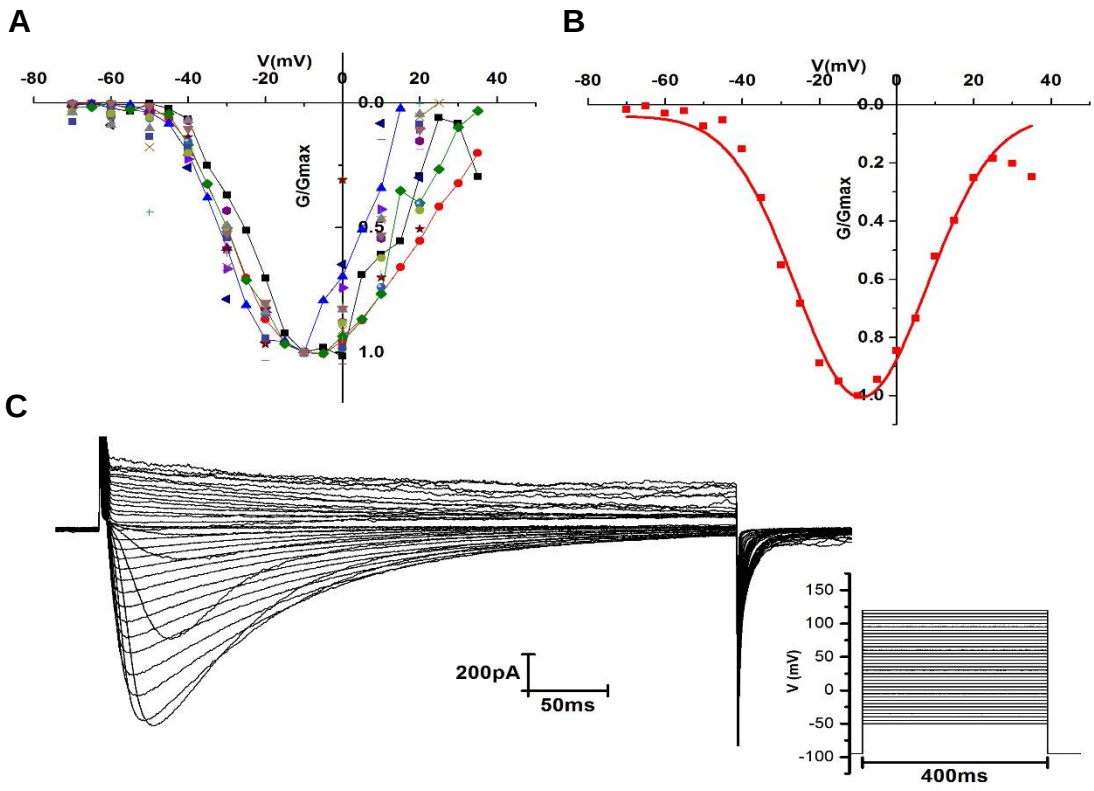

Figure 3.8. SroNa$_v$2 current-voltage relationship

(A) Pooled normalized to peak current IV data of inward current, 2mM $[Ca^{2+}]_{ext}$. (B) Averaged, fitted IV curve analysis of SroNa$_v$2. Maximal conductance occurs at depolarisations to -10mV. (C) Sample trace of expressed SroNa$_v$2 in 2mM $[Ca^{2+}]_{ext}$/[110mM $Cs^{+}]_{int}$

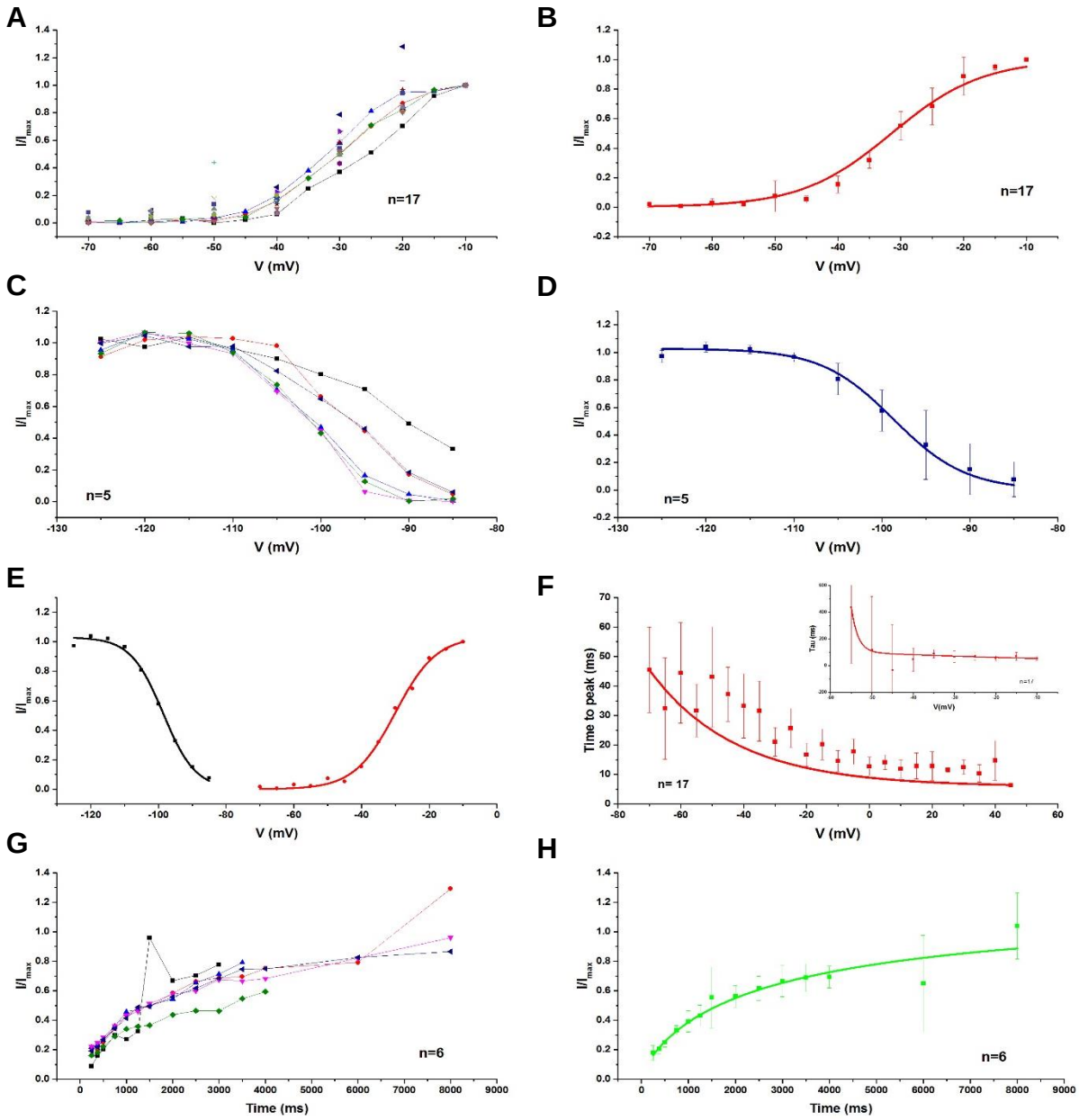

Figure 3.9. SroNa$_v$2 activation-inactivation

SroNav2 Activation/Inactivation Data. (A) Pooled normalized activation data. Peak current size achieved at -10mV. (B) Averaged activation data (C) Pooled inactivation data (D) Averaged inactivation data (E) Combined activation and inactivation data. SroNav2 activation/inactivation curves do not overlap and the channel does not appear to possess a persistent window current. (F) Time to peak data determined from IV trace recordings. Inset: Tau activation data. (G) Pooled recovery from inactivation (RFIA) data (H) Averaged RFIA data

3.4 SroNa$_v$2 Permeability to monovalent ions

To assess ion permeation properties of the SroNa$_v$2 channel Na^+-NMDG perfusion experiments were performed wherein Ca^{2+} ion concentration was kept a constant 2 mM and perfusion of 135 mM $NMDG^+$ was toggled with 135 mM Na^+. SroNav$_v$2 allows the passage of sodium ions alongside calcium through its pore with a ratio of Na^+: Ca^{2+} near 1.6:1 (Fig. 3.9E, F). Some recordings indicated greater than double increase in peak current size while others indicated none to minimal change in current size. The discrepancies could be due to patch current leak during recording, voltage error and shifted peak currents, or differences between experiment-to-experiment setup of perfusion experiments.

To further assess permeability of cations through SroNa$_v$2 and confirm the viability of Na^+ ion permeation seen in Na^+-$NMDG^+$ experiments bi-ionic condition experiments were performed. Monovalent ions at a concentration of 100mM were added to the intracellular solution and external calcium was kept at 4mM. Currents were elicited by voltage steps from -50mV to +100mV, while the cell was held between [-95mV] to [-90mV]. There is a hyperpolarizing shift in the reversal potential as you move up periods on the periodic table. Bi-ionic reversal potential shows permeability to monovalent ions in the order of $Li^+ > K^+ > Na^+ > Cs^+$, with reversal potentials of +7.0mV < +15.0mV, +18.0mV < +42mV, respectively. SroNa$_v$2 produces large outward currents at voltage steps above each respective ions reversal potential. This condition allows for direct measure of the channels ability to pass monovalent ions as there is a large concentration gradient created entirely from the monovalent ion ($100mM_{int} > 0mM_{ext}$) and a lack competition from divalent Ca^{2+} in the extracellular solution.

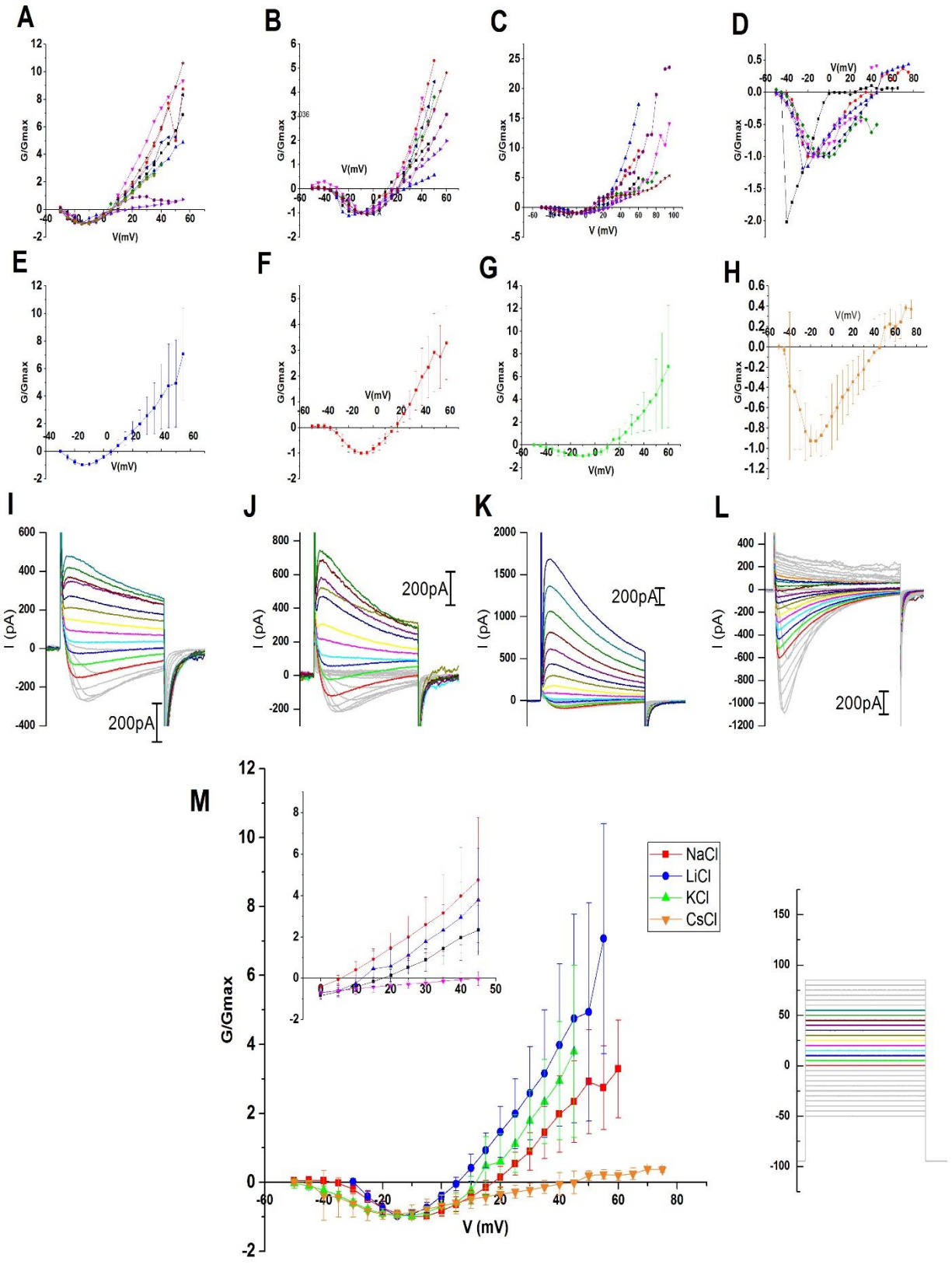
A
B
C
D
E
F
G
H
I
J
K
L
M
G/Gmax
V(mV)
V (mV)
I (pA)
200pA
NaCl
LiCl
KCl
CsCl

Figure 3.10. SroNa$_v$2 Bi-Ionic reversal experiment

[Left to Right; Lithium-Sodium-Potassium-Cesium] (A-D) Pooled recording data normalized to peak conductance for intracellular monovalent ions. (E-H) Averaged pooled data, used to fit to determine reversal potential of each ion. (I-L) Representative traces of each ion. Colours tracings coincide with voltage steps taken from 0mV – 55mV (shown in M, right) from a holding potential of -90mV. (M) Combined graph of figures E-F, with expanded view showing differences in reversal potentials (inset). All recordings done in 4 mM $[Ca^{2+}]_{ext}$

Table 3.1. Bi-ionic reversal potentials of SroNa$_v$2

	Lithium	**Potassium**	**Sodium**	**Cesium**
SroNa$_v$2				
E_{rev} (mV)	6.7809	15.5243	18.76907	42.90918
S.E.M.	1.08614	2.1202	1.38874	4.18464
P_{Ca} / P_x	19.1974	34.90017	41.39771	273.3869
S.E.M.	1.463359	4.325008	3.739147	80.20794
n	10	9	9	7

Values are reported as means ± standard error of mean (S.E.M.), *n* denotes the sample size. P_{Ca}/P_x is the permeability ratio of the monovalent ion (x) in respect to calcium.

3.5 Activity of SroCa$_v$1

SroCa$_v$1 produces measureable currents in 20 mM Ca^{2+}. The current-voltage relationship indicates peak inward currents achieved at approximately -3.5mV (Fig. 3.13A), and a $V_{1/2}$ achieved at -30mV in Ca^{2+} (Fig. 3.14B). SroCa$_v$1 appears to be a rapid channel as complete current decay occurs in approximately 200 ms, and complete recovery from inactivation occurs in approximately 8.1 seconds (Fig. 3.14H). Steady-state current is tested with voltage steps to peak current with increasing holding potentials to determine the percentage of channels available at the varying holding potentials for firing. Half inactivation from this is achieved at holding potential of -47mV, and the overlap in activation and inactivation data shows that there is a small window current of the channel (Fig. 3.14D, E).

SroCa$_v$1 is impermeable to extracellular monovalent ions as tested using the Na^+-$NMDG^+$ experiments (data not shown). No obvious outward current was seen with 110 mM Cs^+ indicating a lack of conduction in either direction of monovalent ions. SroCa$_v$1 appears to be a highly divalent cation selective channel.

Most interestingly, the substitution of 20 mM Ba^{2+} in place of extracellular calcium does not produce the long-lasting currents during depolarisation typical of L-type calcium channels (Fig. 3.15E). However, there is a hyperpolarizing shift in reversal potential and peak of the *I-V* curve with barium and the charge carrier (Fig. 3.16; Table 2). Unlike SroNa$_v$2, Ba^{2+} appears to be equally permeable as Ca^{2+} through SroCa$_v$1 (data not shown).

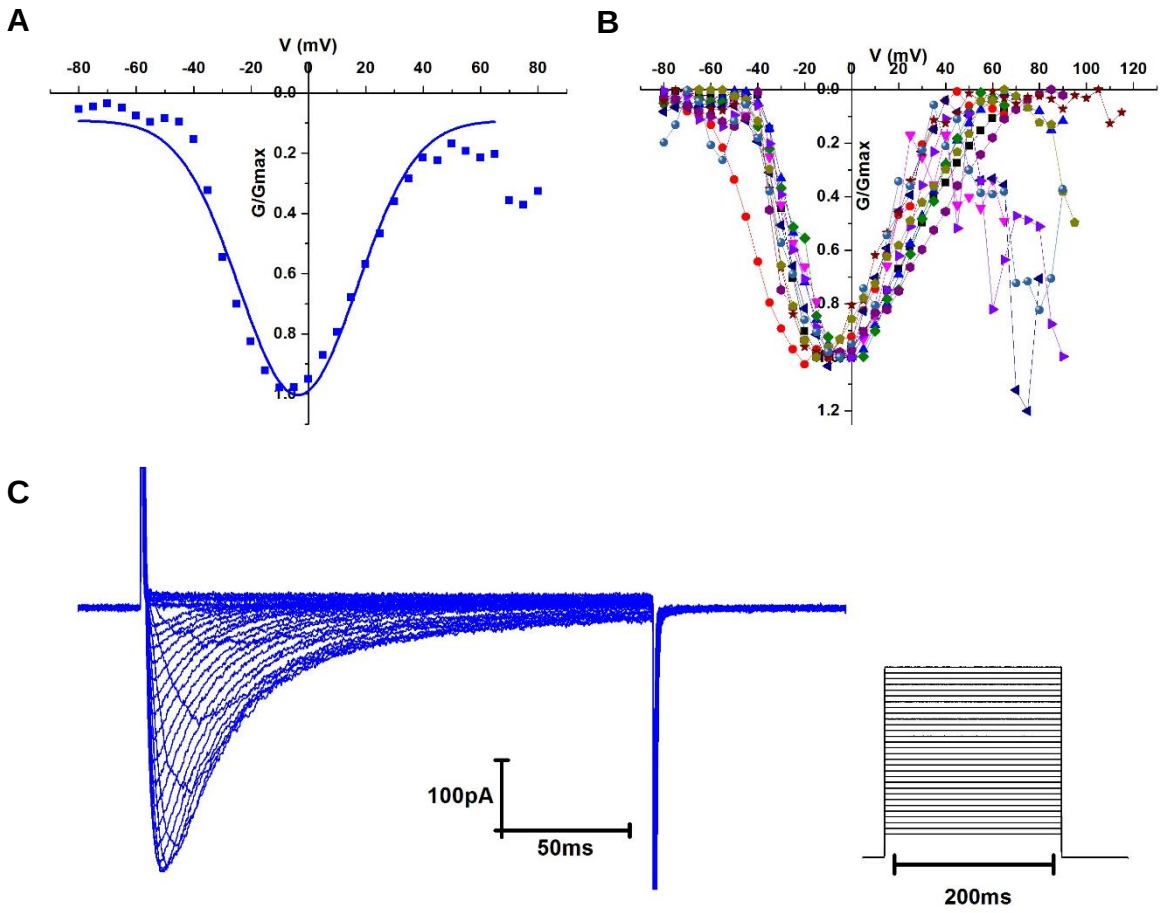

Figure 3.11. SroCa$_v$1 current-voltage relationship

(A) Average normalized, fitted IV analysis. Maximal currents were seen at depolarisations to approximately [-5mV]. (B) Pooled normalized IV curve data of expressed SroCa$_v$1. Recorded in 20mM $[Ca^{2+}]_{ext}$. (C) Sample trace of expressed SroCa$_v$1 in 20mM $[Ca^{2+}]_{ext}$.

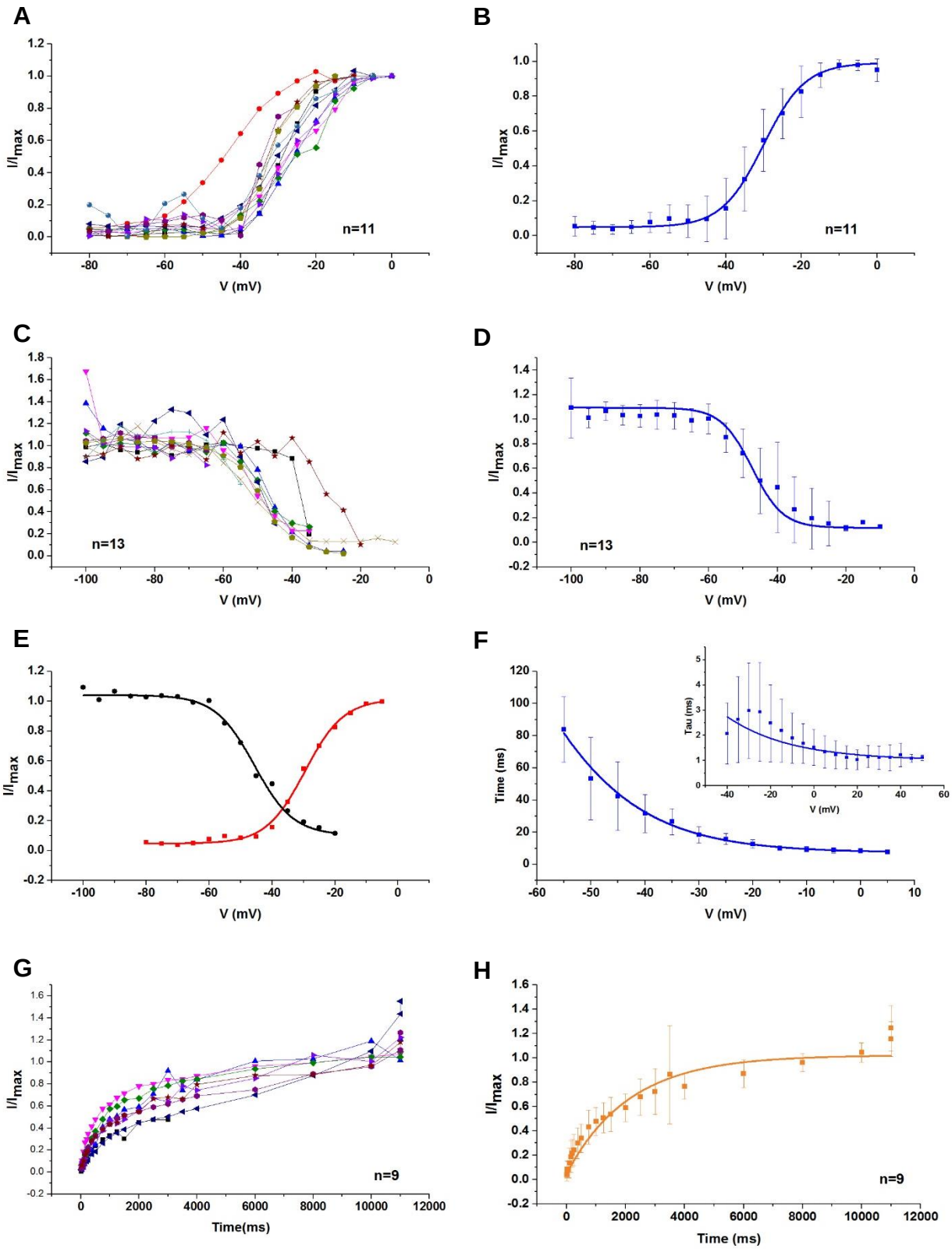
A
B
C
D
E
F
G
H
I/Imax
V (mV)
n=11
n=13
n=9
Time (ms)
Tau (ms)
Time(ms)

Figure 3.12. SroCa$_v$1 activation-inactivation

(A-B) Pooled activation traces and fitted average activation curves (Boltzmann fit), from holding potential of -110mV. (C-D) Steady state inactivation recoding, pooled and fitted average curves (Boltzmann fit). (E) Combined activation and inactivation curves for SroCa$_v$1 (F) Time to peak curve and Tau$_{inact}$ curve [inset] (Boltzmann fit) (G-H) Pooled and average fitted curves (Exponential fit). *n* values denote sample size of presented parameter. Data collected in bath solution containing 20 mM $[Ca^{2+}]_{ext}$

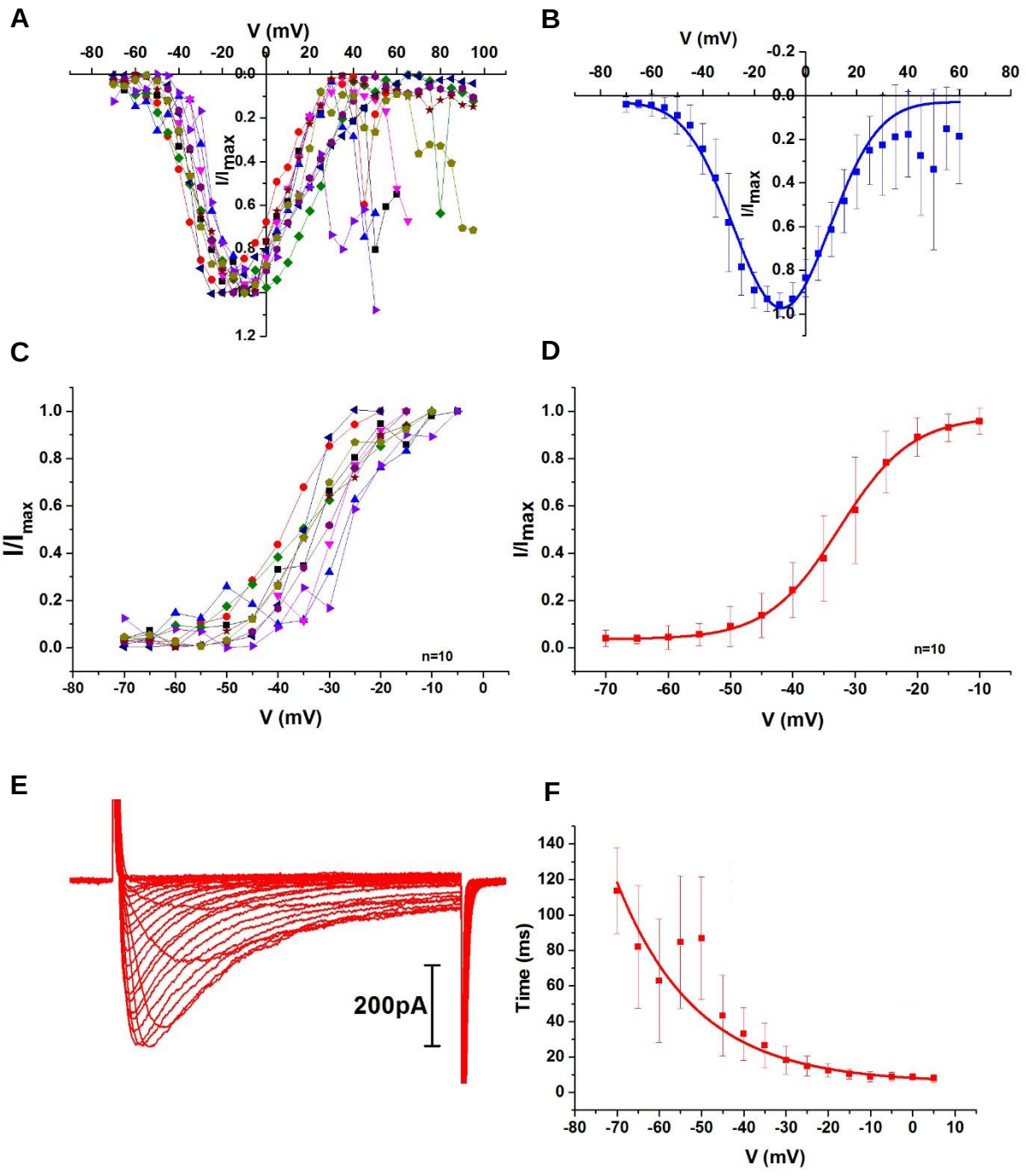

Figure 3.13. SroCa$_v$1 in Ba^{2+} charge carrier

(A-B) Normalized pooled and fitted average *I-V* curves for SroCa$_v$1 with Ba^{2+} as the charge carrier (Gaussian fit). (C-D) Normalized pooled and fitted activation curve (Boltzmann fit) (E) Sample trace of SroCa$_v$1 with Ba^{2+} as charge carrier. (F) Fitted time to peak curve

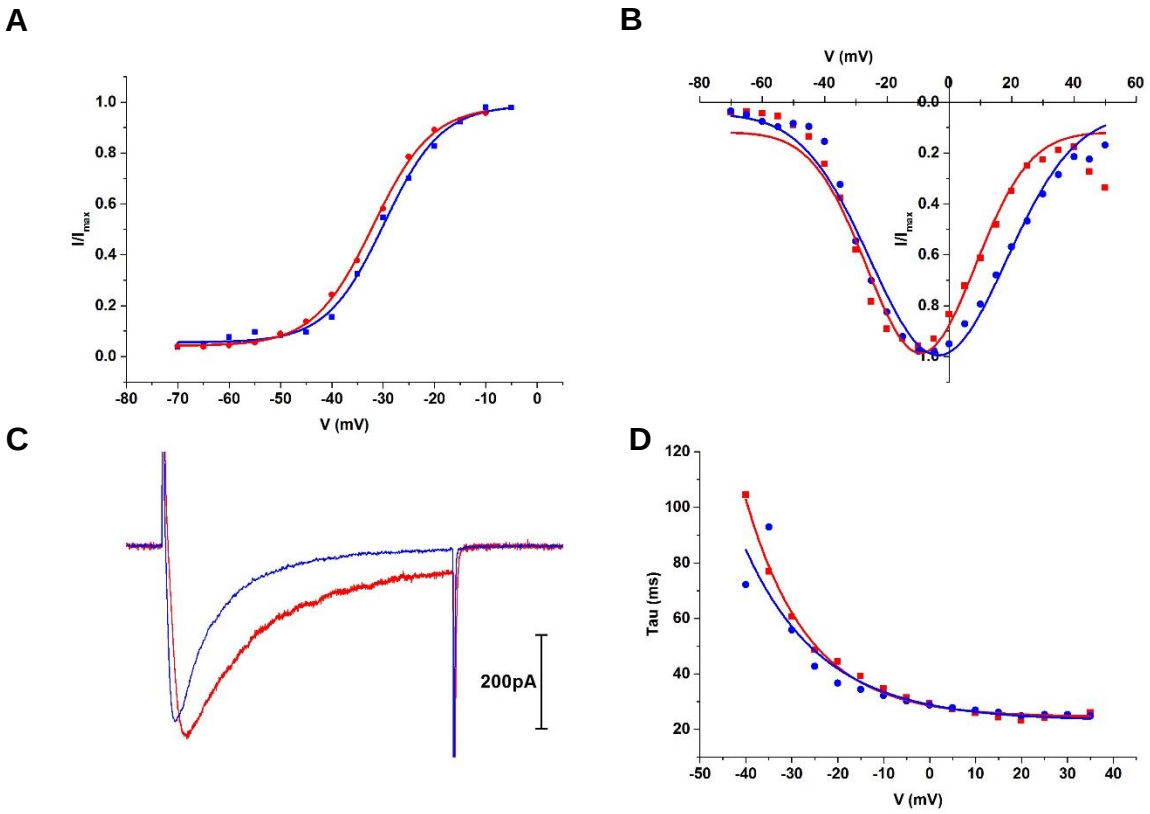

Figure 3.14. SroCa$_v$1 Ca^{2+} vs. Ba^{2+}

(A) Combined activation curves for Ca^{2+} (blue) and Ba^{2+} (blue) (B) Combined *I-V* curves, normalized to peak (C) Sample traces to outline difference in kinetics utilizing either Ca^{2+} (blue) or Ba^{2+} (red) as charge carrier, depolarising voltage step take to -10mV. (D) Combined Tau_{inact} (τ_{inact}) curves.

Table 3.2. Difference in SroCa$_v$1 kinetics dependent on charge carrier

	Calcium	Barium
Activation kinetics		
$V_{1/2}$	-29.83	-31.99
K	5.60	5.75
Peak of IV	-3.5 mV	-9.1 mV
Reversal Potential	+46.25 mV	+34.34 mV
n	11	10

3.6 Bi-ionic analysis SroNa$_v$2 DEKA mutant

The mutant SroNa$_v$2 channel was found to be more stable post-transfection than wild-type. Wild-type channel caused instability cellular membrane resulting unstable and leaky whole-cell patch conditions, and cells were only at acceptable measureable currents for 32 hours post-transfection. HEK cells expressing the SroNa$_v$2-DEKA mutant were able to be held at resting membrane potentials below [-90mV], and cell death during recording was not as prevalent with the mutant versus wild-type channel. Furthermore, the mutant channel requires a minimum 30 hours of incubation post-transfection for observable currents, which could be achieved within 12 hours post-transfection with wild-type SroNa$_v$2.

Mutating the selectivity filter of the SroNa$_v$2 channel Domain III glutamate (E) to lysine (K) to mirror vertebrate Na$_v$1 sodium channels produced a stark change in channel selectivity. Up to 80 hours post-transfection there were not detectable inward currents with bath solutions containing 2-4 mM Ca^{2+}. Na^+-$NMDG^+$ experimentation revealed the first inward currents when 135 mM Na^+ was perfused onto the patched cell. Based on this observation bi-ionic reversal potential experiments were performed to examine the degree of permeability of monovalent ions revealing that the DEKA mutant is exclusively permeable to monovalent ions. With a lack of a peak inward current to standardize against, an average of the first 3 sweeps was taken as baseline/standard.

The bi-ionic condition for the SroNa$_v$2 DEKA mutant produces a dramatic hyperpolarizing shift in reversal potentials of the monovalent ions tested indicating a preferential permeability for intracellular monovalent ions over the extracellular divalent Ca^{2+}. Shifts range from [-27mV] – [-43mV]. Mutant permeability replicates the same order as the wild-type with $Li^+ > K^+ = Na^+ > Cs^+$; however, reversal potentials are shift to -28mV < -12mV = -12mV < -1mV, respectively.

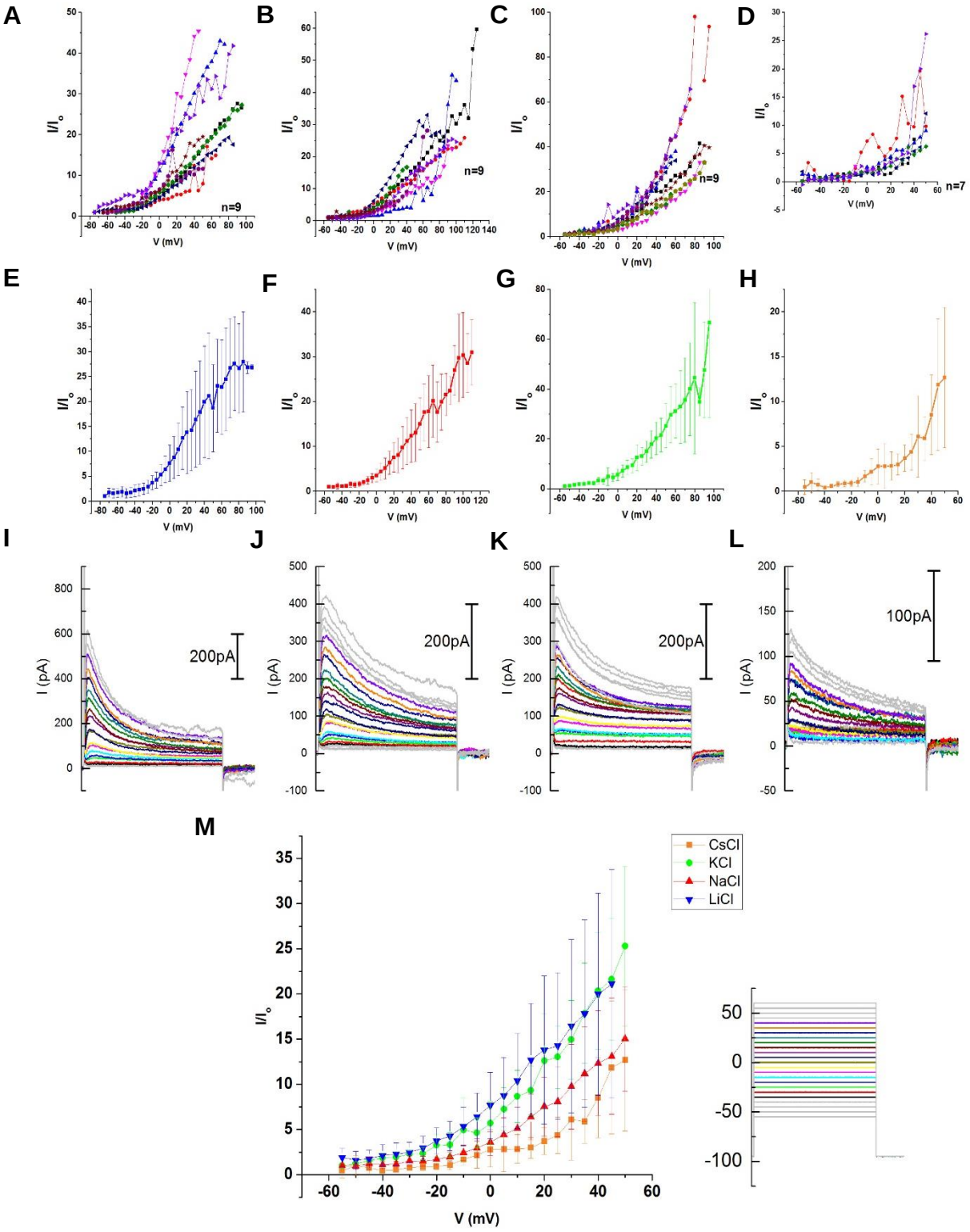
A
B
C
D
E
F
G
H
I
J
K
L
M
I/I$_o$
V (mV)
n=9
n=9
n=9
n=7
I (pA)
200pA
200pA
200pA
100pA
CsCl
KCl
NaCl
LiCl

Figure 3.15. SroNa$_v$2 DEKA mutation bi-ionic reversal

[Left to Right; Lithium-Sodium-Potassium-Cesium] (A-D) Pooled recording data normalized to peak conductance for intracellular monovalent ions. (E-H) Averaged pooled data, used to linear fit to determine reversal potential (I-L) Representative traces of each ion. Colours tracings coincide with voltage steps taken from 0mV – 55mV (shown in M) from a holding potential of [-100mV]. (M) Expanded view of combined graph of figures E-Fdifferences. All recordings done in 4 mM $[Ca^{2+}]_{ext}$

Table 3.3. Bi-ionic reversal potential of wild-type SroNa$_v$2 and DEKA mutant

	Lithium	**Potassium**	**Sodium**	**Cesium**
SroNa$_v$2:DEKA				
E_{rev} (mV)	-28.75749	-12.15726	-12.1704	-1.3319
S.E.M.	1.62473	2.44236	6.00684	8.10938
Permeability ratio				
P_{Ca} / P_X	2.779097	6.916222	9.432046	22.59269
S.E.M.	0.219993	0.96639	2.548279	10.52104
n	9	10	9	6
SroNa$_v$2				
E_{rev} (mV)	6.7809	15.5243	18.76907	42.90918
S.E.M.	1.08614	2.1202	1.38874	4.18464
Permeability ratio				
P_{Ca} / P_X	19.1974	34.90017	41.39771	273.3869
S.E.M.	1.463359	4.325008	3.739147	80.20794
n	10	9	9	7

Values are expressed at means ±standard error of mean (S.E.M.). P_{Ca}/P_x denotes permeability ratio of given ion [X] relative to calcium. *n* denotes sample size for tested ion. All recordings done in 4 mM $[Ca^{2+}]_{ext}$

Chapter 4
Discussion

4.1 Salpingoeca rosetta channels as earliest eukaryotic homologs

Work for this thesis involves an investigation of the earliest eukaryotic homologs for voltage-gated sodium and calcium channels. Recent analyses have consistently placed choanoflagellates as the most basal eukaryotic sister group to the Metazoa to have diverged following the animal-fungal split. The choanoflagellate species of *Salpingoeca rosetta*, is the simplest known candidate to possess voltage-gated sodium channels, SroNa$_v$2, and calcium channels, SroCa$_v$1 and SroCa$_v$3 (Moran et al., 2015; Moran & Zakon, 2014; Richter & King, 2013). Described here, we isolated the full length homologs and functionally characterize SroNa$_v$2 and SroCa$_v$1 electrophysiologically *in vitro*, providing an opportunity to evaluate the common and different features in the earliest branching sodium and calcium channels. It is important to note that previously cloned and expressed cnidarian and arthropod Na$_v$2 channels were heterologously expressed in *Xenopus* oocytes which possess very large calcium-dependent chloride currents, and prevented analyses of direct measurement of inward calcium currents. Previously all voltage-sensitive Na$_v$2 currents were assessed from tail currents in *Xenopus* oocytes. The mammalian HEK-293T cell host allowed a direct analysis of Ca^{2+} ion containing conductances through Na$_v$2 channels, which enabled the first evaluation of the contribution of sodium and calcium ion selectivity on Na$_v$2 channels, as well as being able to evaluate a homolog from an extant species, representative of a possible earliest diverging ancestor.

PCR amplification of target cDNA from *Salpingoeca rosetta* generated by RT-PCR produced a full length Na$_v$2 channel transcript of 5502 base pair (bp) resulting in an 1831 amino acid (AA) polypeptide that contained no alternative splicing in any sequenced PCR product. The isolated Ca_v^{2+} channel and associated β-subunit have a transcript and protein lengths of 4998bp/1666 AA and 1190bp/381 AA, respectively, also lacking in any obvious alternative splicing. SroNa$_v$2 and SroCa$_v$1 possess a 4x6 transmembrane domain protein structure of voltage-gated sodium and calcium channels (Fig. 1.2). They are true homologs of eukaryotic voltage-gated ion channels, (SroCa$_v$1) as their high degree of sequence similarity of the *Salpingoeca rosetta* channels (illustrated in Figures 3.4A, 3.4B), to other homologs in the classes

suggest. Sequence identity of SroNa$_v$2, SroCa$_v$1 and SroCa$_v$β are 33%-51%, 45%-58%, and 24%-26%, respectively. The key residue in all four ion selectivity filters of the isolated SroNa$_v$2 channel that is expected to be primarily responsible for their ion selectivity is DEEA (aspartate-glutamate-glutamate-alanine). The DEEA selectivity filter is consistent with those of previously characterized invertebrate Na$_v$2 channels, including that of *Blattella germanica* (cockroach), *Drosophila melanogaster* (fruit fly), and *Nematostella vectensis* (sea anemone). The more basal, apusozoan homolog, *Thecamonas trahens* has the only differing selectivity filter sequence as DEES (Fig. 3.3 – *T. trahens* filter not shown) (Cai, 2012). A major differentiating factor of Na$_v$2 channels from Na$_v$1 channels is in the replacement of the lysine (K) residue with a glutamate (E) in Domain III of vertebrate homologs or Domain II of cnidarian homologs (Cai, 2012; Catterall, 2012). This single amino acid change to a lysine residue is expected to be responsible for altering channel ion selectivity toward higher preference for sodium ions (Gur Barzilai et al., 2012b; Lipkind & Fozzard, 2008). SroNa$_v$2 demonstrates a relaxed cation selectivity with equal passage of sodium, calcium or potassium ions associated (Fig. 3.9, 3.12) with the DEEA selectivity filter and mimics the cation selectivity of other recorded Na$_v$2 channels from *N. vectensis* and *D. melanogaster* (Gur Barzilai et al., 2012b; Zhang et al., 2011). SroCa$_v$1 is most closely-related to vertebrate voltage-activated (HVA) Ca$_v$1.2 channels and other invertebrate Ca$_v$1 homologs (Fig. 3.4). It is the only observed Ca$_v$1 or Ca$_v$2 channel with an 'EDEE' selectivity filter, although calcium-selective pores of NALCN representatives typically possess an EEEE selectivity filter, but a more unusual EDEE selectivity filter is found in NALCN selectivity filters of a cnidarian (*Nematostella*) or mollusk (*Aplysia*) (Senatore et al., 2013). SroCa$_v$1 shares ~39% identity with the calcium binding domain to human HVA channels in the proximal C-terminus with a calcium-calmodulin binding 'IQ' domain substituted with 'LQ'. SroCa$_v$1, like other Ca$_v$1 or Ca$_v$2 channel homologs requires co-expression of its own Ca$_v$β-subunit. The SroCa$_v$β subunit is not found in other single cell eukaryotes such as *Monosiga* or *Thecamonas* which lack a Ca$_v$1 channel homolog but possess an Nav2 homolog. The association of a Ca$_v$β gene only in genomes which also contain a Ca$_v$1 channel homolog, is consistent with a proposed requirement of Ca$_v$β subunits in the expression of Ca$_v$1 channels (Nishimura et al., 1993; Welling et al., 1993). SroCa$_v$β subunit shares only 24-26% sequence identity with mammalian (human or rat) and *Lymnaea* snail LCa$_v$β subunit isoforms (Dawson et al., 2014) which is likely a factor in our observation

that other snail or mammalian $Ca_v\beta$-subunit homologs will not facilitate the membrane expression of the *Salpingoeca* Ca_v1 channel.

4.2 Unique non-selective ion permeability characteristics of SroNa$_v$2

We illustrate in patch clamp recording that SroNa$_v$2 is a non-selective for extracellular sodium and calcium ions. We observed inward currents with extracellular calcium or barium solutions, and an approximate increase of 1.6x current size when extracellular sodium ions replace equimolar, larger and impermeant N-methyl-D-glucamine (NMDG) along with extracellular calcium or barium ions, indicating an expected non-selectivity of Na_v2 channels allowing passage of both incoming sodium and calcium ions (Du et al., 2016; Gur Barzilai et al., 2012b; Zhang et al., 2011; Zhou et al., 2004). We had confirmed the dual monovalent and divalent ion selectivity in bi-ionic conditions, where high intracellular monovalent ion concentrations lead to large outward currents observed in the order of $Li^+ > Na^+ \approx K^+ > Cs^+$ to large depolarizing voltage-steps beyond the reversal potential, and a generation of large inward calcium currents at steps to lower voltages, due to the presence of extracellular calcium ions. This rank order of monovalent ions of $Li^+ > Na^+ \approx K^+ > Cs^+$ follows the Eisenman's ion selectivity model (Eisenman et al., 1967) and has been previously shown to be true of other type of voltage-gated channels including the invertebrate T-type calcium channel variants in *Lymnaea stagnalis* (Senatore, et al., 2014). The equal permeability of sodium and calcium ions is consistent with the DEEA selectivity filter that allow the passage of cations in a non-selective manner in Na_v2 channel homologs (Gur Barzilai et al., 2012b; Zhang et al., 2011; Zhou et al., 2004). Some calcium-selective channels generate larger or smaller ionic currents when divalent ion barium replaces equimolar calcium ions in the external medium. SroNa$_v$2 has reduced conductance with barium ions with peak current sizes reduced by 30% or 0.7x.

DSC1, the Na_v2 channel from *Drosophila* passes extracellular cations in the order of $Ba^{2+}>Ca^{2+}>Na^+$ (Zhang et al., 2011) which is different from SroNa$_v$2 which is much weaker in passing barium ions, with a rank order of passing extracellular cations of $Ca^{2+}>Na^+>Ba^{2+}$. Ba^{2+} is a much larger ion, with an ionic radius of 1.44 Å compared to Ca^{2+} and Na^+ which have ionic radii of 1.08 and 1.07 Å, respectively (Whittaker & Muntus, 1970). A small relative barium current is consistent with a greatly reduced outward current of larger monovalent Cs^+ with an

ionic radius of 1.78 Å that we recorded in bi-ionic conditions (Fig. 3.10). On the other hand, larger barium currents have often been attributed to a greater ligand binding of native calcium ions to channel pores compared to barium ions, in what has been termed the "sticky pore" hypothesis that limits the conductance rate of calcium through calcium-selective channels. No explanation is satisfactory in explaining what causes the differing relative permeability for calcium or barium ions.

SroNa$_v$2 exhibits a slow activation of gating and slow inactivation gating relative to typical fast vertebrate Na$_v$1 channels upon depolarizing voltage steps in patch clamp recording. Average time to peak data indicates that SroNa$_v$2 is upwards of 15x slower than neuronal Na$_v$1.1 and Na$_v$1.3, and cardiac Na$_v$1.5 (Chen et al., 2015; Veerman et al., 2015). Inactivation is 50x slower than typical brain sodium channel sodium channel of less than 1 ms, and more similar to slow-inactivating cardiac Na$_v$1.5 which requires ~50 ms to inactivate (Veerman et al., 2015); the inactivation decay rate of SroNa$_v$2 is consistent with previously reported data from expressed cockroach BSC1 Na$_v$2 channels (Zhou et al., 2004). Fast inactivation kinetics and fast recovery rates from inactivation allow typical Na$_v$1 sodium channels to generate action potential spikes at rates of 100 Hz in nervous systems (Catterall, 2012). SroNa$_v$2 appears to have a very slow recovery rate from 100% inactivation of ~15s, at a holding potential of -100 mV. Such a channel would not be a good candidate for fast inter-cellular communication as the rate of membrane depolarization would be very slow due to its slow activation gating, and limited in number of spikes generated with sustained depolarization because of its slow recovery rate from accumulated inactivation.

A most unique feature of SroNa$_v$2 lies in its odd pairing of the voltage dependence of activation and inactivation. SroNa$_v$2 is completely inactivated at normal resting membrane potentials ([-90mV] to [-45mV]) (Fig. 3.8E), with a midpoint (50%) of voltage-dependent inactivation of SroNa$_v$2 of ~[-103mV]) which theoretically would mean that a large hyperpolarizing input below -95 mV would be required to remove SroNa$_v$2 from complete inactivation. We don't know the resting membrane potential of *Salpingoeca rosetta* to determine whether membrane potentials could fall below 95 mV to remove the inactivation of SroNa$_v$2 channels.

Usually when voltage-sensitivities of ion channels are dramatically shifted to hyperpolarizing or depolarizing directions, they are usually more equally leftward shifted in the midpoints of 50% voltage of activation and inactivation, contributing to a changing operating window of channel excitability and refractoriness to more hyperpolarized potentials (i.e. low voltage activated channels) or depolarized potentials (i.e. high voltage-activated channels) (Chen et al., 2015; Loussouarn et al., 2016; Veerman et al., 2015). The most similar mammalian sodium channel as SroNa$_v$2 with a leftward shifted inactivation curve is heart sodium channel Na$_v$1.5 which exhibits a 50% voltage-dependent inactivation at ~[-89mV]. But Na$_v$1.5 also possess a hyperpolarizing shift in the voltage-dependence of activation compared to typical sodium channels, where $V_{50.activation}$ of ~[-41mV]) (Veerman et al., 2015; Zhang et al., 2013). SroNa$_v$2 is not only left shifted in the midpoint of the voltage dependence of inactivation compared to Na$_v$1.5 by more than 10 mV, but it is ~20 mV more right-shifted in the 50% of voltage dependence of activation compared to Na$_v$1.5. With a large, ~80 mV voltage-divide between the voltage-dependence of inactivation and activation, would mean that hyperpolarization input which would adequately recover SroNa$_v$2 from inactivation, would need to be succeeded by 80 mV of depolarizing input to adequately recruit SroNa$_v$2 channels to open. The strangely wide gap between the voltage-sensitivities of activation and inactivation, may be understood in the context of SroNa$_v$2 in its native environment. The native *Salpingoeca* environment may possess second messenger signalling or biological components not present in HEK293T cells that may be required for the native properties of the SroNa$_v$2 channel. For example, the voltage-dependent inactivation of SroNa$_v$2 may be strongly influenced by G-protein coupled receptor signalling like vertebrate Ca$_v$2 channels (Gray et al., 2007; Huang et al., 2010), or perhaps there is an auxiliary subunit of SroNa$_v$2 within native *Salpingoeca rosetta* that dramatically alters voltage dependent properties of SroNa$_v$2 channels, such as the Cavβ or vertebrate Na$_v$ β subunit. Another consideration is that SroNa$_v$2 is unusual as a sodium channel in passing lots of calcium ions, and perhaps there are intracellular calcium-associated modulators of gating such as the calcium calmodulin IQ motif that generates a calcium dependent inactivation of typical invertebrate and vertebrate Ca$_v$1 channels (Byerly et al., 1985; Taiakina et al., 2013; Zamponi & Snutch, 1996). Lastly, theoretically, SroNa$_v$2 is a channel serves only as a voltage-sensor or salt-sensor, such as mammalian Cav1.1 or Nax channels, respectively which are non-conducting, but couple ion binding to a downstream signalling mechanisms (Watanabe et al., 2002).

The SroNa$_v$2 channel was cloned, like other Na$_v$2 channels by its homology to Na$_v$1 channels in coding sequence. No one has tried to isolate a specific Na$_v$2 accessory subunit complexed with the Nav2 channels in a protein homogenate. It is logical to assume that Na$_v$2 channels may lack an accessory subunit because they Na$_v$2 channels express well in vitro without an accessory subunit (Gur Barzilai et al., 2012b; Zhang et al., 2011; Zhou et al., 2004). To date it remains that all functionally expressed Na$_v$2 channel α-subunits have been done without the use of accessory subunits (Gur Barzilai et al., 2012b; Zhang et al., 2011; Zhou et al., 2004). It is also noteworthy to consider that *Drosophila* fruit fly mutants of Na$_v$2 genes, generate an olfactory sensing impairment, and no other *Drosophila* mutant has a similar phenotype that would suggest co-requirement for Na$_v$2 channel function. *Drosophila* mutant *para* is a paralytic phenotype as a result of a lack of Nav1 channel gene, and its accessory subunit TipE causes a comparable paralytic phenotype as a result of its mutation in *Drosophila* (Feng et al., 1995; Li et al., 2011). Functional activity of Na$_v$1 channels are observed *in vitro* only after co-expression of an accessory Na$_v$β subunit. The Spafford lab found a barely detectable size of maximal current expression *in vitro* of *Lymnaea* pond snail LNa$_v$1 channel, and its expression was not compatible with *Drosophila* or vertebrate Na$_v$β accessory subunits for expression (unpublished). There might be an auxiliary subunit present in the native *S. rosetta* environment responsible for modulating SroNa$_v$2 channel functions. β-subunits are required auxiliary subunits with all Na$_v$1 channels and possess similar tissue-specific expression patterns as Na$_v$1 α-subunits. Vertebrate β-subunits are transmembrane proteins encoded by four genes (Scna1b – Scna4b) and each subunit interacts with the core α-subunit via either disulfide bonds or non-covalent interactions in a 1:1 stoichiometric fashion (Brackenbury & Isom, 2011; Catterall, 1988; Morgan et al., 2000; Yu et al., 2003). They are typically found expressed in a paired combinations of β_1 or β_3 with β_2 or β_4 (Namadurai et al., 2015; Yu et al., 2003) in mammals, or TipE and TEHs (TipE Homologous proteins) in *Drosophila*, or unique CUB domain containing Na$_v$β subunits in *Lymnaea* pond snail (Feng et al. 1995; Li et al., 2011; Zhang et al., 2011). Like the calcium channels, the β-subunits of sodium channels increase membrane expression of the pore forming α-subunits, and modify channel kinetic properties (Fang & Colecraft, 2011; Morgan et al., 2000; Yu et al., 2005). Combinations of different invertebrate Ca$_v$β (Dawson et al., 2014) or vertebrate Cavβ_1 to Cav β_4 subunits results in altered inactivation and current decay kinetics compared expression of the calcium channels α-subunit alone (Yu et al., 2003). It remains to be clearly demonstrated

whether SroNa$_v$2 is susceptible to modulation by co-expression of known auxiliary sodium channel β-subunits from other species, such as the ones found in *Drosophila, Lymnaea* or mammalian Na$_v$β subunits.

4.3 Change in selectivity with selectivity filter mutation DEKA

Changing the Domain III glutamate (E) residue to lysine (K) in the selectivity filter to replicate the selectivity filter of non-cnidarian, neuronal Na$_v$1 channels dramatically increases the selectivity of SroNa$_v$2. Previous investigators mutated the same Na$_v$2 channel residue from *Nematostella vectensis* (Gur Barzilai et al., 2012b) but extracellular calcium ion selectivity was not tested, a consequence of working with *Xenopus* oocytes, where calcium-activated chloride currents obscure the detection of calcium currents.

The Na$_v$1 sodium channel family is encoded by 10 genes, and nine of these Na$_v$1 genes possess the DEKA selectivity filter (outside of SCN7A gene with selectivity filter DENA), and are highly selective to sodium ions. The Na$_v$ channel pore likely resembles the pore dimensions of bacterial sodium channel, NavAb, for example, resolved as a high resolution X-ray crystal structure (Payandeh et al., 2011). It is believed through molecular modeling experiments that in the absence of Na^+ ions the carboxylate group of glutamate (DII) forms a hydrogen bond with lysine (DIII) thereby stabilizing the channel and preventing permeation of cations. The ionic size and hydration shell of Na^+ allow it to replace lysine (DIII) more easily than other ions (Lipkind & Fozzard, 2008). Mutations of the selectivity filter to the Na$_v$2.1 channel from *N. vectensis* produces a functional channel that is less selective for potassium over sodium (Gur Barzilai et al., 2012b). However, the degree of change in selectivity depended on the magnitude of mutation, with a single amino acid change within the selectivity filter (DII/III E→K) producing the smallest change, and altering the entire pore loops of each domain inferring the greatest change in sodium to potassium ion selectivity. In *Salpingoeca*, we report that just changing the single glutamate to lysine residue change in Domain III selectivity filter generated sodium channels with no selectivity for calcium ions, but may have some permeability to K ions as large outward K^+ or Na^+ currents were observable in bi-ionic conditions with Ca^+ as the external ion, and K^+ ion or Na^+ ion as the only internal ion.

4.4 Functional role of the Na_v2 channel family

The function of Na_v2 channels has been linked to olfaction sensing in fruit flies, and a motor related function, where *Drosophila* mutants have a hyperkinetic response to threatening external stimuli (Dong et al., 2015). It may be that $SroNa_v2$ has a parallel role to play in single cell *Salpingoeca*, in transduction of chemical sensing, a single cell functional correlate to olfaction.

4.5 Quintessential high voltage-activated calcium channel, $SroCa_v1$

$SroCa_v1$ is a functional homolog of vertebrate $Ca_v1.2$ calcium channels which is widely expressed in the brain and heart (Brickley et al., 1995; Catterall et al. 2005; Hofmann et al., 2014), and to single Ca_v1 homologs in invertebrates, such as LCa_v1 from *Lymnaea* pond snail. $SroCa_v1$ is the most basal eukaryotic organism to possess a high voltage-activated calcium channel.

$SroCa_v1$ also exhibits many of the same features characteristic of invertebrate Ca_v1 or mammalian $Ca_v1.2$ calcium channel homologs including the generation of a calcium current that begins to activate at -40 mV and peaks near the overshoot (0 mV). Like other Ca_v1 channels $SroCa_v1$ possess faster kinetics compared to $SroNa_v2$ with peak currents attained in under 10ms, but are much slower than the typical invertebrate or vertebrate Na_v1 channel from nervous systems. Another unique feature of Ca_v1 channels that $SroCa_v1$ possesses is a current rundown which can be remedied by using GTP and ATP in the intracellular recording pipette. The most characteristic feature of L-type calcium channels shared in invertebrate Ca_v1 or mammalian $Ca_v1.2$ channels comes from a slowing of inactivation when Ba^{2+} is substituted in the bath solution for Ca^{2+} resulting in long-lasting currents during sustained membrane depolarization (Hofmann et al., 2014; Senatore et al., 2011; Wheeler et al., 2012). The faster inactivation kinetics when calcium is the charge carrier is an effect known as calcium-dependent inactivation (CDI), resulting from calcium binding to an IQ motif in the proximal C-terminus of L-type Cav1calcium channels. Vertebrate $Ca_v2.1$ and $Ca_v2.2$ channels lack a calcium-dependent inactivation also. Instead it has a calcium-calmodulin regulated facilitation of calcium currents

involving the homologous IQ motif common in vertebrate Cav2 channels. P/Q-type and N-type channels are responsible for neurotransmitter release at the synaptic terminal and play a role in synaptic plasticity in hippocampal neurons (Nanou et al., 2016). In all cases calmodulin (CaM), a calcium-sensing bi-lobed protein covalently linked to the proximal C-termini of calcium channels, plays a role in modulating channel kinetics whether this is CDI and calcium-dependent facilitation (CDF) (Zuhlke et al., 1999). It currently remains to be shown whether CaM is associated with SroCa$_v$1 which appears to possess a conserved calcium-calmodulin IQ motif.

When substituting extracellular Ba^{2+} for Ca^{2+} there is a depolarizing shift in $V_{1/2}$ of activation, a shift in the reversal potential, and a shift in the peak of the I-V curve. This phenomenon is consistent with previously documented data on α_{1A}/ P/Q-type channels from vertebrates that shift as much as +15mV in a depolarizing direction, and in the invertebrate jellyfish *Cyanea capillata* L-type calcium channels to near similar magnitude of [+11mV] to [+12mV] (Jeziorski et al., 1998; Zamponi et al., 1996). This effect has been theorized as a result of charge screening of extracellular cations to the channel's protonation site causing conformational changes in the tertiary structure of the channel to coordinate Ca^{2+} binding (Hom et al., 1989; Zamponi et al., 1996). This phenomenon may likely be occurring in SroCa$_v$1 as evidenced by the differences in Ca^{2+} versus Ba^{2+} kinetics (Fig. 3.13).

4.6 Functional role of the SroCa$_v$1

High voltage-activated channels have critical sets of roles in both vertebrates and invertebrates including coupling excitation to muscle contraction (smooth and striated), neurotransmitter release, hormone regulation, neuroplasticity, pain perception, and vision (Beam, et al.,, 1989; Lipscombe, 2004; Mcrory et al., 2004; Murakami et al., 2002). In the genome of sister choanoflagellate, *Monosiga brevicolis*, exists genes encoding for α-, β-, βH-spectrins, and a complete set of SNARE proteins (synaptobrevin 2, syntaxin 1, SNAP-25), which have roles in cytoskeleton formation and stabilization and establishing epithelial cell polarity, and vesicle secretion, respectively (Baines, 2010; Burkhardt et al., 2011; Williams et al., 2014). In invertebrates, spectrins establish epithelial brush border polarity in the gut of *Drosophila* (Phillips & Thomas, 2006), while SNARE proteins were found restricted to the posterior end of *M. brevicolis* (Burkhardt et al., 2011). *M. brevicolis* also produces an extracellular matrix likely

allowing for cell-cell interactions composed of various components including proteins related to collagen, epithelial growth factor, laminin G, and fibrinogen among others (Williams et al., 2014). The morphology of *S. rosetta* is highly related to choanoflagellate *M. brevicolis* so it is likely to possess the same complement of homologous genes as *Monosiga* (Fairclough et al., 2013). Burkhardt and colleagues have shown that prey capture in *S. rosetta* occurs at the posterior pole via vesicular engulfment of targets and is facilitated by cilia (Burkhardt et al., 2011). It could be possible that SroCa$_v$1 is co-localized with SNARE proteins, and plays a role in a form of calcium-mediated vesicle release. This parallels the neurotransmitter release in pre-synaptic terminals of invertebrate and vertebrate nervous systems which is initiated by an influx of calcium through calcium channels causing intracellular vesicles to fuse to the cellular membrane through the action of SNARE proteins and release their contents (Catterall, 1999). Another possible role of L-type calcium channels is in a calcium dependent, muscular contraction and cellular mobility, in a manner that parallels roles that L-type calcium channels play in initiating muscle contraction of heart and skeletal muscle of invertebrates and vertebrates. Other protozoans, *Paramecium* (unicellular ciliates) swim by beating their cilia, and make turns by transiently reversing their power stroke. This ciliary reversal is caused by Ca^{2+} entering the cilium through voltage-gated Ca$_v$1 channels that are found exclusively in the cilia (Kink et al., 1990; Lodh et al., 2016). *Salpingoeca* rosetta have a collar of cilia surrounding the posterior flagellum for driving bacteria towards the cell to phagocytose. It is possible that Salpingoeca rosetta also use L-type calcium channels within their posterior collar of cilia to regulate ciliary beating.

The choanoflagellates offer a window to early eukaryotic development and the origins of multicellularity. Their emergence occurs at a time just after the fungal-animal split and prior to the expansion of multicellular organism. There are parallels to a commensalism of the human gut microbiome and the effect of native gut bacteria on the metabolism, and possible nervous system related activity including neurotransmitter release (Cryan et al., 2012; Stilling et al. 2016). In their native environments choanoflagellates form commensal relationships with bacteria in which they not only feed on those bacteria but are influenced by their by-products to form multicellular complexes (Alegado et al., 2012; Woznica et al., 2016). The genome size of *Salpingoeca rosetta* is the largest among other basal extant Opisthokonta (placozoa, cnidaria, ctenophora) and the number of orthologue clusters nearly matches that of higher Metazoa (Fairclough et al., 2013;

Osigus et al., 2013). The presence of a single member of each voltage-gated ion channel homolog (Na_v2, Ca_v1 and Ca_v3) and accessory calcium channel subunits $Ca_v\beta$ and Ca_v-$\alpha2\delta$ in *Salpingoeca* allows for direct evaluation of the consequences of manipulation of genes without the complexity resulting from multiple calcium and sodium channel isoforms, but a total gene pool that reflex a metazoan type cellular complexity.

4.7 Future directions and considerations

There is a number of opportunities for future research involving both in-vitro work of the Salpingoeca rosetta voltage-gated ion channels *in vitro* and in-vivo experimentation within *Salpingoeca rosetta*.

SroNa_v2 has been shown to be a non-selective channel allowing the passage of both sodium and calcium ions. A short term experiment is to test whether there is competition between calcium and sodium for pore binding. Anomalous mole fraction experimentation can be performed where sodium is held at a constant concentration while perfusion of increasing calcium concentrations to examine the ability of calcium ions to displace sodium ions in passing through SroNa_v2.

In combination of the DEKA selectivity filter mutation that dramatically changes ionic selectivity to match the selectivity filter of Na_v1 channels, a mutation involving the IFM-motif of the III-IV linker can be examined in an attempt to accelerate channel inactivation to resemble Na_v1 channels. The IFM-motif is largely responsible for the rapid inactivation of the Na_v1 family of channels and is often key component behind the 'ball-and-chain' or 'hinge-lid' mechanism often referred to in topic of fast inactivation.

Another experiment is to mutate the Domain II glutamate (E) to lysine (K) to produce a DKEA selectivity filter that is the condition present in cnidarians such as jellyfish *Polyorchis penicillatus* (Spafford et al. 1996) and sea anemone *Nematostella vectensis* (Zakon, 2012). Our goal will be to address whether the cnidarian DKEA selectivity filter is equivalent to the DEKA selectivity filter in Na_v1 channels of non-cnidarian metazoans in generating a high sodium selectivity.

In preliminary experiments, SroNa$_v$2 has been shown to be highly sensitive to block by the channel blocker lidocaine in the low µM ranges (data not shown). Determining the state-dependent block and other modulatory properties of lidocaine can be fully assessed, as well assessment of the drug blockade with other known sodium channel blockers including tetrodotoxin and saxitoxin. Highly selective drug blocker can be used to directly test the role of SroNa$_v$2 channels on *Salpingoeca rosetta* behavior *in vivo*. We can carry out time-lapse microscopy before and drug application to evaluate the physiological relevance of SroNa$_v$2 in the behavioral context of *S. rosetta*.

SroCa$_v$1 appears to be a quintessential high voltage-activated Ca$_v$1 calcium channel homolog that requires co-expression of auxiliary subunits for functional expression. Thus far to invertebrate or mammalian Ca$_v$β-subunits other than SroCa$_v$β do not promote the membrane expression and recording of SroCa$_v$1. *Salpingoeca rosetta* also appears to possess the gene encoding an $\alpha_2\delta$-subunit. We are currently trying to isolate this auxiliary subunit and test whether it can be used in conjunction with native β-subunits to put together the native assembly of calcium channel subunits *in vitro*. In vertebrates, it is thought that both Ca$_v$β and Ca$_v$-$\alpha_2\delta$ have roles to play outside of their functions with calcium channels. We are now generating SroCa$_v$1 and SroNa$_v$2 antibodies, and also SroCa$_v$β and SroCa$_v$-$\alpha_2\delta$ antibodies to evaluate the spatial co-localization of calcium and sodium channel subunits within *Salpingoeca*. In no other eukaryotic model than *Salpingoeca* is there only a single calcium channel and solitary Cavβ and Cav$\alpha_2\delta$ subunits, for evaluating the relationship between subunits without the complexity of other multiple isoforms in the cell.

Since SroCa$_v$1 is structurally homologous and shares many key sequence features with vertebrate L-type calcium channels we expect that SroCa$_v$1 can be blocked with calcium channel blockers that are potent in vertebrates. We will be testing the isradapine, nifedipine, verapamil and diltiazem for their ability to block SroCa$_v$1. As with SroNa$_v$2, we can then test these drug effects directly on *Salpingoeca rosetta* to assess consequences of ion channel loss to behavior.

Calmodulin, a bilobed calcium-binding protein, has been shown to play a role in modulating properties of calcium and sodium voltage-gated channels. It has been found to have effects not only on vertebrate L-type calcium channels, but also invertebrates, such as *Cyanea capillata* (jellyfish) (Jeziorski et al., 1998), *Lymnaea stagnalis* (pond snail) (Taiakina et al.,

2013) and likely unicellular ciliate, *Paramecium*. We are curious as to whether a similar conservation of calmodulin regulation is shared for SroCa$_v$1 or SroNa$_v$2.

Transcriptome data reveals that Salpingoeca rosetta also possesses the gene for a homologous low voltage-activated (T-type) calcium channel. Thus far we have isolated 2/3 of the channel and will be working towards isolating the channel in its entirety. The barrier to overcome lies in the difficult nature of the S. rosetta genome which has a high GC content (~60%), and what appears to be 'lazy' intron splicing evidenced by several isolated PCR products of both SroCa$_v$1 and SroNa$_v$2 contaminated with intron sequence.

Chapter 5
General Conclusions

We have isolated and electrophysiologically characterized two voltage-gated ion channel homologs (SroNa$_v$2 and SroCa$_v$1) from the most basal, extant eukaryote known to date to possess them, the choanoflagellate, Salpingoeca rosetta. The channels follow the 4 domain, 6 transmembrane helix architecture characteristic of the eukaryotic voltage-gated ion channel superfamily. The original hypothesis for this thesis was to assess the similarity of SroNa$_v$2 to other Na$_v$2 channels with the identical DEEA selectivity filter, and to compare SroCa$_v$1 to vertebrate and invertebrate high voltage-activated L-type calcium channels. This thesis has confirmed that even in the most basal sodium channel the slow activation-inactivation kinetics of the Na$_v$2 channel family are conserved, as well as their non-selective nature for permeating ions. Replacing the Domain III glutamate (E) with a lysine (K) in the selectivity filter to replicate vertebrate neural and cardiac sodium channel homologs causes a significant change in selectivity. SroCa$_v$1 supports evidence that the co-expression of auxiliary subunits is required for functional expression of the core α-subunit *in vitro*. The channel maintains high selectivity for divalent ions and has kinetics properties faster than SroNa$_v$2, but slower than Na$_v$1 channels. SroCa$_v$1 lacks both the slowing of kinetics and the prominent calcium-dependent inactivation observed through the long lasting currents during depolarization characteristic of L-type channels when barium is substituted as the charge carrier.

This thesis has provided evidence for the basic functions and characteristics of sodium and calcium channels. The presence of these channels in a single-celled extant eukaryote brings into question the purpose for the evolution of electrical signalling through such facilitated means.

References

Alegado, R. A., Brown, L. W., Cao, S., Dermenjian, R. K., Zuzow, R., Fairclough, S. R., … King, N. (2012). A bacterial sulfonolipid triggers multicellular development in the closest living relatives of animals. *eLife*, *2012*(1), 1–16. http://doi.org/10.7554/eLife.00013

Alegado, R. A., Grabenstatter, J. D., Zuzow, R., Morris, A., Huang, S. Y., Summons, R. E., & King, N. (2013). *Algoriphagus machipongonensis* sp. nov., co-isolated with a colonial choanoflagellate. *International Journal of Systematic and Evolutionary Microbiology*, *63*(1), 163–168. http://doi.org/10.1099/ijs.0.038646-0

Altier, C., Garcia-caballero, A., Simms, B., You, H., Chen, L., Walcher, J., … Zamponi, G. W. (2010). The $Ca_v\beta$ subunit prevents RFP2-mediated ubiquitination and proteasomal degradation of L-type channels. *Nature Publishing Group*, *14*(2), 173–180. http://doi.org/10.1038/nn.2712

Anderson, P. A. V, & Spencer, A. N. (1989). The Importance of Cnidarian Synapses for Neurobiology, *20*(5), 435–457.

Armstrong, C. M., Bezanilla, F., & Rojas, E. (1973). Destruction of Sodium Conductance Inactivation in Squid Axons Perfused with Pronase. *Journal of General Physiology*, *62*, 375–391.

Baines, A. J. (2010). Evolution of the spectrin-based membrane skeleton. *Transfusion Clinique et Biologique*, *17*(3), 95–103. http://doi.org/10.1016/j.tracli.2010.06.008

Beagle, S. D., & Lockless, S. W. (2015). Electrical signalling goes bacterial. *Nature*, *527*, 44–45.

Beam, K. G., Tanabe, T., & Numa, S. (1989). Structure , Function , and Regulation of the Skeletal Muscle Dihydropyridine Receptor ". *Annals of the New York Academy of Sciences*, *560*, 127–137.

Bean, B. P. (1985). Two kinds of calcium channels in canine atrial cells. Differences in kinetics, selectivity, and pharmacology. *The Journal of General Physiology*, *86*(1), 1–30. http://doi.org/10.1085/jgp.86.1.1

Bendahhou, S., Cummins, T. R., Tawil, R., Waxman, S. G., & Ptácek, L. J. (1999). Activation and inactivation of the voltage-gated sodium channel: role of segment S5 revealed by a novel hyperkalaemic periodic paralysis mutation. *The Journal of Neuroscience : The Official Journal of the Society for Neuroscience*, *19*(12), 4762–71. Retrieved from http://www.ncbi.nlm.nih.gov/pubmed/10366610

Ben-Johny, M., & Yue, D. T. (2014). Calmodulin regulation (calmodulation) of voltage-gated calcium channels. *The Journal of General Physiology*, *143*(6), 679–692. http://doi.org/10.1085/jgp.201311153

Bezanilla, F. (2000). The voltage sensor in voltage-dependent ion channels. *Physiological Reviews*, *80*(2), 555–592. http://doi.org/10.1126/science.279.5349.403

Boda, D., Leaf, G., Fonseca, J., & Eisenberg, B. (2015). Energetics of ion competition in the DEKA selectivity filter of neuronal sodium channels. *Condensed Matter Physics*, *18*(1), 1–14. http://doi.org/10.5488/CMP.18.13601

Borowiec, M. L., Lee, E. K., Chiu, J. C., & Plachetzki, D. C. (2015). Dissecting phylogenetic signal and accounting for bias in whole-genome data sets: a case study of the Metazoa. *bioRxiv*, 13946. http://doi.org/10.1101/013946

Brackenbury, W. J., & Isom, L. L. (2011). Na^+ channel β subunits : overachievers of the ion channel family, *2*(September), 1–11. http://doi.org/10.3389/fphar.2011.00053

Brehm, P., & Eckert, R. (1978). Calcium entry leads to inactivation of calcium channel in *Paramecium*. *Science (New York, N.Y.)*. Retrieved from http://www.ncbi.nlm.nih.gov/pubmed/103199

Brickley, K., Campbell, V., Berrow, N., Leach, R., Norman, R. I., Wray, D., … Baldwin, S. A. (1995). Use of site-directed antibodies to probe the topography of the of voltage-gated Ca^{2+} channels subunit, *364*, 129–133.

Brickley, K., Campbell, V., Berrow, N., Leach, R., Norman, R. I., Wray, D., … Uk, L. S. (1995). Use of site-directed antibodies to probe the topography of the of voltage-gated Ca^{2+} channels subunit, *364*, 129–133.

Brunet, T., & Arendt, D. (2016). From damage response to action potentials: early evolution of

neural and contractile modules in stem eukaryotes. *Philosophical Transactions of the Royal Society of London. Series B, Biological Sciences*, *371*(1685), 20150043-. http://doi.org/10.1098/rstb.2015.0043

Bullerwell, C. E., Forget, L., Lang, B. F., Edouard-montpetit, B., & Ht, Â. (2003). Evolution of monoblepharidalean fungi based on complete mitochondrial genome sequences, *31*(6), 1614–1623. http://doi.org/10.1093/nar/gkg264

Buraei, Z., & Yang, J. (2010). Structure and function of the beta subunit of voltage-gated Ca^{2+} channels, *48*(Suppl 2), 1–6. http://doi.org/10.1097/MPG.0b013e3181a15ae8.Screening

Burger, G., Forget, L., Zhu, Y., Gray, M. W., & Lang, B. F. (2003). Unique mitochondrial genome architecture in unicellular relatives of animals. *Proceedings of the National Academy of Sciences of the United States of America*, *100*(3), 892–897. http://doi.org/10.1073/pnas.0336115100

Burkhardt, P., Stegmann, C. M., Cooper, B., Kloepper, T. H., Imig, C., Varoqueaux, F., … Fasshauer, D. (2011). Primordial neurosecretory apparatus identified in the choanoflagellate *Monosiga brevicollis*. *Proc. Natl. Acad. Sci. USA*, *108*(37), 15264–9. http://doi.org/10.1073/pnas.1106189108

Byerly, L. O. U., Chase, P. B., & Stimers, J. R. (1985). Permeation and Interaction of Divalent Cations in Calcium Channels of Snail Neurons. *J. Gen. Physiol.*, *85*(April).

Cai, X. (2012). Ancient origin of four-domain voltage-gated Na^{+} channels predates the divergence of animals and fungi. *Journal of Membrane Biology*, *245*(2), 117–123. http://doi.org/10.1007/s00232-012-9415-9

Canti, C., Davies, A., & Dolphin, A. C. (2003). Calcium channel α2δ subunits - Structure, functions and target site for drugs. *Current Neuropharmacology*, *1*, 209–217. http://doi.org/10.2174/1570159033477116

Carpenter, J. (2012). Multicellularity Driven by Bacteria. *Science, 337*, 510 http://doi.org/10.1126/science.337.6094.510

Carr, M., Leadbeater, B. S. C., Hassan, R., Nelson, M., & Baldauf, S. L. (2008). Molecular phylogeny of choanoflagellates , the sister group to Metazoa, 7–9.

Catterall, W. A. (1988). Structure and Function of Voltage-Sensitive Ion Channels. *Science*, *242*(4875), 50–61.

Catterall, W. A. (1999). Interactions of Presynaptic Ca^{2+} Channels and Snare Proteins in Neurotransmitter Release. *Annals of the New York Academy of Sciences*, 144–159.

Catterall, W. A. (2011). Voltage-Gated Calcium Channels. *Cold Spring Harbor Perspectives in Biology* , *3*(8). http://doi.org/10.1101/cshperspect.a003947

Catterall, W. A. (2012). Voltage-gated sodium channels at 60: structure, function and pathophysiology. *The Journal of Physiology*, *590*(Pt 11), 2577–89. http://doi.org/10.1113/jphysiol.2011.224204

Catterall, W. A., Cestèle, S., Yarov-Yarovoy, V., Yu, F. H., Konoki, K., & Scheuer, T. (2007). Voltage-gated ion channels and gating modifier toxins. *Toxicon*, *49*(2), 124–141. http://doi.org/10.1016/j.toxicon.2006.09.022

Catterall, W. a, Perez-Reyes, E., Snutch, T. P., & Striessnig, J. (2005). International Union of Pharmacology. XLVIII. Nomenclature and structure-function relationships of voltage-gated calcium channels. *Pharmacological Reviews*, *57*(4), 411–425. http://doi.org/10.1124/pr.57.4.5.units

Chen, Y. J., Shi, Y. W., Xu, H. Q., Chen, M. L., Gao, M. M., Sun, W. W., … Liao, W. P. (2015). Electrophysiological Differences between the Same Pore Region Mutation in SCN1A and SCN3A. *Molecular Neurobiology*, *51*(3), 1263–1270. http://doi.org/10.1007/s12035-014-8802-x

Cox, D. H., & Dunlap, K. (1992). Pharmacological discrimination of N-type from L-type calcium current and its selective modulation by transmitters. *The Journal of Neuroscience : The Official Journal of the Society for Neuroscience*, *12*(3), 906–14. Retrieved from http://www.ncbi.nlm.nih.gov/pubmed/1347563

Cryan, J. F., Dinan, T. G., Bernard, C., Pavlov, I., Beaumont, W., James, W., … Charles, E. (2012). Mind-altering microorganisms : the impact of the gut microbiota on brain and behaviour of the nineteenth century through the pioneering work, *13*. http://doi.org/10.1038/nrn3346

Dawson, T. F., Boone, A. N., Senatore, A., Piticaru, J., Thiyagalingam, S., Jackson, D., … Spafford, J. D. (2014). Gene Splicing of an Invertebrate Beta Subunit (LCavβ) in the N-Terminal and HOOK Domains and Its Regulation of LCa_v1 and LCa_v2 Calcium Channels, *9*(4). http://doi.org/10.1371/journal.pone.0092941

Dayel, M. J., Alegado, R. A., Fairclough, S. R., Levin, T. C., Nichols, S. A., McDonald, K., & King, N. (2011). Cell differentiation and morphogenesis in the colony-forming choanoflagellate Salpingoeca rosetta. *Developmental Biology*, *357*(1), 73–82. http://doi.org/10.1016/j.ydbio.2011.06.003

Dayel, M. J., & King, N. (2014). Prey capture and phagocytosis in the choanoflagellate *Salpingoeca rosetta*. *PLoS ONE*, *9*(5), 1–6. http://doi.org/10.1371/journal.pone.0095577

DeMaria, C. D., Soong, T. W., Alseikhan, B. A., Alvania, R. S., & Yue, D. T. (2001). Calmodulin bifurcates the local Ca^{2+} signal that modulates P/Q-type Ca^{2+} channels. *Nature*, *411*(0028–0836 SB–IM), 484–489. http://doi.org/10.1038/35078091

Dick, I. E., Tadross, M. R., Liang, H., Hock Tay, L., Yabg, W., & Yue, D. T. (2008). A modular switch for sptial Ca^{2+} selectivity in the calmodulin regulation of Ca_V channels. *Nature*, *451*(7180), 830–834. http://doi.org/10.1038/nature06529.A

Dolphin, A. C. (2012). Calcium channel auxiliary $\alpha_2\delta$ and β subunits : trafficking and one step beyond. *Nature*, *13*(August), 542–555. http://doi.org/10.1038/nrn3311

Dolphin, A. C., Wyatt, C. N., Richards, J., Beattie, R. E., Craig, P., Lee, J., … Volsen, S. G. (1999). The effect of $\alpha_2\delta$ and other accessory subunits on expression and properties of the calcium channel á1G, 35–45.

Dong, K., Du, Y., Rinkevich, F., Wang, L., & Xu, P. (2015). The Drosophila Sodium Channel 1 (DSC1): The founding member of a new family of voltage-gated cation channels. *Pesticide Biochemistry and Physiology*, *120*, 36–39. http://doi.org/10.1016/j.pestbp.2014.12.005

Doyle, D. A., Cabral, J. M., Pfuetzner, R. A., Kuo, A., Gulbis, J. M., Cohen, S. L., … MacKinnon, R. (1998). The structure of the potassium channel: molecular basis of K^+ conduction and selectivity. *Science (New York, N.Y.)*, *280*(5360), 69–77. http://doi.org/10.1126/science.280.5360.69

Dreyfus, F. M., Tscherter, A., Errington, A. C., Renger, J. J., Shin, H.-S., Uebele, V. N., … Leresche, N. (2010). Selective T-type calcium channel block in thalamic neurons reveals channel redundancy and physiological impact of I(T)window. *The Journal of Neuroscience : The Official Journal of the Society for Neuroscience*, *30*(1), 99–109. http://doi.org/10.1523/JNEUROSCI.4305-09.2010

Du, H., Wang, Y., Shi, Y., Yu, J., Sun, W., & Zhang, Y. (2016). Effect of Traditional Chinese Medicine on Inflammatory Mediators in Pediatric Asthma, *2016*.

Dzhura, I., & Neely, A. (2003). Differential Modulation of Cardiac Ca^{2+} Channel Gating by β-Subunits. *Biophysical Journal*, *85*(1), 274–289. http://doi.org/10.1016/S0006-3495(03)74473-7

Eisenman, A. G., Sandblom, J. P., & Walker, J. L. (1967). Membrane Structure and Ion Permeation. Study of ion exchange membrane structure and function is relevant to analysis of biological ion permeation, *155*(3765), 965–974.

Eisenman, G. (1962). Cation selective glass electrodes and their mode of operation. *Biophysical Journal*, *2*(2 Pt 2), 259–323. http://doi.org/10.1016/S0006-3495(62)86959-8

Fairclough, S. R. (2011). The Cellular and Molecular Basis of Multicellular Development in the Choanoflagellate.

Fairclough, S. R., Chen, Z., Kramer, E., Zeng, Q., Young, S., Robertson, H. M., … King, N. (2013). Premetazoan genome evolution and the regulation of cell differentiation in the choanoflagellate *Salpingoeca rosetta*. *Genome Biology*, *14*(2), R15. http://doi.org/10.1186/gb-2013-14-2-r15

Fairclough, S. R., Dayel, M. J., & King, N. (2010). Multicellular development in a choanoflagellate. *Current Biology*, *20*(20), 875–876. http://doi.org/10.1016/j.cub.2010.09.014

Fang, K., & Colecraft, H. M. (2011). Mechanism of auxiliary β-subunit-mediated membrane targeting of L-type ($Ca_V1.2$) channels. *The Journal of Physiology*, *589*(Pt 18), 4437–4455. http://doi.org/10.1016/j.bpj.2010.12.3088

Favre, I., Moczydlowski, E., & Schild, L. (1996). On the Structural Basis for Ionic Selectivity

Among Na^+, K^+, and Ca^{2+} in the Voltage-Gated Sodium Channel, *71*(December), 3110–3125.

Feng, G., Dedk, P., Chopra, M., & Hall, L. M. (1995). Cloning and Functional Analysis of TipE , a Novel Membrane Protein That Enhances *Drosophila* para Sodium Channel Function Deduced Amino Acid Position, *82*, 1001–1011.

Gerster, U., Neuhuber, B., Groschner, K., Striessnig, J., & Flucher, B. E. (1999). Current modulation and membrane targeting of the calcium channel α1C subunit are independent functions of the beta subunit. *The Journal of Physiology*, *517 (Pt 2*, 353–368. http://doi.org/PHY_8939 [pii]

Glockling, S. L., Marshall, W. L., & Gleason, F. H. (2013). Phylogenetic interpretations and ecological potentials of the *Mesomycetozoea* (Ichthyosporea). *Fungal Ecology*, *6*(4), 237–247. http://doi.org/10.1016/j.funeco.2013.03.005

Goldin, A. L. (2003). Mechanisms of sodium channel inactivation. *Current Opinion in Neurobiology*, *13*(3), 284–290. http://doi.org/10.1016/S0959-4388(03)00065-5

Gray, A. C., Raingo, J., & Lipscombe, D. (2007). Neuronal calcium channels: Splicing for optimal performance. *Cell Calcium*, *42*(4–5), 409–417. http://doi.org/10.1016/j.ceca.2007.04.003

Gur Barzilai, M., Reitzel, A. M., Kraus, J. E. M., Gordon, D., Technau, U., Gurevitz, M., & Moran, Y. (2012a). Convergent Evolution of Sodium Ion Selectivity in Metazoan Neuronal Signaling. *Cell Reports*, *2*(2), 242–248. http://doi.org/10.1016/j.celrep.2012.06.016

Gur Barzilai, M., Reitzel, A. M., Kraus, J. E. M., Gordon, D., Technau, U., Gurevitz, M., & Moran, Y. (2012b). Convergent Evolution of Sodium Ion Selectivity in Metazoan Neuronal Signaling. *Cell Reports*, *2*(2), 242–248. http://doi.org/10.1016/j.celrep.2012.06.016

Hedges, S. B., Blair, J. E., Venturi, M. L., & Shoe, J. L. (2004). A molecular timescale of eukaryote evolution and the rise of complex multicellular life, *BMC Evolutionary Biology*, *9*, 1–9.

Heinemann, S. H., Terlau, H., Stuehmer, W., Imoto, K., & Numa, S. (1992). Calcium-channel characteristics conferred on the sodium-channel by single mutations. *Nature*, *356*(6368),

441–443. Retrieved from http://pubman.mpdl.mpg.de/pubman/item/escidoc:602454:2

Hendrich, J., Van Minh, A. T., Heblich, F., Nieto-Rostro, M., Watschinger, K., Striessnig, J., … Dolphin, A. C. (2008). Pharmacological disruption of calcium channel trafficking by the $\alpha_2\delta$ ligand gabapentin. *Proc Natl Acad Sci U S A*, *105*(9), 3628–3633. http://doi.org/10.1073/pnas.0708930105

Hille, B. (1975). Ionic selectivity, saturation, and block in sodium channels. A four-barrier model. *The Journal of General Physiology*, *66*(5), 535–60. http://doi.org/10.1085/jgp.66.5.535

Hille, B. (2001). Ion Channel Excitable Membranes. *Sunderland Massachusetts USA*. http://doi.org/10.1007/3-540-29623-9_5640

Hodgekin, A. L., & Huxley, A. F. (1952). Currents carried by sodium and potassium ions through the mmebrane of the giant axon of Loligo. *J. Physiol.*, *116*, 449–472.

Hofmann, F., Flockerzi, V., Kahl, S., & Wegener, J. W. (2014). L-Type $Ca_V1.2$ Calcium Channels: From In Vitro Findings to In Vivo Function. *Physiological Reviews*, *94*(1), 303–326. http://doi.org/10.1152/physrev.00016.2013

Hom, B. P., Pietrobon, D., & Hess, P. (1989). Interactions of Protons with Single Open L-Type Calcium Channels Location of Protonation Site and Dependence of Proton-induced Current Fluctuations on Concentration and Species of Permeant Ion. *J. Gen. Physiol.*, *94*(94), 23–42.

Huang, X., Senatore, A., Dawson, T. F., Quan, Q., & Spafford, J. D. (2010). G-proteins modulate invertebrate synaptic calcium channel (LCa_v2) differently from the classical voltage-dependent regulation of mammalian $Ca_v2.1$ and $Ca_v2.2$ channels. *The Journal of Experimental Biology*, *213*(Pt 12), 2094–103. http://doi.org/10.1242/jeb.042242

Jarrett, H. W., & Madhavan, R. (1991). Calmodulin-binding proteins also have a calmodulin-like binding site within their structure: The flip-flop model. *Journal of Biological Chemistry*, *266*(1), 362–371.

Jekely, G. (2013). Global view of the evolution and diversity of metazoan neuropeptide signaling. *Proc Natl Acad Sci U S A*, *110*(21), 8702–8707. http://doi.org/Doi

10.1073/Pnas.1221833110

Jeziorski, M. C., Greenberg, R. M., Clark, K. S., Anderson, P. A. V, & Augustine, S. (1998). Cloning and Functional Expression of a Voltage-gated Calcium Channel α_1 Subunit from Jellyfish *, *273*(35), 22792–22799.

Kass, R. S. (2004). Sodium channel inactivation goes with the flow. *The Journal of General Physiology*, *124*(1), 7–8. http://doi.org/10.1085/jgp.200409123

Kim, M. S., Morii, T., Sun, L. X., Imoto, K., & Mori, Y. (1993). Structural determinants of ion selectivity in brain calcium channel. *FEBS Letters*, *318*(2), 145–148. http://doi.org/10.1016/0014-5793(93)80009-J

King, N. (2004). The Unicellular Ancestry of Animal Development, *Developmental Cell*, *7*, 313–325.

Kink, J. A., Maley, M. E., Preston, R. R., Ling, K., & Waken-friedman, M. A. (1990). Mutations in *Paramecium* Calmodulin Indicate Functional Differences between the C-Terminal and N-Terminal Lobes In Vivo, *62*, 165–174.

Kovalevskaya, N. V., Van De Waterbeemd, M., Bokhovchuk, F. M., Bate, N., Bindels, R. J. M., Hoenderop, J. G. J., & Vuister, G. W. (2013). Structural analysis of calmodulin binding to ion channels demonstrates the role of its plasticity in regulation. *Pflugers Archiv European Journal of Physiology*, *465*(11), 1507–1519. http://doi.org/10.1007/s00424-013-1278-0

Krauss, D., Eisenber, B., & Gillespie, D. (2011). Selectivity sequences in a model calcium channel: role of electrostatic field strength. *European Journal of Biophysics*, *141*(4), 520–529. http://doi.org/10.1016/j.surg.2006.10.010.Use

Kulkarni, N. H., Yamamoto, A. H., Robinson, K. O., Mackay, T. F. C., & Anholt, R. R. H. (2002). The DSC1 channel, encoded by the smi60E locus, contributes to odor-guided behavior in *Drosophila melanogaster*. *Genetics*, *161*(4), 1507–1516. http://doi.org/10.1126/science.287.5461.2185

Lang, B. F., O'Kelly, C., Nerad, T., Gray, M. W., & Burger, G. (2002). The closest unicellular relatives of animals. *Current Biology*, *12*(20), 1773–1778. http://doi.org/10.1016/S0960-9822(02)01187-9

Lee, A., Scheuer, T., & Catterall, W. a. (2000). Ca^{2+}/Calmodulin-Dependent Facilitation and Inactivation of P/Q-Type Ca^{2+} Channels. *Journal of Neuroscience*, *20*(18), 6830–6838.

Lee, A., Wong, S. T., Gallagher, D., Li, B., Storm, D. R., Scheuer, T., & Catterall, W. a. (2000). Ca^{2+}/ calmodulin binds to and modulates P / Q-type calcium channels. *Nature*, *399*(May 1999), 155–159.

Levin, T. C., Greaney, A. J., Wetzel, L., & King, N. (2014). The Rosetteless gene controls development in the choanoflagellate *S. rosetta*. *eLife*, *3*, e04070. http://doi.org/10.7554/eLife.04070

Levin, T. C., & King, N. (2013). Report Evidence for Sex and Recombination in the Choanoflagellate *Salpingoeca rosetta*. *CURBIO*, *23*(21), 2176–2180. http://doi.org/10.1016/j.cub.2013.08.061

Ley, R. E., Hamady, M., Lozupone, C., Turnbaugh, P. J., Ramey, R. R., Bircher, J. S., … Gordon, J. I. (2008). Evolution of mammals and their gut microbes. *Science*, *777*(November).

Li, J., Waterhouse, R. M., & Zdobnov, E. M. (2011). A remarkably stable TipE gene cluster : evolution of insect Para sodium channel auxiliary subunits, *BMC Evolutionary Biology*, *11*, 1–11.

Lipkind, G. M., & Fozzard, H. a. (2008). Voltage-gated Na^{+} channel selectivity: the role of the conserved domain III lysine residue. *The Journal of General Physiology*, *131*(6), 523–9. http://doi.org/10.1085/jgp.200809991

Lipscombe, D. (2004). L-Type Calcium Channels: The Low Down. *Journal of Neurophysiology*, *92*(5), 2633–2641. http://doi.org/10.1152/jn.00486.2004

Lodh, S., Yano, J., Valentine, M. S., & Houten, J. L. Van. (2016). Voltage-gated calcium channels of *Paramecium* cilia. *J. Exper. Buiol.*, *219*, 3028–3038. http://doi.org/10.1242/jeb.141234

Long, S. B., Campbell, E. B., & Mackinnon, R. (2005). Crystal Structure of a Mammalinan Voltage-Dependent Shaker Family K^{+} Channel. *Science*, *897*(August), 897–903. http://doi.org/10.1126/science.1116269

Lory, P., Varadi, G., & Schwartz, A. (1992). The beta subunit controls the gating and dihydropyridine sensitivity of the skeletal muscle Ca^{2+} channel. *Biophysical Journal*, *63*(5), 1421–4. http://doi.org/10.1016/S0006-3495(92)81705-8

Loussouarn, G., Sternberg, D., Nicole, S., Marionneau, C., Le Bouffant, F., Toumaniantz, G., … Charpentier, F. (2016). Physiological and pathophysiological insights of $Na_v1.4$ and $Na_v1.5$ comparison. *Frontiers in Pharmacology*, *6*(JAN). http://doi.org/10.3389/fphar.2015.00314

Love, G. D., Grosjean, E., Stalvies, C., Fike, D. a, Grotzinger, J. P., Bradley, A. S., … Summons, R. E. (2009). Fossil steroids record the appearance of Demospongiae during the Cryogenian period. *Nature*, *457*(7230), 718–21. http://doi.org/10.1038/nature07673

Mackie, G. O. (2004). Central Neural Circuitry in the Jellyfish Aglantha, *5*, 5–19. http://doi.org/10.1159/000076155

Marais, E., Klugbauer, N., & Hofmann, F. (2001). Calcium channel $\alpha_2\delta$ subunits-structure and Gabapentin binding. *Molecular Pharmacology*, *59*(5), 1243–8. http://doi.org/10.1124/mol.59.5.1243

Mcrory, J. E., Hamid, J., Doering, C. J., Garcia, E., Parker, R., Hamming, K., … Snutch, T. P. (2004). The CACNA1F Gene Encodes an L-Type Calcium Channel with Unique Biophysical Properties and Tissue Distribution, *24*(7), 1707–1718. http://doi.org/10.1523/JNEUROSCI.4846-03.2004

Moran, Y., Barzilai, M. G., Liebeskind, B. J., & Zakon, H. H. (2015). Evolution of voltage-gated ion channels at the emergence of Metazoa. *The Journal of Experimental Biology*, *218*(Pt 4), 515–25. http://doi.org/10.1242/jeb.110270

Moran, Y., & Zakon, H. H. (2014). The evolution of the four subunits of voltage-gated calcium channels: Ancient roots, increasing complexity, and multiple losses. *Genome Biology and Evolution*, *6*(9), 2210–2217. http://doi.org/10.1093/gbe/evu177

Morgan, K., Morgan, K., Stevens, E. B., Shah, B., Cox, P. J., Dixon, A. K., … Jackson, A. P. (2000). β3 : An additional auxiliary subunit of the voltage- sensitive sodium channel that modulates channel gating with distinct kinetics, *PNAS*, *97*(5), 2308-2313. http://doi.org/10.1073/pnas.030362197

Moroz, L. L. (2015). Convergent evolution of neural systems in ctenophores, 598–611. http://doi.org/10.1242/jeb.110692

Murakami, M., Fleischmann, B., De Felipe, C., Freichel, M., Trost, C., Ludwig, A., … Cavali??, A. (2002). Pain perception in mice lacking the β3 subunit of voltage-activated calcium channels. *Journal of Biological Chemistry*, *277*(43), 40342–40351. http://doi.org/10.1074/jbc.M203425200

Namadurai, S., Yereddi, N. R., Cusdin, F. S., Huang, C. L., Chirgadze, D. Y., Jackson, A. P., & Jackson, A. P. (2015). A new look at sodium channel β subunits. *Open Biology*, *5*.

Nanou, E., Sullivan, J. M., Scheuer, T., & Catterall, W. A. (2016). Calcium sensor regulation of the $Ca_v2.1$ Ca^{2+} channel contributes to short-term synaptic plasticity in hippocampal neurons, *113*(4), 1062–1067. http://doi.org/10.1073/pnas.1524636113

Nichols, S. A., Roberts, B. W., Richter, D. J., Fairclough, S. R., & King, N. (2012). Origin of metazoan cadherin diversity and the antiquity of the classical cadherin/β-catenin complex. *Proc. Natl. Acad. Sci. USA*, *109*(32), 13046–51. http://doi.org/10.1073/pnas.1120685109

Nishimura, S., Takeshima, H., Hofmann, F., Flockerzib, V., & Imoto, K. (1993). Requirement of the calcium channel β subunit for functional conformation. *FEBS Letters*, *324*(3), 283–286.

Nosenko, T., Schreiber, F., Adamska, M., Adamski, M., Eitel, M., Hammel, J., … Wörheide, G. (2013). Deep metazoan phylogeny: When different genes tell different stories. *Molecular Phylogenetics and Evolution*, *67*(1), 223–233. http://doi.org/10.1016/j.ympev.2013.01.010

Opatowsky, Y., Chen, C.-C., Campbell, K. P., & Hirsch, J. a. (2004). Structural analysis of the voltage-dependent calcium channel β subunit functional core and its complex with the α_1 interaction domain. *Neuron*, *42*, 387–399. http://doi.org/10.1016/S0896-6273(04)00250-8

Osigus, H., Eitel, M., & Schierwater, B. (2013). Molecular Phylogenetics and Evolution Chasing the urmetazoon : Striking a blow for quality data?, *Molecular Phylogenetics and Evolution*, *66*, 551–557. http://doi.org/10.1016/j.ympev.2012.05.028

Pakendorf, B., & Stoneking, M. (2005). Mitochondrial DNA and human evolution. *Annu. Rev. Genomics Hum. Genet.*, (6), 165–183. http://doi.org/10.1146/annurev.genom.6.080604.162249

Paps, J., Medina-chacón, L. A., Marshall, W., Suga, H., & Ruiz-, I. (2015). Molecular phylogeny of Unikonts : new insights into the position of apusomonads and ancyromonads and the internal relationships of opisthokonts, *Protist*, *164*(1), 2–12. http://doi.org/10.1016/j.protis.2012.09.002.Molecular

Parfrey, L. W., Lahr, D. J. G., Knoll, A. H., & Katz, L. A. (2011). Estimating the timing of early eukaryotic diversification with multigene molecular clocks. *Proceedings of the National Academy of Sciences of the United States of America*, *108*(33), 13624–9. http://doi.org/10.1073/pnas.1110633108

Payandeh, J., Scheuer, T., Zheng, N., & Catterall, W. A. (2011). The crystal structure of a voltage-gated sodium channel. *Nature*, *475*(7356), 353–358. http://doi.org/10.1038/nature10238

Payandeh, J., Scheuer, T., Zheng, N., & Catterall, W. A. (2012). The Crystal Structure of a Voltage-Gated Sodium Channel. *Nature*, *475*(7356), 353–358. http://doi.org/10.1038/nature10238.THE

Peterson, B. Z., DeMaria, C. D., & Yue, D. T. (1999). Calmodulin is the Ca^{2+} sensor for Ca^{2+}dependent inactivation of L-type calcium channels. *Neuron*, *22*, 549–558.

Philippe, H., Lartillot, N., & Brinkmann, H. (2005). Multigene analyses of bilaterian animals corroborate the monophyly of Ecdysozoa, Lophotrochozoa, and protostomia. *Molecular Biology and Evolution*, *22*(5), 1246–1253. http://doi.org/10.1093/molbev/msi111

Phillips, M. D., & Thomas, G. H. (2006). Brush border spectrin is required for early endosome recycling in Drosophila. http://doi.org/10.1242/jcs.02839

Prindle, A., Liu, J., Asallay, M., Ly, S., Garcia-Ojalvo, J., & Suel, G. M. (2015). Ion channels enable electrical communication in bacterial communities. *Nature*, *527*, 59–70. http://doi.org/10.1038/nature15709

Richter, D., & King, N. (2013). The Genomic and Cellular Foundations of Animal Origins. *Annual Review of Genetics*, 1–31. http://doi.org/10.1146/annurev-genet-111212-133456

Ruiz-Trillo, I., Burger, G., Holland, P. W. H., King, N., Lang, B. F., Roger, A. J., & Gray, M. W. (2007). The origins of multicellularity : a multi-taxon genome initiative, *Genetics*, *23*(3).

http://doi.org/10.1016/j.tig.2007.01.005

Ruiz-Trillo, I., Roger, A. J., Burger, G., Gray, M. W., & Lang, B. F. (2008). A phylogenomic investigation into the origin of Metazoa. *Molecular Biology and Evolution*, *25*(4), 664–672. http://doi.org/10.1093/molbev/msn006

Saimi, Y., & Kung, C. (1994). Ion channel regulation by calmodulin binding. *FEBS Lett*, *350*(2–3), 155–158. http://doi.org/0014-5793(94)00782-9 [pii]

Sands, Z., Grottesi, A., & Sansom, M. S. P. (2005). Voltage-gated ion channels. *Current Biology : CB*, *15*(2), R44–R47. http://doi.org/10.1016/j.cub.2004.12.050

Senatore, A., Boone, A. N., Lam, S., Dawson, T. F., Zhorov, B. S., & Spafford, J. D. (2011). Mapping of dihydropyridine binding residues in a less sensitive invertebrate L-type calcium channel (LCa_v1). *Channels*, *5*(2), 173–187. http://doi.org/10.4161/chan.5.2.15141

Senatore, A., Boone, A. N., & Spafford, J. D. (2011). Optimized Transfection Strategy for Expression and Electrophysiological Recording of Recombinant Voltage-Gated Ion Channels in HEK-293T Cells, *JOVE*, 4–11. http://doi.org/10.3791/2314

Senatore, A., Guan, W., Boone, A. N., & Spafford, J. D. (2014). T-type channels become highly permeable to sodium ions using an alternative extracellular turret region (s5-p) outside the selectivity filter. *Journal of Biological Chemistry*, *289*(17), 11952–11969. http://doi.org/10.1074/jbc.M114.551473

Senatore, A., Guan, W., & Spafford, J. D. (2014). Ca_v3 T-type channels: Regulators for gating, membrane expression, and cation selectivity. *Pflugers Archiv European Journal of Physiology*, *466*(4), 645–660. http://doi.org/10.1007/s00424-014-1449-7

Senatore, A., Monteil, A., Minnen, J. Van, Smit, A. B., & Spafford, J. D. (2013). NALCN Ion Channels Have Alternative Selectivity Filters Resembling Calcium Channels or Sodium Channels, *8*(1). http://doi.org/10.1371/journal.pone.0055088

Senatore, A., Zhorov, B. S., & Spafford, J. D. (2012). Ca_v3 T-type calcium channels. *Wiley Interdisciplinary Reviews: Membrane Transport and Signaling*, *1*(4), 467–491. http://doi.org/10.1002/wmts.41

Shalchian-tabrizi, K., Minge, M. A., Espelund, M., Orr, R., Ruden, T., Kjetill, S., & Cavalier-smith, T. (2008). Multigene Phylogeny of Choanozoa and the Origin of Animals, *3*(5). http://doi.org/10.1371/journal.pone.0002098

Simms, B. A., & Zamponi, G. W. (2014). Neuronal voltage-gated calcium channels: Structure, function, and dysfunction. *Neuron*, *82*(1), 24–45. http://doi.org/10.1016/j.neuron.2014.03.016

Smith, M. R., Yu, E. J., & Goldin, A. L. (1997). Interaction between the putative sodium channel inactivation particle and domain III S4-S5. *Biophysical Journal*, *72*(2), A261.

Sogin, M. L. (1991). Early evolution and the origin of eukaryotes.*Current Biology, 1,* 457-463

Song, W., Liu, Z., Tan, J., Nomura, Y., & Dong, K. (2004). RNA editing generates tissue-specific sodium channels with distinct gating properties. *Journal of Biological Chemistry*, *279*(31), 32554–32561. http://doi.org/10.1074/jbc.M402392200

Spafford, J. D., Grigoriev, N. G., & Spencer, A. N. (1996). Pharmacological properties of voltage-gated Na^+ currents in motor neurones from a hydrozoan jellyfish Polyorchis penicillatus. *Journal of Experimental Biology*, *199*, 941–948.

Spafford, J. D., Van Minnen, J., Larsen, P., Smit, A. B., Syed, N. I., & Zamponi, G. W. (2004). Uncoupling of calcium channel α_1 and β subunits in developing neurons. *Journal of Biological Chemistry*, *279*(39), 41157–41167. http://doi.org/10.1074/jbc.M403781200

Spencer, A. N. (1979). Neurobiology of Polyorchis. II. Structure of effector systems, *J. Neurobio., 10*(2), 95–117.

Spencer, A. N. (1995). Modulatory Mechanisms at a Primitive Neuromuscular Synapse : Membrane Currents, Transmitter Release and Modulation by Transmitters in a Cnidarian Motor Neuron, *Amer. Zool. 528*, 520–528.

Stephens, R. F., Guan, W., Zhorov, B. S., & Spafford, J. D. (2015). Selectivity filters and cysteine-rich extracellular loops in voltage-gated sodium, calcium, and NALCN channels. *Frontiers in Physiology*, *6*, 153. http://doi.org/10.3389/fphys.2015.00153

Stephens, R., Zhorov, B. S., & Spafford, J. D. (2015). Regulation of ion selectivity in voltage-

gated sodium channels, calcium channels and NALCN pores by selectivity filter residues and extracellular turrets. *Frontiers in Physiology*, *53*(9), 1689–1699. http://doi.org/10.1017/CBO9781107415324.004

Stilling, R. M., Dinan, T. G., & Cryan, J. F. (2016). The brain's Geppetto — microbes as puppeteers of neural function and behaviour ?, *Journal of NeuroVirology*, (22), 14–21. http://doi.org/10.1007/s13365-015-0355-x

Suga, H. (2015). Filastereans and Ichthyosporeans : Models to Understand the Origin of Metazoan, 117–128. http://doi.org/10.1007/978-94-017-9642-2

Taiakina, V., Boone, A. N., Fux, J., Senatore, A., Weber-adrian, D., Guillemette, G., & Spafford, J. D. (2013). The Calmodulin-Binding , Short Linear Motif , NSCaTE Is Conserved in L-Type Channel Ancestors of Vertebrate. *PLoS ONE*, *8*(4). http://doi.org/10.1371/journal.pone.0061765

Tarvin, R. D., Santos, J. C., O'Connell, L. A., Zakon, H. H., & Cannatella, D. C. (2016). Convergent Substitutions in a Sodium Channel Suggest Multiple Origins of Toxin Resistance in Poison Frogs. *Molecular Biology and Evolution*, *33*(4), msv350. http://doi.org/10.1093/molbev/msv350

Torruella, G., Derelle, R., Paps, J., Lang, B. F., Roger, A. J., Salchian-Tabrizi, K., & Ruiz-Trillo, I. (2012). Phylogenetic Relationships within the Opisthokonta Based on Phylogenomic Analyses of Conserved Single-Copy Protein Domains Research article, *29*(2), 531–544. http://doi.org/10.1093/molbev/msr185

Van Petegem, F., Clark, K. A., Chatelain, F. C., & Minor, D. L. (2004). Structure of a complex between a voltage-gated calcium channel β-subunit and an α-subunit domain. *Nature*, *429*(6992), 671–5. http://doi.org/10.1038/nature02588

Vandenberg, C. A., & Bezanilla, F. (1991). A sodium channel gating model based on single channel, macroscopic ionic, and gating currents in the squid giant axon. *Biophysical Journal*, *60*(6), 1511–1533. http://doi.org/10.1016/S0006-3495(91)82186-5

Veerman, C. C., Wilde, A. A. M., & Lodder, E. M. (2015). The cardiac sodium channel gene SCN5A and its gene product $Na_V1.5$: Role in physiology and pathophysiology. *Gene*,

573(2), 177–187. http://doi.org/10.1016/j.gene.2015.08.062

Wakefield, W. S., Powell, M. J., Barr, D. J. S., Churchill, P. F., Longcore, J. E., & Chen, S. (2010). A molecular phylogenetic evaluation of the Spizellomycetales, *102*(3), 596–604. http://doi.org/10.3852/09-120

Watanabe, E., Hiyama, T. Y., Kodama, R., & Noda, M. (2002). Na_x sodium channel is expressed in non-myelinating Schwann cells and alveolar type II cells in mice. *Neuroscience Letters*, *330*(1), 109–113. http://doi.org/10.1016/S0304-3940(02)00708-5

Watanabe, H., Fujisawa, T., & Holstein, T. W. (2009). Cnidarians and the evolutionary origin of the nervous system. *Development Growth and Differentiation*, *51*(3), 167–183. http://doi.org/10.1111/j.1440-169X.2009.01103.x

Wegener, L., Lahr, D. J. G., Knoll, A. H., & Katz, L. A. (2011). Estimating the timing of early eukaryotic diversification with multigene molecular clocks, *108*(33), 13624–13629. http://doi.org/10.1073/pnas.1110633108

Weissgerber, P., Held, B., Bloch, W., Kaestner, L., Chien, K. R., Fleischmann, B. K., … Freichel, M. (2006). Reduced cardiac L-type Ca2+ current in $Ca_v\beta_2$-/- embryos impairs cardiac development and contraction with secondary defects in vascular maturation. *Circulation Research*, *99*(7), 749–757. http://doi.org/10.1161/01.RES.0000243978.15182.c1

Welling, B. Y. A., Bosse, E. V. A., Cavalie, A., Ludwig, A., Nastainczykt, W., Psychiatrie, I., & Klopferspitz, A. (1993). Stable co-expresion of calcium channel α_1, β and $\alpha_2\delta$ subunits in somatic cell line. *J. Physiol*, *471*, 749–765.

West, J. W., Patton, D. E., Scheuer, T., Wang, Y., Goldin, A. L., & Catterall, W. A. (1992). A cluster of hydrophobic amino acid residues required for fast Na^+-channel inactivation. *Proceedings of the National Academy of Sciences of the United States of America*, *89*(22), 10910–4. http://doi.org/10.1073/pnas.89.22.10910

Wheeler, D. G., Groth, R. D., Ma, H., Barrett, C. F., Owen, S. F., Safa, P., & Tsien, R. W. (2012). Ca_V1 and Ca_V2 channels engage distinct modes of Ca^{2+} signaling to control CREB-dependent gene expression. *Cell*, *149*(5), 1112–1124.

http://doi.org/10.1016/j.cell.2012.03.041

Whittaker, E. W., & Muntus, R. (1970). Ionic radii for use in geochemistry, *Geochimica et cosmochimica Acta, 34*, 945-956.

Williams, F., Tew, H. A., Paul, C. E., & Adams, J. C. (2014). The predicted secretomes of *Monosiga brevicollis* and *Capsaspora owczarzaki*, close unicellular relatives of metazoans , reveal new insights into the evolution of the metazoan extracellular matrix. *Matrix Biology, 37*, 60–68. http://doi.org/10.1016/j.matbio.2014.02.002

Wiser, O., Trus, M., Tobi, D., Halevi, S., Giladi, E., & Atlas, D. (1996). The $\alpha_2\delta$ subunit of voltage sensitive Ca^{2+} channels is a single transmembrane extracellular protein which is involved in regulated secretion. *FEBS Letters*, *379*(1), 15–20. http://doi.org/10.1016/0014-5793(95)01475-6

Woznica, A., Cantley, A. M., Beemelmanns, C., Freinkman, E., & Clardy, J. (2016). Bacterial lipids activate , synergize , and inhibit a developmental switch in choanoflagellates, *113*(28). http://doi.org/10.1073/pnas.1605015113

Yamagishi, T., Janecki, M., Marban, E., & Tomaselli, G. F. (1997). Topology of the P segments in the sodium channel pore revealed by cysteine mutagenesis. *Biophysical Journal*, *73*(1), 195–204. http://doi.org/10.1016/S0006-3495(97)78060-3

Yu, E. J., Ko, S., Lenkowski, P. W., Pance, A., Patel, M. K., & Jackson, A. P. (2005). Distinct domains of the sodium channel β_3-subunit modulate channel-gating kinetics and subcellular location, *526*, 519–526. http://doi.org/10.1042/BJ20050518

Yu, F. H., Westenbroek, R. E., Silos-santiago, I., Mccormick, K. A., Lawson, D., Ge, P., … Curtis, R. (2003). Sodium Channel β_4, a New Disulfide-Linked Auxiliary Subunit with Similarity to β_2, *J. NeuroSci. 23*(20), 7577–7585.

Yu, F. H., Yarov-Yarovoy, V., Gutman, G. a, & Catterall, W. a. (2005). Overview of molecular relationships in the voltage-gated ion channel superfamily. *Pharmacological Reviews*, *57*(4), 387–395. http://doi.org/10.1124/pr.57.4.13.1

Zakon, H. H. (2012). Adaptive evolution of voltage-gated sodium channels: the first 800 million years. *Proceedings of the National Academy of Sciences of the United States of America*,

109 Suppl(Supplement_1), 10619–25. http://doi.org/10.1073/pnas.1201884109

Zamponi, G. W., & Snutch, T. P. (1996). Evidence for a specific site for modulation of calcium channel activation by external calcium ions, *Eur. J. Physiol., 431*, 470–472.

Zhang, T., Liu, Z., Song, W., Du, Y., & Dong, K. (2011). Molecular Characterization and Functional Analysis of the DSC1 Channel. *Insect Biochem Mol Biol*, *41*(7), 451–458. http://doi.org/10.1016/j.ibmb.2011.04.010.MOLECULAR

Zhang, T., Wang, Z., Wang, L., Luo, N., Jiang, L., Liu, Z., … Dong, K. (2013). Role of the DSC1 Channel in Regulating Neuronal Excitability in *Drosophila melanogaster*: Extending Nervous System Stability under Stress. *PLoS Genetics*, *9*(3). http://doi.org/10.1371/journal.pgen.1003327

Zhang, Z., Zhao, Z., Liu, Y., Wang, W., Wu, Y., & Ding, J. (2013). Kinetic Model of $Na_v1.5$ Channel Provides a Subtle Insight into Slow Inactivation Associated Excitability in Cardiac Cells, *PLoS One, 8*(5). http://doi.org/10.1371/journal.pone.0064286

Zhou, W., Chung, I., Liu, Z., Goldin, A. L., & Dong, K. (2004). A voltage-gated calcium-selective channel encoded by a sodium channel-like gene. *Neuron*, *42*(1), 101–112. http://doi.org/10.1016/S0896-6273(04)00148-5

Zuhlke, R. D., Pitt, G. S., Deisseroth, K., Tsien, R. W., & Reuter, H. (1999). Calmodulin supports both inactivation and facilitation of L-type calcium channels. *Nature*, *42*(1995), 159–162.